JMENTATION PAGE

Form Approved
OMB No. 0704-0188

2. REPORT DATE	3. REPORT TYPE AND DATES COVERED
Jan. 92	Final 15Jul88-30Sep91

4. TITLE AND SUBTITLE

Tunable Solid State Lasers Based on Molecular Ions

5. FUNDING NUMBERS

DAALO3-88-K-0103

6. AUTHOR(S)

A. Lempicki and Cz. Koepke

7. PERFORMING ORGANIZATION NAME(S) AND ADDRESS(ES)

Boston University - Chemistry Dept
881 Commonwealth Ave. Boston, MA 02215

8. PERFORMING ORGANIZATION REPORT NUMBER

9. SPONSORING/MONITORING AGENCY NAME(S) AND ADDRESS(ES)

U. S. Army Research Office
P. O. Box 12211
Research Triangle Park, NC 27709-2211

10. SPONSORING/MONITORING AGENCY REPORT NUMBER

ARO 25631.13-PH

11. SUPPLEMENTARY NOTES

The view, opinions and/or findings contained in this report are those of the author(s) and should not be construed as an official Department of the Army position, policy, or decision, unless so designated by other documentation.

12a. DISTRIBUTION/AVAILABILITY STATEMENT

Approved for public release; distribution unlimited.

12b. DISTRIBUTION CODE

13. ABSTRACT *(Maximum 200 words)*

The main objective of this program was to investigate the possibility of developing tunable solid state lasers based on complexes of Transition Metal Ions in their highest valency state or equivalently d^0 configuration. This is a class of materials, often referred to as "phosphors" with strong absorption bands in the UV, and thus well suited for excimer laser pumping. We have found that, contrary to initial arguments, Excited State Absorption processes are very strong and overlapping the emission spectrum. Indications are that octahedral complexes, rather than tetrehedral may have a greater chance, especially in inorganic glasses. Additionally photochromic effects in BGO are reported and a study of non–radiative processes in broad band emitters, the later showing the inadequacy of present theoretical approach.

14. SUBJECT TERMS

Solid State Laser, Excited State Absorption, Photochromizm, Non-radiative processes

15. NUMBER OF PAGES

160

16. PRICE CODE

17. SECURITY CLASSIFICATION OF REPORT	18. SECURITY CLASSIFICATION OF THIS PAGE	19. SECURITY CLASSIFICATION OF ABSTRACT	20. LIMITATION OF ABSTRACT
UNCLASSIFIED	UNCLASSIFIED	UNCLASSIFIED	UL

FINAL REPORT

to

US ARMY RESEARCH OFFICE
(DAALO3 – 88 – K – 0103)

TUNABLE SOLID STATE LASERS BASED ON MOLECULAR IONS

A. Lempicki and Cz. Koepke *
Boston University,
Chemistry Department,
Boston, MA 02215

July 15, 1988 to September 30, 1991.

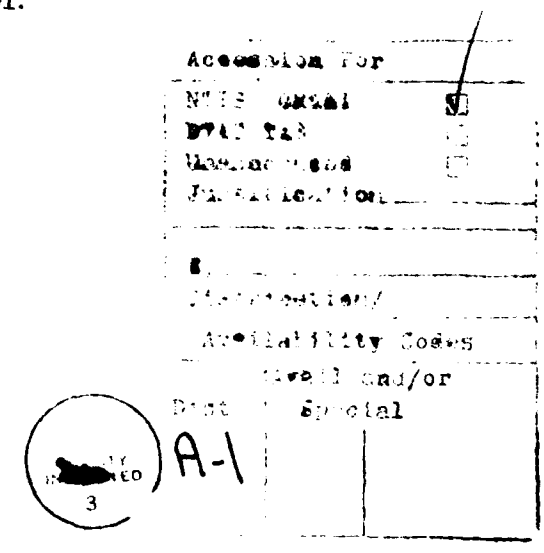

* On leave from Institute of Physics, Copernicus University, Torun, Poland.

TABLE OF CONTENTS

1. INTRODUCTION

This program was aimed at finding if d^0 – molecular complexes in crystals and glasses are capable to yield net optical gain, and in consequence, tunable laser action in the blue–green. d^0 type, crystalline materials are quite well known as efficient, broad–band lamp and cathodo–luminescent phosphors. They have never been investigated as possible laser media. Glasses containing molecular d^0 complexes are new materials and their luminescent properties are quite interesting and, in some cases, promising. A list of ions and their valence states giving rise to d^0 configuration, is given in Table I.

Table I *Closed Shell Transition Metal Ions*

Valence	+4	+5	+6	+7
3d	Ti	V	Cr	Mn
4d	Zr	Nb	Mo	–
5d	Hf	Ta	W	–

Table II lists the known oxy–complexes of the ions, their coordination and reported observation of luminescence. The table is based on a review article by Blasse [1]. Aside from efficiency and broad–band emission of these materials there are the following reasons why they may be considered as potential laser materials:

(a) The absorption (pump) bands are invariably situated in the near UV. They are quite intense being of a "charge transfer" character [1]. Excimer lasers could therefore be excellent pumping sources.

(b) The decay times of this class of materials are of the order of 10^{-6} sec, hence typically 10^3 times longer than for dyes. Lasers based on these materials would then have considerably higher energy storage, although naturally lower gain.

(c) Generally the existence of the Excited State Absorption (ESA) is recognized as a problem, whose existence may prevent laser action. At the onset of this program there were good reasons to believe that ESA should not represent much of a problem. These reasons were based on the following considerations. If one takes a very simple minded view of the charge transfer from a ligand to the central metal ion, the ion finds itself then in a

Table II *Complexes of Transition Metal Ions*

Ion valence	Complex		Structure	Luminescence	Example
+4	TiO_4^{4-}	Titanate	Tetr.	yes	
	TiO_6^{8-}	Titanate	Oct.	yes	$BaTi(PO_4)_2$
	TiO_5^{6-}	Titanate	Square pyram.	?	
	ZrO_6^{8-}	Zirconate		?	
	HfO_6^{8-}	Hafneate		?	
+5	VO_4^{3-}	Vanadate	Tetr.	yes	
	NbO_4^{3-}	Niobate	Tetr.	yes	
	NbO_6^{3-}	Niobate	Oct.	yes	$LiNbO_3$
	NbO_6^{7-}	Niobate	Oct.	yes	Li_3NbO_4
	TaO_4^{3-}	Tantalate	Tetr.	yes	
	TaO_6^{7-}	Tantalate	Oct.	yes	$Mg_4Ta_2O_9$ $MgTa_2O_6$
	TaO_8^{11-}	Tantalate	Zircon	yes	
+6	CrO_4^{2-}	Chromate	Tetr.	no	
	MoO_4^{2-}	Molybdate	Tetr.	yes	$CaMoO_4$
	MoO_6^{6-}	Molybdate	Oct.	no	
	WO_4^{2-}	Tungstate	Tetr.	yes	$CaWO_4$ $ZnWO_4$ etc.
	WO_6^{6-}	Tungstate	Oct.	yes	A_2BWO_6
+7	MnO_4^-	Manganate	Tetr.	no	

d^1–like state and next higher excited state is again a d–orbital, split off by the crystal field by an energy of 10Dq. The transition between these d–orbitals, which would correspond to ESA is parity forbidden and in the case of tetrahedral complexes should lie in the near IR. Thus, this simple model would predict a weak ESA at wavelength range shifted away from the luminescence band. A molecular–orbital picture of the described process is shown in Fig. 1 of Appendix 7.

Our investigation required single crystals of few mm length and at least a mm in thickness. These are not widely available and we were therefore limited to the following samples:

$CaMoO_4$	from Dr. L.H. Brixner of Du Pont de Nemours
$CaWO_4$	as above
$ZnWO_4$	from Dr. K. Nassau

In addition we have obtained samples of the following glasses from Corning Glass Works (courtesy of Dr. G.H. Beall):

zirconate glasses, doped with ZrO_2 of 4,6, and 8% concentration
tungstate glass, doped with 20 % of WO_3
niobate glass, doped with 1 % of Nb_2O_5.

We concentrated mostly on spectroscopic characteristics, which are related to potential laser applications i.e. on measurements of excited–state absorption and determination of stimulated emission. The results allowed us to draw some conclusions about the second excited state of these systems. In some cases, we measured basic spectroscopic characteristics: absorption, emission spectra, and temperature dependence of light yield and decay time.

Several publications, (Appendices A1, A2, A5 and A6) deal with properties of Bismuth Germanate, BGO, (ns^2 electronic configuration). Thematically they are rather loosely connected with the main goal: search among d^0 materials. However the technology of BGO is well established and large crystals are available. The luminescent properties of BGO have been widely investigated and its broad–band emission and reasonable efficiency, made it a good candidate for laser exploration.

2. SUMMARY OF BASIC OPTICAL SPECTROSCOPY

All investigated materials have similar, very broad emission spectra, which are not overlapped by ground state absorption (GSA). This fact allowed us to neglect the GSA absorption term in evaluation of excited–state absorption (ESA) crossection. The

measurements of GSA are especially difficult because of enormously high oscillator strength of absorption transitions (historically known as "charge transfer" ones). We did, however, several such measurements, usually to determine the temperature dependence of the absorption edge [A6]. Using a very intense source of excitation: excimer laser and wavelength falling in the vicinity of the absorption edge we observed interesting, thermally induced nonlinear effects, especially distinct in BGO crystals, [A6].

In order to determine the quantum efficiency of our samples (especially unknown in glasses) we carried–out the measurements of temperature dependence of the light yield andluminescence decay time. In the case of glasses it led to the surprising result that the Mott – Seitz frequency factor, well known from the theory of nonradiative transitions, appeared to be unusually small. This fact inspired us to make quantum–mechanical calculations of Struck–Fonger type, in order to find, if possible, a universal reason for very different values of the frequency factor, obtained for various materials, [A11]. Our conclusion is that both linear or nonlinear coupling to just one fully symmetrical mode is incapable to reasonably fit the parameters required by this type of theory and hence radiationless transitions should be treated by more sophisticated models e.g. the linear coupling to one and quadratic coupling to another mode [See references in A11].

For all materials we performed measurements of ESA and luminescence decays. In all cases the temporal behavior of ESA and luminescence was exactly the same, proving that both ESA and luminescence occur from the same state i.e. the initial state of ESA transitions is just the luminescing one. They also are both mostly single–exponential, suggesting just one active site. Among crystals, the only exceptions from this rule are ESA decays in $CaWO_4$, distorted somehow by a long ESA component originating in well known phosphorescent traps and contributions from the WO_3 group.

3. SUMMARY OF EXCITED–STATE SPECTROSCOPY

Under the name of ESA spectroscopy we understand all measurements of Excited–State Absorption and optical gain leading to the numerical evaluation of the corresponding crossections, σ_{ESA} and σ_{ST}, (ST – standing for stimulated emission). The determination of S_{ST}, follows the McCumber theory of phonon–terminated lasers [See A7, Sec.5]. Measurements of the ESA crossection σ_{ESA}, are described in most Appendices. From the laser point of view, the real issue is which of these two crossections is larger in the wavelength region corresponding to the emission spectrum.

Unfortunately in all cases we have studied, Excited–State Absorption shows a very broad spectrum, overlapping the emission spectrum, often spreading even farther. In all

these cases $\sigma_{ESA} > \sigma_{ST}$. There are however some promising observations in glasses, to which we shall return later.

We first concentrated on BGO because of the readily available large crystals. The obviously large light output under 308 nm excimer excitation, made it an excellent medium for initial experiments on excited state absorption. However the measurements of ESA spectra, in presence of overlapping luminescence proved to be extremely difficult. The problem was solved by using a gated OMA system working in a synchronous mode. The BGO crystal displayed broad–band ESA, precluding a possible lasing. Additionally, measuring the temporal characteristics of ESA, we found an interesting behavior: the excited–state absorption value $\{ESA = 1 - \exp(-\alpha_{ESA}L)\}$ increased with probe beam intensity, being, thus, a kind of excited–state photochromism. The effect proved to be extremely difficult to interpret. Finally we settled on a hypothesis of inhomogeneously distributed traps, fed by a higher excited state, [A1,A2,A5]. We have also observed an interesting thermal effect under very intense excimer excitation. This was iterpreted as an internal feedback between thermally increased absorption and localL temperature. It caused a nonlinear increase of excitation and, in consequence, an elevation of the excitation strength by some two orders of magnitude, [A6]. Later this discovery proved to be of significance and value in thermal tuning of the absorption in other materials, [A7].

Almost all d^0 materials, studied under this program happened to be of four–fold coordination. This was originally thought to be an advantage because 4–fold coordination provides a lower crystal field splitting of the d levels, (compared to 6–fold), and would therefore tend to move the ESA spectra more to the red of the luminescence. The detailed study proved that when term splitting and lattice relaxation are taken into account, this is not generally true and the ESA spectra are broad and tend to ovrlap the luminescence. If there is any hope of obtaining d^0 systems free of ESA, the 6–fold coordination may be more desirable, [A12].

The first measured material of d^0 type was a $CaMoO_4$ crystal [A4], showing a very broad and quite symmetrical ESA spectrum of very high crossection. The ratio: σ_{ESA}/σ_{ST} reached an extraordinarily high value ~ 160. This fact indicates that the higher excited state must be of the same character as the first excited state, and therefore a triplet. This turned out to be an universal feature of our tetroxo–complex materials.

Next two tungstate crystals: $CaWO_4$ and $ZnWO_4$ [A7,A8] showed similar, asymmetrical ESA spectra peaking around 22000 cm^{-1}. $CaWO_4$ crystal displayed additionally a very long–lived ESA component, which in all likelihood is connected with well known phosphorescent traps, existing in this material [A7]. We provide an

interpretation of this phenomenon in terms of simple kinetics, involving the traps fed from the first excited (luminescing) state, and being a source for additional ESA. $CaWO_4$ crystal appeared to be very tricky to get resonable data. First of all, it had rather small absorption at 308 nm (excimer line) and had to be heated to increase the GSA, utilizing the red shift of the absorption edge. It had, however, the advantage that at higher temperatures, the 308 nm line excited mostly the WO_4^{2-} complex, whereas at room temperature we could see in luminescence a quite large contribution from WO_3 Schottky defects. The paper on $CaWO_4$, [A7], reports various aspects of very high excitation by a line falling in the vicinity of the absorption edge, and how it reflects in the luminescence and ESA characteristics. $ZnWO_4$ crystal had much simpler properties, although we had to switch to another, longer–wavelength source of excitation (N_2 laser, 337.1 nm) in order to provide a sufficient excitation depth. Both these crystals provided the experimental data producing qualitatively the same SCC diagrams, with large delocalization of the terminal state of the ESA transition {of $(t_1^5, 4t_2)$ configuration}.

A new class of materials are glasses containing transition metal ions in d^0 configuration. We measured the following glasses: zirconate glass (of concentration: 4, 6, and 8% of ZrO_2), tungstate glass (20% of WO_3), and niobate glass (1% of Nb_2O_5), (A9,A10). Similarly to the crystals, ESA was here also very strong and broad–band. However, what is interesting, ESA spectra peaked at higher energy than for crystals by some 2000 cm^{-1}, (this was the case of zirconate and tungstate glasses), and in the case of niobate in quite far UV (we could only see a tail of ESA spectrum). We believe that this fact is strongly associated with the symmetry of molecular complex, because ESA occurs between configurations which are separated by 10Dq energy. The exact structure of our glasses is not yet well documented, but in the case of tungstate glass, Raman spectra suggest a nearly perfect tetrahedral coordination [A9]. Because the ESA spectra of zirconate glasses were very similar to those of tungstate glass, then, in view of rather confusing data on their symmetry, we assumed also tetrahedral coordination for these glasses. The only exception among our glasses is the niobate glass whose ESA is remarkably shifted towards UV. From the point of view of possible laser action this fact could be very beneficial. However the value of σ_{ESA} in the ESA tail covering the stimulated emission region, is still much larger than σ_{ST}, and thus, still precludes any possibility of laser action. In our opinion, the fact of UV–situated peak of ESA spectrum must be connected with octahedral coordination of the niobate glass, because $10Dq(O_h) = 9/4\{10Dq(T_d)\}$. A highly distorted 5– or 6–fold coordination of Nb complex in this glass was suggested before by Ellison and Hess [see A9]. The basic spectroscopic evaluation of these glasses showed in some cases their high quantum efficiency (~ 88 % for

zirconate glasses) and an extraordinarily small frequency factor, as defined by the Mott–Seitz theory of nonradiative transitions in strongly lattice–coupled systems, [A11].

5. CONCLUSIONS

In tetroxo systems the ESA transitions occur between $(t_1^5,2e)$ and $(t_1^5,4t_2)$ configurations and hence, are related to 10Dq energy. The one–electron molecular orbital energetic diagrams, where 10Dq falls into infrared region, do not give any reasonable indication if in such systems ESA overcomes optical gain or vice–versa. In one–electron model terms, ESA would then be a parity forbidden, single–line, pure d–d transition, which is of course untrue, and a proper approach needs to take into account various aspects of a very strong electron–lattice coupling. To get a feeling, how the electron–lattice coupling affects the ESA, we applied, wherever possible, the Single Configuration Coordinate (SCC) model with the simplest assumptions of linear coupling to a single, full symmetry mode. The model required the construction of a parabola corresponding to the higher (terminal ESA state) excited state. We did this by using experimentally obtained lineshapes of the emission and ESA, and a theoretical value for the 10Dq energy, which provided the spacing between the excited state parabolas, taken at equilibrium point of ground state parabola. This model is of course a greatly simplified picture, but in absence of better experimental data, provides at least a framework for further discussion of ESA in tetroxo complexes. For a full disussion see A7 and A8.

For the tungstate materials ($CaWO_4$, $ZnWO_4$, and tungstate glass), the higher excited–state parabola (corresponding to $(t_1^5,4t_2)$ configuration) appears to be shifted towards small values of the Configuration Coordinate, showing thus, a remarkable delocalization of the excited configuration. This has been interpreted as a considerable admixture of p–orbitals of the central ion into its d–orbitals. This admixture, possibly together with a contribution of $2p_\sigma$ ligand orbitals, causes an essential charge redistribution, (with respect to the ground state) and, in view of large displacement of higher excited–state parabola, is responsible for the large ESA linewidth. Also, what is perhaps most important, under the mixing of the p–orbitals into the higher excited configuration, the $4t_2$ one–electron state ceases to be pure d–state. Thus, the Laporte selection rule which precludes d–d transitions, because of the same parity of 2e and $4t_2$ states (assuming elcctric–dipole transition moment), ceases to be valid. This can be one of the causes of very high ESA transition oscillator strength. Moreover, as long as molecular terms are considered, the higher excited configuration $(t_1^5,4t_2)$ results in several singlet and triplet terms, the latter ones are presumably of lowest energy. ESA, very much like GSA, chooses these transitions which are spin–allowed. Hence ESA, starting from the lowest

triplet of $(t_1^5,2e)$ configuration, terminates on one of the higher configuration triplet terms and this is an additional cause of the high ESA strength.

In our last paper on tetroxo–complexes [11], we collected all the SCC diagrams for $CaWO_4$, $ZnWO_4$, tungstate glass, and $CaMoO_4$. All the tungstates display virtually the same diagrams, with large displacement of the higher excited–state parabola. The only difference between tungstate glass and tungstate crystals is the higher–energy peak of ESA spectrum in the glass, which may be connected with the higher Stokes shift, the fact often observed in glasses. The only exception from this picture is the SCC diagram of $CaMoO_4$ which displays rather small displacement of the higher excited–state parabola with respect to the lower one. This would predict a rather narrow ESA spectrum, contrary to the experiment. We believe that this is the point where our simple model, assuming harmonic potential and linear coupling to a single fully symmetrical mode, fails. However, it is well documented in literature [A7 ref 15 and 34] that $CaMoO_4$ reveals very large static Jahn–Teller effect in the excited state. The displacement of the first excited–state parabola under Jahn–Teller distortion, must then be responsible for the large observed ESA linewidth in this particular crystal. Another issue, which may be mentioned here is very different spin–orbit coupling for tungstates (central atom Z = 74) and molybdates (Z = 42). This interaction, mixing the multiplicities can affect differently the shapes of ESA spectra of tungstates and molybdates.

The conclusions from this series of papers on d^0 complexes, [A3, A4, A7 – A11] is contained in the "Conclusion" Section of A11. Briefly we have shown that an intense ESA spreads over the emission region and in general has a larger crossection than the stimulated crossection. The basic reason for this is the large electron – lattice coupling and the fact that ESA transitions are more allowed than the luminescent transitions. This derives from the singlet nature of the ground state, the triplet nature of the luminescent level and triplet–like nature of the higher excited states. This sequence is difficult to avoid. The only hope of defeating the overlap of ESA and emission is a spectral separation, resulting from the use of complexes in which the splitting of the d levels by crystal field is much larger. Hence our suggestion that octahedral complexes have a greater chance if efficient luminescence is observed. Since our data on ESA of transition metal complexes are the first ones collected on this class of compounds, it is hoped that they will stimulate further experimental and theoretical work.

The last paper of this series, [A12], departs somewhat from the main theme and addresses the general subject of nonradiative transitions in broad band emitters. This has been the subject of concern because there is no comprehensive theory of radiationless

processes in strongly coupled systems. The paper reviews briefly the history of the subject and shows conclusively that models based on linar and nonlinear coupling to a single vibrational mode or existence of selection rules are not adequate.

APPENDICIES

A1. *Cz. Koepke and A. Lempicki, "Excited State "Photochromism" in Bismuth Germanate", Chem. Phys. Lett. 172, 224 (1990)*

A2. *Cz. Koepke and A. Lempicki, "Excited State Absorption in $Bi_4Ge_3O_{12}$", Chem. Phys. Lett. 172, 227 (1990)*

A3. *Cz. Koepke and A. Lempicki, "Excited State Absorption in Solid State Molecular Complexes", in OSA Annual Meeting Technical Digest 1990, Vol.15 of the OSA Technical Digest Series (Optical Society of America, Washington, D.C., 1990)*
p. 192

A4. *Cz. Koepke and A. Lempicki, "Excited State Absorption in $CaMoO_4$", J. Luminescence, 47, 189 (1991)*

A5. *Cz. Koepke and A. Lempicki, "Electronic Photochromism: Case Study of Bismuth Germanate", J. Luminescence, 47, 227 (1991)*

A6. *Cz. Koepke, A.J. Wojtowicz, and A. Lempicki, "Thermal Effects in Excimer-Excited Bismuth Germanate", J. Opt. Soc. Amer. B 8, 1831 (1991)*

A7. *Cz. Koepke, A.J. Wojtowicz, and A. Lempicki, "Excited-State Absorption in Excimer-Pumped $CaWO_4$ Crystal", submitted to J. Luminescence*

A8. *Cz. Koepke and A. Lempicki, "Excited-State Absorption in $ZnWO_4$ Crystal", to be published.*

A9. Cz. Koepke, A. Lempicki, and C.H. Beall, "Glasses Containing Closed-Shell Molecular Complexes, I: Luminescence", to be published.

A10. Cz. Koepke, A. Lempicki, and C.H. Beall, "Glasses Containing Closed-Shell Molecular Complexes, II: Excited State Absorption", to be published.

A11. Cz. Koepke, A.J. Wojtowicz, and A. Lempicki, "Study of Molecular Tetroxo Complexes as Possible Laser Media", to be published.

A12. Cz. Koepke, A. Lempicki, and A.J. Wojtowicz, "Luminescence Quenching of Strongly Coupled Systems", to be published.

APPENDIX 1

Volume 172, number 3,4 CHEMICAL PHYSICS LETTERS 7 September 1990

Excited state "photochromism" in bismuth germanate

Cz. Koepke [1] and A. Lempicki

Chemistry Department, Boston University, 590 Commonwealth Avenue, Boston, MA 02215, USA

Received 17 May 1990

We report first time observation of transient excited state absorption (ESA) whose magnitude *increases* with the intensity of the probe beam. The effect is observed in bismuth germanate ($Bi_4Ge_3O_{12}$) and behaves as a sort of an excited state photochromism (ESP). In this material ESA increases from ≈20% up to ≈76% when the probe beam intensity increases from 1 to 16 W/cm^2. It has been measured with two different methods and occurs even with a Xe flash lamp used as a probe beam source. Several possible mechanisms of the ESP effect are considered.

Excited state absorption (ESA) has recently become a focus of attention because of its detrimental effect upon laser action [1,2]. We report a first time observation of transient ESA (following pulsed excitation), which increases with the intensity of a probe beam propagating through the excited medium. Because the medium becomes more opaque as the intensity of the probe beam increases, we call this effect excited state photochromism (ESP), in obvious analogy to photochemical effects causing light-induced absorption. We have observed this effect in $Bi_4Ge_3O_{12}$ (BGO) which due to its broad and intense luminescence has been the subject of some interest as a potential laser material. The absorption edge of BGO rises strongly below 320 nm and the emission band peaking at 480 nm has a halfwidth of 6400 cm^{-1}. Room temperature decay time is ≈500 ns. The absorption band is most likely due to a charge transfer transition characterized by a large Stokes shift (more than 15000 cm^{-1}) [3]. Our results indicate that the ESA spectrum overlaps the luminescence and even spreads further. Because of this, BGO cannot be considered as a potential laser material[#1].

The samples used in our experiment were crystal cubes of typically 0.8 cm edge length (Bicron Corp.). The excitation was provided by an unfocused excimer laser beam covering the whole face area (308 nm, pulse duration ≈30 ns, energy falling on the sample ≈30 mJ/pulse, repetition rate 14 pps). The probe beam was propagated transverse to the excitation. Two different probe beam-detection schemes were used:

(1) A chopped (3 ms duration, 14 pps) cw laser beam (He–Ne or other) and fast silicon photodiode. The chopper provided the trigger to the excimer and the diode output was directed to two channels of a boxcar. Gate widths of both channels were set at 30 or 50 ns, the gate of first channel delayed 30 ns from the peak of the pumping pulse, the second delayed ≈600 μs. Thus, the first channel measured the signal when ESA reaches its maximum whereas the second measured only the probe beam intensity.

(2) A pulsed xenon lamp (pulse duration ≈0.5 μs, 7 pps) and an OMA detector system set up to register a spectrum from 320 to 690 nm.

In both measurements the probe beam intensities were measured after passing through the pumped and unpumped sample. Ground state absorption at the probe beam wavelengths plays no role because of the large Stokes shift and the complete transparency of BGO in the visible. Extreme care was taken to eliminate luminescence contributions. Both measurements provided the ratio $(I_0-\delta I)/I_0$, where I_0 is the probe beam intensity after passing through an unpumped sample and δI the decrease of the beam due

[1] On leave from Institute of Physics, N. Copernicus University, 87-100 Toruń, Poland.

[#1] A detailed account of this work will be published elsewhere.

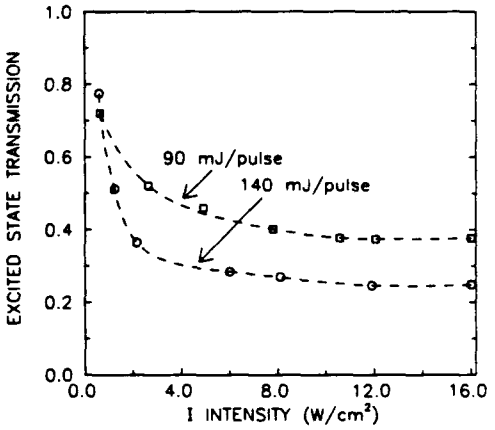

Fig. 1. Probe beam intensity dependence of EST for two different strengths of excitation: 90 and 140 mJ/pulse (laser output energy). Squares and circles represent experimental data for lower and higher excitation.

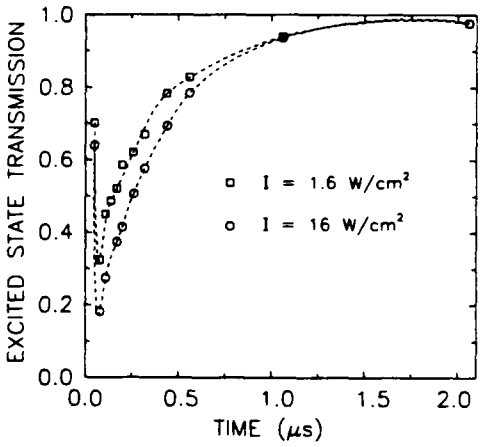

Fig. 2. Temporal dependence of EST for two I intensities: 1.6 and 16 W/cm². Circles and squares denote experimental data for higher and lower I, dashed lines are added to make those decays more readable.

to ESA. This ratio defines the excited state transmission (EST = 1 − ESA).

Fig. 1 shows a direct dependence of EST on I, for two different excitation strengths. In this case the source of the probe beam was a He–Ne laser (632.8 nm). Squares and circles correspond to excimer laser pulse energies of 90 and 140 mJ, respectively. A distinct, hyperbolic-like EST(I), is especially interesting in the region of small Is, where the most of EST drop (ESA increase) occurs, followed by a sort of saturation. At much larger intensities (≈ 70 W/cm²) we observe a gradual increase of EST (footnote 1).

Fig. 2 illustrates the temporal dependence of EST for two different intensities of the probe beam, provided by the He–Ne laser. Squares and circles represent data points corresponding to lower and higher I values respectively. One can note a very sudden, initial decrease of EST, lasting about 30 ns occurring during the pump pulse excitation. For higher I, EST decreases down to about 18%. Dashed lines represent a "french curve" type traces through the measured data.

We now turn to results obtained with experimental setup (2) utilizing the OMA and a broad band probe beam. This experiment should provide us with a spectral distribution of ESA (or EST) if it were not for the highly structured spectrum of the Xe lamp (insert in fig. 3). The variation of spectral intensity of the lamp tends to distort the EST spectrum in such a manner that it becomes a *nonlinear* folding of the

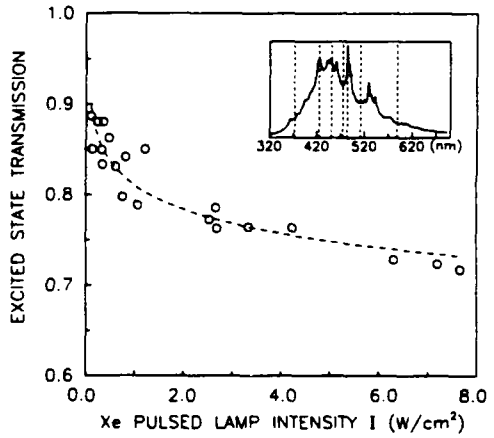

Fig. 3. Intensity dependence of EST measured by ungated OMA with Xe-pulsed lamp as a probe beam. Experimental data were taken here from three different EST spectra measured for various lamp intensities. Insert shows lamp spectrum and the wavelengths at which these data were taken.

lamp spectrum and true EST spectrum. Thus, the lamp spectrum peaks cause the appearance of valleys in the EST spectrum. The result is that the EST spectra measured by the OMA are a sort of distorted negative reflection of the Xe lamp spectrum. This, of course, makes it difficult to determine an actual EST spectrum but indications are that it is very broad, encompassing most of the visible. Assuming a flat spectral distribution of EST in the range of the lamp spectrum, we can use the OMA results and compare

them with the results obtained with a laser probe beam. In order to do this, we determine Xe lamp intensity using the following formula:

$$I = P\frac{\delta\lambda}{\Delta\lambda\, d}, \qquad (1)$$

where P is peak power entering the sample, $\Delta\lambda$ is width of the entire lamp spectrum, $\delta\lambda$ is the average width of prominent lamp spectrum peaks (about 10 nm, according to measured spectrum and manufacturers data [4]), and d is the area of the probe beam spot on the sample. The results are presented in fig. 3. Three complete EST spectra were taken here for three different lamp intensities. The values of EST were then plotted as a function of I chosen at indicated wavelengths. A distinct decreasing of EST with lamp intensity confirms the results obtained with laser–boxcar setup. It is noteworthy that this dependence was obtained under the assumption of a flat ESA spectrum.

Several attempts were made to find a mechanism which would account for the measured ESP effect. The assumption was made that the ESP effect induced by the probe beam can result either from a significant change of population of the first excited state or through the action of additional absorbing centers populated by a form of energy transfer. We considered the following models (footnote 1):

(a) a three-level model involving radiationless transitions from upper- to lower-excited states (states, between which ESA transitions occur),

(b) a four-level model involving a trap level (that evidence was proved by thermoluminescence measurements [5] and which is also mentioned by-Moncorgé et al. [6]) laying below the lower-excited state and possibly providing the populations to this state,

(c) a four-level model where the probe beam would contribute to the formation of free carriers and lead to free carrier absorption [7],

(d) five-level model involving a separate trap fed by the second-excited state and capable of providing the additional absorption. This is a mechanism similar to that proposed by Macfarlane in connection with hole-burning [8].

All of these models (except (b)) are capable of describing the results. However, all of them require an unphysically large σ cross section which would be responsible for I-induced part of ESA. Thus, so far the problem of ESP mechanism remains open.

In conclusion we believe that we have measured a new photochromic effect which specifically occurs when excited states are involved. The value of ESA cross section σ_{ESA} estimated from experimental data is $\approx 4\times10^{-19}$ cm^2 (for excited state population of about 5×10^{18} cm^{-3} derived from material and excitation parameters) and is about one order of magnitude greater than σ_{ST} for the stimulated emission in the spectral region of the probe beams (σ_{ST} was estimated from the measured luminescence spectrum, using McCumber theory of phonon-terminated lasers (footnote 1) [9], and for 632.8 nm $\sigma_{ST}\approx 1.9\times10^{-20}$ cm^2). According to calculation of BGO electronic structure [6], it would suggest that ESA transitions are mostly spin forbidden and the upper-excited state should then be a singlet state.

The observed effect could have some useful applications for creating an active, transient, self-tunable filter. Also, it may serve as a warning that broad band ESA spectra, overlapping luminescence bands, may be distorted by the dependence on probe beam intensity.

We are grateful to M. Mayhew of BICRON for supplying the BGO crystals and to A.J. Wojtowicz for some spectroscopic characterization of these samples. The support by the US Army Research Office under Grant DAAL03-88-K-0103 is also gratefully acknowledged.

References

[1] L.J. Andrews, S.M. Hitelman, M. Kokta and D. Gabbe, J. Chem. Phys. 84 (1986) 5229.
[2] S.A. Payne, L.L. Chase and G.D. Wilke, Phys. Rev. B 37 (1988) 998.
[3] R. Moncorgé, B. Jacquier and G. Boulon, J. Luminescence 14 (1976) 337.
[4] Short-Arc Xenon Flashlamps and Power Supplies, EG&G Electro-Optics product information and data sheet.
[5] C.L. Melcher, Nature 313 (1985) 465.
[6] R. Moncorgé, B. Jacquier, G. Boulon, F. Gaume-Mahn and J. Janin, J. Luminescence 12/13 (1976) 467.
[7] W.W. Piper and D.T.F. Marple, J. Appl. Phys. 32 (1961) 2237.
[8] R.M. Macfarlane and R.M. Shelby, in: Persistent spectral hole-burning: science and applications, ed. W.E. Moerner (Springer, Berlin, 1988) p. 127.
[9] D.E. McCumber, Phys. Rev. A 134 (1964) 299.

APPENDIX 2

Volume 172, number 3,4 CHEMICAL PHYSICS LETTERS 7 September 1990

Excited state absorption in $Bi_4Ge_3O_{12}$

Cz. Koepke [1] and A. Lempicki

Chemistry Department, Boston University, 590 Commonwealth Avenue, Boston, MA 02215, USA

Received 17 May 1990

Excited state absorption (ESA) spectra can sometimes be distorted by the dependence of ESA on probe beam intensity. An example of such a case is encountered in bismuth germanate, where severe distortion of ESA spectrum is caused by the strong increase of ESA with the intensity of the probe beam. We describe a method which extracts the true ESA spectrum and allows to ascribe the effect to concrete states. The method may be useful in other cases when strong dependence on probe beam intensity occurs.

Excited state absorption (ESA) has recently become a subject of great interest [1–4] because of new and extensive development of tunable, solid state lasers. One of the ESA features, qualitatively well understood, is the saturation of ESA transitions which results in decreasing of ESA with probe beam intensity. In two previous papers [5] [#1] we reported on an entirely opposite behavior. In bismuth germanate ($Bi_4Ge_3O_{12}$ – BGO) ESA increases with probe beam intensity, I, during pulsed excitation. The effect, which we call excited state photochromism (ESP), is very distinct (ESA increases from $\approx 20\%$ to $\approx 80\%$, when I increases from 1 to ≈ 20 W/cm^2), and possibly involves some trap levels in its mechanism [6,7].

In order to measure the ESP effect in BGO, we used two different experimental setups, both using an excimer laser as a source of 308 nm excitation, and a transverse pumping beam geometry. The first setup involved a monochromatic probe beam source (He–Ne or Ar lasers) and a photodiode detector coupled to a two-channel boxcar. The other used a polychromatic probe beam (Xe-flash lamp) and an OMA detection system. The laser–boxcar setup was used to measure excited state transmission (EST = 1 – ESA) as a function of time and probe beam intensity, whereas the Xe lamp–OMA system which, in principle, should yield the complete ESA spectrum, distorted it severely because of the ESP effect (see footnote 1). The measurements of luminescence decay time were carried out with a fast transient recorder (1024 channels × 10 ns interval).

There remained the problem of extracting an actual ESA spectrum from the measured one. Indications were that it is very broad, even broader than the practically white BGO luminescence.

Fig. 1 presents the time decay of ESA(t) after a 30

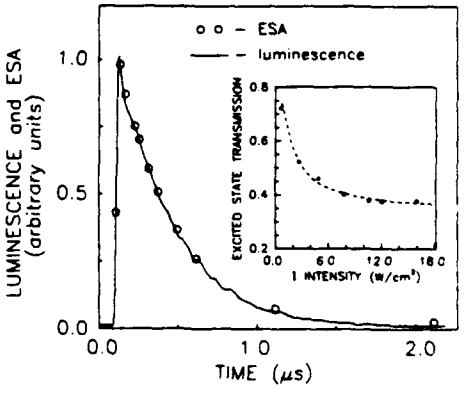

Fig. 1. The comparison of the temporal dependence of EST and luminescence, following ≈ 30 ns long excitation pulse (308 nm line, excimer laser). Insert shows a typical experimental EST(I) dependence (points) fitted by analytical curve used in our procedure.

[1] On leave from Institute of Physics, N. Copernicus University, 87-100 Toruń, Poland.

[#1] A detailed account of this work will be published elsewhere.

ns excitation (circles) compared with the luminescence decay measured under the same conditions (solid line). A distinct identity of the decays shows that both ESA and luminescence transitions are governed by virtually the same kinetics. The insert shows a typical EST(I) dependence (ESP effect) where experimental points are fitted by an analytical curve, used in our extraction method.

The very distinct EST(I) dependence, as seen in insert, and the highly structured spectrum of probe beam (Xe-pulsed lamp) strongly influences the EST spectrum. Indeed, the measured spectrum looks like a sort of distorted reflection of Xe lamp spectrum. The highly structured EST spectrum clearly reflects the lamp spectrum and does not allow to determine an *actual shape* of EST(λ), i.e. such a shape which would correspond to an *entirely flat* spectrum of $I(\lambda)$.

The method to obtain an actual ESA spectrum from measured spectrum is schematically illustrated in fig. 2. The lamp spectrum is sketched in quarter a of the figure, EST(I) in quarter b. The dashed curve in quarter c of the figure shows the EST[$I(\lambda)$] dependence resulting from applying of lamp spectrum $I(\lambda)$ in measured EST(I) dependence. In order to do this we used analytical functions which fit experimental EST(I) dependence very precisely, with a R^2 correlation parameter of 0.9927–0.9972. Using these functions we essentially simplified our procedure without loosing any physical information. The thin line in quarter c schematically represents the measured excited state transmission: $\mathrm{EST}^{\mathrm{m}}(\lambda)$. An actual EST "shape function" $F_{\mathrm{EST}}(\lambda)$ is hence given by the following ratio:

$$F_{\mathrm{EST}}(\lambda)=\frac{\mathrm{EST}^{\mathrm{m}}(\lambda, I)}{\mathrm{EST}[I(\lambda)]}. \qquad (1)$$

In the denominator of (1) the dependence on λ is implicit and is a result of folding of EST(I), which, we assume, is independent of λ explicitly, with the lamp spectrum $I(\lambda)$. Thus, the only dependence of the denominator on λ originates from Xe lamp spectrum. Unlike the denominator, the numerator of (1) depends on λ explicitly, containing an information on true EST spectrum. Relation (1) also indicates that $F_{\mathrm{EST}}(\lambda)$ would reach the unity level at a point λ_0 where I in the denominator equals I in the numerator. To make such an approach legal, the used EST(I) dependence should correspond to that value of excitation parameter $p=N^*/N$ which is typical for Xe lamp–OMA measurement. Also the range of I intensity should correspond to optics used with the Xe lamp [5].

The family of $F_{\mathrm{EST}}(\lambda)$ "shape functions" and the measured $\mathrm{EST}^{\mathrm{m}}(\lambda)$ spectrum are illustrated in fig. 3 where "shape functions" are parameterized by the range of I. One can see that for $I=7$ W/cm^2 most of X. lamp features vanish (see especially the region from 480 to 620 nm), whereas they appear for other

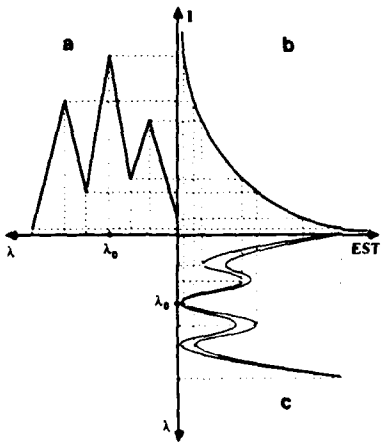

Fig. 2. Schematic presentation of used method for extracting of an actual shape of EST spectrum from measured one.

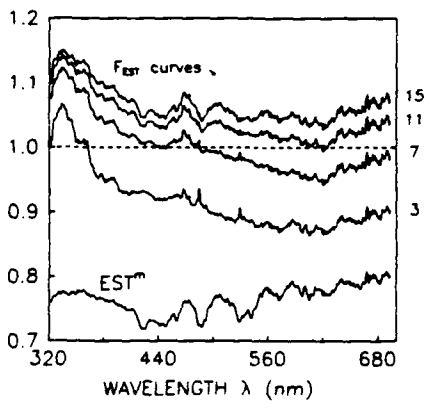

Fig. 3. The family of EST "shape functions" $F_{\mathrm{EST}}(\lambda)$, obtained with various ranges of $I(\lambda)$ intensity, and $\mathrm{EST}^{\mathrm{m}}$ spectrum measured by OMA. The numbers on the right-hand side denote the altered $I(\lambda_0)$ intensities (in W/cm^2).

intensities. For lower I intensities there are some peaks at wavelengths where the Xe lamp spectrum has its characteristic maxima, and for higher I intensities these peaks convert into valleys. Moreover, this curve crosses the unity level for $\lambda_0 \approx 484$ nm, the wavelength of the particular lamp peak for which the I intensity was scaled. It should also be pointed out that in ref. [5] the estimated value of I for the Xe lamp was 8 W/cm^2. All these facts convince us that $F_{EST}(\lambda, 7\ \mathrm{W/cm^2})$ corresponds well to an actual shape of the EST(λ) spectrum. Hence, to get an actual EST(λ) spectrum one needs to multiply $F_{EST}(\lambda)$ by EST$^m(\lambda_0)$ (in our case by 0.72, the value of measured EST for $\lambda_0 \approx 484$ nm, as seen in lower part of fig. 3).

So far we have been dealing only with transmission (EST). It is more useful to convert the results to cross sections which are proportional to the natural logarithm of EST (with ($-$) sign). We can then define a cross section "shape function" as

$$F_{CR}(\lambda) = \frac{\ln[\mathrm{EST}^m(\lambda, I)]}{\ln\{\mathrm{EST}[I(\lambda)]\}} . \qquad (2)$$

Having F_{CR}, an actual ESA cross section corresponding to a measured EST spectrum, can be expressed as

$$\sigma^m_{ESA}(\lambda) = F_{CR}(\lambda)\, \sigma_{ESA}(\lambda_0) , \qquad (3)$$

where $\sigma_{ESA}(\lambda_0)$ is an experimental value taken from the maximum of ESA(t) (fig. 1) at λ_0. Thus, eq. (3) corresponds to a transient excited state absorption. We should emphasize here that the $\sigma^m_{ESA}(\lambda)$ spectrum involves also a contribution from stimulated emission $\sigma_{ST}(\lambda)$ via the relation

$$\sigma^m_{ESA}(\lambda) = \sigma_{ESA}(\lambda) - \sigma_{ST}(\lambda) . \qquad (4)$$

The stimulated emission spectrum $\sigma_{ST}(\lambda)$ can be derived in terms of McCumber theory of phonon-terminated lasers [8] using the measured luminescence spectrum, quantum efficiency and spontaneous emission lifetime, as shown in ref. [9], and see footnote 1.

Fig. 4 shows the excited state absorption spectrum $\sigma_{ESA}(\lambda)$ in comparison with stimulated emission spectrum $\sigma_{ST}(\lambda)$. The distinct depression of the σ^m_{ESA} curve proves the existence of stimulated emission in BGO excited by an excimer laser. Indeed, $\sigma_{ST}(\lambda)$ fills this depression very effectively, making

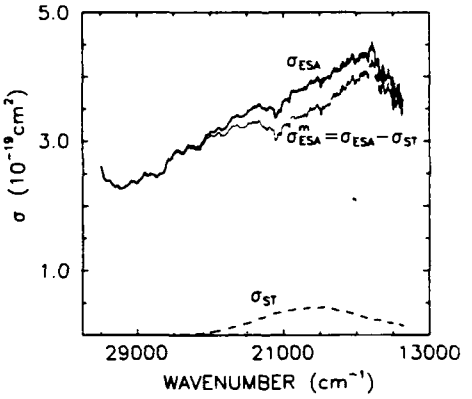

Fig. 4. An actual ESA spectrum expressed by means of cross section σ_{ESA} and stimulated emission spectrum σ_{ST} (dashed curve). Thinner line shows global σ^m_{ESA} spectrum, resulting directly from our measurements.

the $\sigma_{ESA}(\lambda)$ spectrum monotonically increasing with the wavelength in the 17000–25000 cm^{-1} range. However, $\sigma_{ST}(\lambda)$ being so much smaller than $\sigma_{ESA}(\lambda)$ does not provide any hope for possible laser action in BGO.

The $\sigma_{ESA}(\lambda)$ spectrum appears to be very broad, covering most of the visible and peaking around 16000 cm^{-1} (≈ 620 nm, ≈ 2 eV). This agrees with our previous observations [6], that in red region ESA in BGO is most efficient.

We thus have extracted an actual ESA spectrum for BGO, the measurement being very tricky because of ESA(I) specific dependence.

The magnitude ($\approx 10^{-19}$ cm^2) of the two cross sections σ_{ESA} and σ_{ST} makes it rather plausible that both correspond to spin forbidden transitions. On the other hand, we know that both ESA and luminescence transitions are governed by the kinetics of the luminescing state (temporal results of fig. 1). Since the ground state of the BiO_6 complex is assumed to be a singlet ^{1}A and the luminescing state a triplet [7,10], this would mean that the terminal state of the ESA transition is again a singlet. The ESA spectrum peaks around 2 eV, and it is likely that the state (zero-phonon line) is at somewhat lower energy. Taking this into account and with BGO electronic structure derived from molecular orbital model including spin–orbit and configuration interactions among all states, as shown in ref. [7], it is possible that ESA transitions occur from ^{T}E to ^{1}E state,

whereas stimulated emission – and luminescence transitions occur from ^{T}E to totally symmetric ground state ^{1}A.

We are thankful to M. Mayhew of Bicron Corp. for supplying the BGO crystals and to A.J. Wojtowicz for some spectroscopic evaluation of these samples. The support by the US Army Research Office under the Grant DAAL03-88-0103 is also gratefully acknowledged.

References

[1] L.J. Andrews, S.M. Hitelman, M. Kokta and D. Gabbe, J. Chem. Phys. 84 (1986) 5229.
[2] S.A. Payne, L.L. Chase and G.D. Wilke, Phys. Rev. B 37 (1988) 998.
[3] D.S. Hamilton, S.K. Gayen, G.J. Pogatshnik, R.D. Ghen and W.J. Miniscalco, Phys. Rev. B 39 (1989) 8807.
[4] T. Wegner and K. Peterman, Appl. Phys. B 49 (1989) 275.
[5] Cz. Koepke and A. Lempicki, Chem. Phys. Letters 172 (1990) 224.
[6] C.L. Melcher, Nature 313 (1985) 465.
[7] R. Moncorgé, B. Jacquier, G. Boulon, F. Gaume-Mahn and J. Janin, J. Luminescence 12/13 (1976) 467.
[8] D.E. McCumber, Phys. Rev. A 134 (1964) 299.
[9] A.J. Wojtowicz, W. Meng, A. Lempicki, G.H. Beall, D.W. Hall and T.C. Chin, IEEE J. Quantum Electron. QE-24 (1988) 1109.
[10] R. Moncorgé, B. Jacquier and G. Boulon, J. Luminescence 14 (1976) 337.

APPENDIX 3

gence, the amount of feedback will depend on the location of the $\lambda/4$ plate. We observed that the feedback is smaller when the $\lambda/4$ plate is located in front of the amplifier system (two Nd:YAG rods) than when it is behind the amplifier system. A matrix theory describing the birefringent effect is developed to explain the experimental result. The ratio of feedback intensities corresponding to the $\lambda/4$ plate's being behind versus being in front of the amplifiers depends on the ratio of the depolarization coefficient to the linear-polarized amplification coefficient.

ThY13 Excited-state absorption in solid-state molecular complexes

Cz. Koepke and A. Lempicki*
Boston University, Chemistry Deptartment, 590 Commonwealth Avenue, Boston, Massachusetts 02215

Molecular complexes in solids have never been treated as possible laser materials. Among them are known luminophors and scintillators of pronounced luminescence over the range of some 150 nm and thus being potential candidates for tunable laser media (acting in blue-green region). In the few cases studied so far distinct excited state absorption (ESA), usually overlapping the luminescence and spreading even further, was observed. We have investigated $CaMoO_4$, $CaWO_4$ (of nd^0 electronic configuration) and $Bi_4Ge_3O_{12}$ (BGO) (ns^2 configuration). Interesting properties are displayed by BGO, where ESA increases with probe-beam intensity, the phenomenon being a sort of excited-state photochromism (ESP), possibly involving some trap levels in its mechanism. BGO has the best (smallest) ratio of ESA to stimulated emission crossections (σ_{ESA}/σ_e) of about one order of magnitude (e.g., for 632.8nm $\sigma_{ESA} \sim 4\times10^{-19}\,cm^2$ $\sigma_e \sim 2\times10^{-20}\,cm^2$), which precludes a chance for lasing in this crystal. The two other crystals reveal rather "standard", broad ESA spectra of absorption crossections σ_{ESA} of the order of 10^{-19}, 10^{-18} cm^2 whereas emission cross sections are $\sim 10^{-21}$, 10^{-20} cm^2. The results, though precluding laser action in these materials, provide spectroscopic data, which, we believe, are new in the field of solid state optics.

ThY14 Photorefractive mode coupling between two unidirectional ring oscillators

Li-Xuo Dai, Yih-Shun Gou, Pochi Yeh, and Claire Gu**
National Chiao Tung University, Hsinchu, Taiwan, China

Photorefractive mode coupling between resonators provides a simple model for self-pumped phase conjugators,[1] in which instability may occur because of energy transfer among different oscillation modes inside the crystal. In this paper, we consider the coupling between two unidirectional ring resonators.[2] The first resonator is driven by an external laser beam by means of photorefractive two-wave mixing. The internal oscillating beam is then employed to drive the second ring resonator by the same mechanism. We find that with proper choice of resonator parameters, two type of oscillations may occur. In the first type the primary resonator, which is driven by thr external laser, oscillates, but the secondary resonator, which is driven by the primary resonator, does not oscillate. In the second type the primary and secondary resonators oscillate simultaneously, and the oscillation of one resonator affects that of the other. We also find that even though the two resonators can oscillate separately, they may not perform steady-state oscillation when they are coupled. In this case the coupled system is not stable, which may result in temporal instability similar to that which occurs in self-pumped phase conjugators. Our results include the conditions for each of the above operation modes, the intensities and frequencies for steady-state oscillations, and the change of oscillation in one resonator that is brought about by detuning the other one.

*Rockwell International Science Center, 1049 Camino Dos Rios, Thousand Oaks, California 91360.

References

1. M. D. Ewbank and P. Yeh, Proc. Soc. Photo-Opt. Instrum. Eng. 613, 59, (1986).
2. P. Yeh, J. Opt. Soc. Am. B 2, 1924, (1985).

ThY15 Effects of a pulsed Gaussian beam on photorefractive materials

Chibing Xu, John K. McIver, and David Statman
Department of Physics and Astronomy, University of New Mexico, Albuquerque, New Mexico 87131

The band-transport model is used to study the effects of a pulsed Gaussian laser beam on photorefractive materials. Attention is paid to the relaxation of the polarization of the materials. When the relaxation time of the polarization is much shorter than the pulse length, the results differ little from those obtained when the relaxation is omitted. The induced electrical field in the illuminated area reaches its steady-state value much faster than in the dark area because there are many more photocarriers in the illuminated area. Although electron density and ionized-donor density decrease rapidly because of recombination when the light is turned off, the total charge density, which determines the induced field, keeps growing as a result of a nonzero electrical current. After the initial growth, the field remains unchanged for a long time, i.e., there is long-term storage of the induced field. When the relaxation time is longer than the pulse length, then the longer the relaxation time, the faster the induced field grows when the light is on, but the slower it reaches steady state when the light is off. This occurs because the polarization slowly follows the change in the field.

ThY16 Modal properties of nonlinear parabolic graded-index optical guides

L. Gagnon and C. Paré
Centre d'optique, photonique et laser, Université Laval, Québec, Québec, G1K 7P4, Canada

We study the propagation modes in nonlinear planar and circular media that have a transverse parabolic index profile.[1] The first mode profiles, as well as their dispersion curves, are calculated numerically. In particular, one observes a splitting of some linear degenerate modes and cutoff of nonlinear modes because of self-focusing limits. A numerical scheme (beam propagation method) is also used to study near-modal propagation under the paraxial approximation. Those results are compared with an approximate analytical calculation based on the variational principle.[2] This approach is not limited to small nonlinearities; it describes quite well the amplitude-dependent quasiperiodic propagation observed numerically. Furthermore, it reproduces the modal dispersion curves in a simple way. These results can also be applied to the study of nonlinear radiation modes of the free three-dimensional paraxial wave equation.

References

1. J. T. Manassah, P. L. Baldeck, and R.R. Alfano, Opt. Lett. 13, 589 (1988).
2. D. Anderson, Phys. Rev. A 27, 3135 (1983).

ThY17 Backseeded stimulated photorefractive scattering phase conjugation in SBS niobate fibers

Lambertus Hesselink, Ruth Ann Mullen, and Dave Pepper
Stanford University, Room 359 B Durand, Stanford, California 94305-4035

Back-seeded stimulated photorefractive scattering phase conjugation is demonstrated in SBN fibers for the first time. A 7 mm long by 0.8 mm diameter 0.01% Ce:SBN fiber oriented with its c-axis along the length of the fiber is used for the measurement. The seed is provided by placing a retroreflecting screen in the path of the beam that is transmitted by the fiber. Reflectivities of 28% and 49%, accounting for reflection losses, are achieved by using light with wavelengths of 515 nm and 638 nm, respectively. Previously seeded stimulated phase conjugation (SSPC) has been demonstrated in bulk photorefractive $BaTiO_3$,[1,2] by using retroreflector arrays. Good fidelity of the back-reflected signal is achieved with reflectivities approaching 60%. The geometry for optimum results requires that an index-matching fluid surround the crystal; pixel-based image processing appears to be difficult to achieve in bulk crystals. In the new approach a synthetic material is constructed by bundling SBN fibers. This allows parallel, pixel-based image processing to be accomplished[3] with low-power (milliwatt) laser beams. By employing a polarization

Journal of Luminescence 47 (1991) 189–191
North-Holland

Excited state absorption in $CaMoO_4$

Cz. Koepke [1] and A. Lempicki

Boston University, Chemistry Dept., 590 Commonwealth Ave., Boston, MA 02215, USA

Received 14 May 1990
Revised 5 July 1990
Accepted 6 July 1990

We report the first measurement of excited state absorption (ESA) in a calcium molybdate ($CaMoO_4$) crystal, and compare the ESA spectrum with a stimulated emission spectrum calculated in terms of the McCumber theory of phonon terminated lasers. It appears that the magnitude of ESA would preclude laser action in this crystal. The temporal ESA dependence has been measured and discussed in terms of the most likely assignment of energy levels involved in ESA.

Calcium molybdate ($CaMoO_4$) is a well known luminescent material and its spectral properties have been reported in numerous papers [1–6]. The MoO_4^{2-} complex of tetrahedral coordination and of $4d^0$ electronic configuration has a characteristically strong absorption in the ultraviolet range and emission peaking in the green. Both absorption and emission involve charge transfer from ligands (O) to transition metal (Mo) (absorption) or vice versa (emission). This is a simplified picture and more exact results for tetra-oxo ions are reported in ref. [7]. The absorption of $CaMoO_4$, at room temperature, starts at 340 nm and for shorter wavelengths can easily reach thousands of cm^{-1}. The emission is very broad (400–750 nm), peaking around 520 nm at room temperature, and rather structureless. Both, absorption and emission are described in various publications and the electronic structure of this material (especially dealing with the ground, and lower excited states) is rather well known [1–3]. The material can be regarded as a prototype candidate for tunable solid state lasers based on d^0 configuration [8].

In the present paper we report on excited state absorption (ESA) in $CaMoO_4$, measured with two entirely different methods and compare the ESA cross section with the stimulated emission cross section, calculated via the McCumber theory [9] based on a measured luminescence spectrum. We shall refer to ESA as a phenomenon as well as quantitatively as the absorption, expressed in percents.

The $CaMoO_4$ single crystal used in our measurements, was carefully polished, especially the entrance and exit faces of the probe beam. The sample length was 1.6 cm. All measurements were carried out at room temperature. The excite-and-probe beam experiments used virtually the same kind of arrangement as described in detail in ref. [10]. The only essential difference was the replacement of the exciting excimer laser by a nitrogen laser. Two different setups were used in order to eliminate any doubts about observed effects. The first, involved a krypton laser serving as the source of the chopped probe beam, and a fast silicon photodiode connected to a two channel boxcar as a detection system. The other setup used a polychromatic probe beam derived from a pulsed xenon lamp, and a synchronously working optical multichannel analyzer (OMA) system as detection. We chose the N_2 laser for excitation because the 337.1 nm line provided a sufficient excitation depth. At this wavelength the absorption length

[1] On leave from Institute of Physics, N. Copernicus University, Toruń, Poland.

0022-2313/91/$03.50

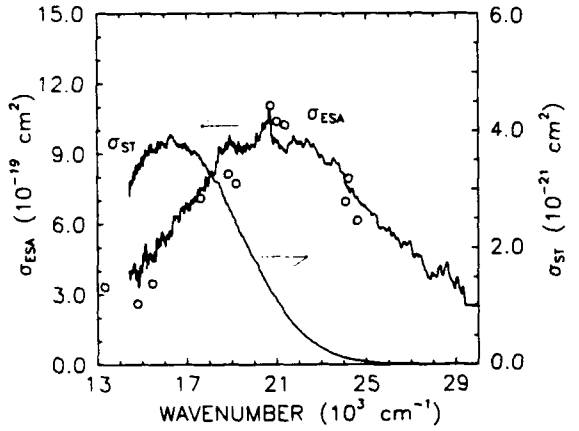

Fig. 1. ESA cross section spectrum measured by boxcar-Kr laser setup (circles) and OMA-Xe pulsed lamp setup (solid line), compared with stimulated emission cross section, obtained from measured luminescence spectrum via McCumber theory.

was ~ 1.3 mm, the 337.1 nm line falling into the lower part of the $CaMoO_4$ absorption edge. This allowed us to carry out successful measurements with the OMAXe lamp setup, where the width of the Xe lamp probe beam was not less than ~ 500 μm.

The ESA spectrum plotted in terms of the cross section σ_{ESA} is shown in fig. 1. Two sets of measurements are shown in the figure. The continuous curve was obtained using the Xe lamp-OMA setup whereas the circles correspond to the krypton laser-boxcar setup. The wavelengths of the circles correspond to the various lines of the krypton laser, whose power was maintained constant in order to eliminate a possible dependence of ESA on probe beam intensity [10–12]. In both cases the σ_{ESA} cross section was calculated from the excited state transmission using an excited state population $N^* = 3.9 \times 10^{17}$ cm^{-3} obtained from the ground state absorption and the intensity of the N_2 laser. The agreement between the two types of measurement is remarkably good. In the same figure we plot the stimulated emission cross section σ_{ST} obtained from the transformation of the luminescence spectrum by means of the McCumber theory. This procedure is described in detail in refs. [10,13]. It is remarkable that σ_{ESA} is about two orders of magnitude higher than σ_{ST}, thus precluding any possibility of laser action in this material.

The temporal dependence of ESA was measured with the boxcar. As probe beam we used the 514.5 nm line of an argon laser which matches the maximum of the luminescence.

The luminescence decay was measured with a photomultiplier tube coupled to a monochromator and the signal was recorded by a fast digitizer. For this measurement we used the 308 nm line of an excimer laser, the luminescence signal being detected at 520 nm. The results of temporal measurements are plotted in fig. 2, where the solid line denotes the luminescence decay curve and circles represent the ESA decay. The identity of both decays proves that both ESA and luminescence transitions occur from the same state.

It is believed [4–6] that the luminescence occurs from molecular triplet states $^3T_2 \simeq {}^3T_1$ resulting, like two other close states $^1T_1$ and $^1T_2$, from the $(t_1)^5(2e)^1$ excited configuration (this picture is a simplification, suitable for isolated MoO_4^{2-} molecular complexes [7]). The obtained ESA spectrum, reaching its maximum around ~ 2.6 eV and having the zero-phonon line probably somewhere around ~ 1.7–1.8 eV would indicate that the terminal state for ESA transitions is $^1T_2$ originating in the $(t_1)^5(4t_2)^1$ excited configuration [1]. In such a case we would deal with triplet–singlet transitions, similar to the case of luminescence:

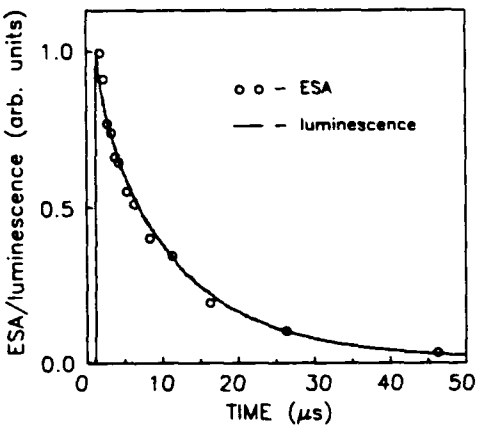

Fig. 2. Normalized temporal decay of ESA (circles) measured with argon laser 514.5 nm line and luminescence (solid line) measured at 520 nm.

$^3T_1 \rightarrow {}^1A_1$. On the other hand, the relatively large σ_{ESA}/σ_{ST} ratio (~ 200) would suggest that the terminal ESA state contains some triplet admixture. The precise assignment of ESA transitions to concrete levels would require more precise knowledge of higher excited $CaMoO_4$ states.

Concluding, we have measured a distinct ESA effect for $CaMoO_4$, whose spectrum and measured ESA(t) dependence suggest transitions between $^3T_1$ and $^1T_2$ states (originating from different excited electronic configurations). The stimulated emission effect is very weak and is practically negligible in comparison with ESA.

We thank Dr. L. Brixner of Du Pont for supplying the $CaMoO_4$ samples and acknowledge the support by the US Army Research Office under the Grant DAAL03-88-0103.

References

[1] R.Grasser, E. Pitt, A. Scharmann and G. Zimmerer, Phys. Stat. Sol. (b) 69 (1975) 359.

[2] C.E. Tyner and H.G. Drickamer, J. Chem. Phys. 67 (1977) 4103.

[3] A.L. Ivanovskii, V.P. Zhukov, V.K. Slepukhin, V.A. Gubanow and G.P. Shveikin, Zh. Struktur. Khimii 21 (1980) 30.

[4] G. Blasse, Structure Bonding 42 (1980) 1.

[5] W. Barendswaard and J.H. van der Waals, Mol. Phys. 59 (1986) 337.

[6] J.H. van der Waals, Acta Phys. Polon. A 71 (1987) 809.

[7] T. Ziegler, A. Rauk and E.J. Baerends, Chem. Phys. 16 (1976) 209.

[8] W. Krupke and M.J. Weber, Prospects for New Dielectric Solid State Lasers, Topical Meeting on Tunable Solid State Lasers, 26–28 October 1987, Williamsburg, Virginia, Technical Digest, Vol. 20.

[9] D.E. McCumber, Phys. Rev. 134 (1964) A299.

[10] Cz. Koepke, A.J. Wojtowicz and A. Lempicki, to be published.

[11] Cz. Koepke and A. Lempicki, Chem. Phys. Lett., in press.

[12] Cz. Koepke and A. Lempicki, Chem. Phys. Lett., in press.

[13] A.J. Wojtowicz, W. Meng, A. Lempicki, G.H. Beall, D.W. Hall and T.C. Chin, IEEE J. Quantum Electron. QE-24 (1988) 1109.

Journal of Luminescence 47 (1991) 227–238
North-Holland

Electronic photochromism: case study of bismuth germanate

Cz. Koepke [1] and A. Lempicki

Boston University, Chemistry Dept., 590 Commonwealth Ave., Boston, MA 02215, USA

Received 31 July 1990
Accepted 7 September 1990

In this paper we examine the various mechanisms which can lead to photochromism, based on electronic rather than chemical effects. We make a distinction between passive and active photochromic materials. We show that in the case of solids, the simple models, adequate for organic molecules, no longer apply. Photochromism encountered in bismuth germanate ($Bi_4Ge_3O_{12}$) requires the postulation of inhomogeneously broadened absorption due to trap states. It is suggested that the results indicate the emergence of a new technique of excited-state site selection spectroscopy.

1. Introduction

In recent times there has been a renewal of interest in materials which exhibit absorption increasing with the intensity of light. Phenomena of this kind are of importance in optical bistability [1–3] and are the subject of numerous papers dealing with "reverse" or "negative" saturable absorption [4–7]. Traditionally these effects have been called photochromism, the most dramatic manifestation being of course the photographic process itself. Photochromism has been associated with chemical changes including isomerization, etc. Contrasted with this narrow view of photochromism have been fast processes which are purely electronic. Since they were first observed in connection with saturable absorption or bleaching under influence of light, they have been designated as reverse saturable absorption (RSA) or negative saturable absorption, all rather unfortunate names in our opinion [7,4]. Another term which has found some acceptance is optical power limiting materials [7] which, like photochromism, refers more to the function than the underlying phenomenon. We too have been guilty of introducing yet another term namely excited state photochromism (ESP) [8], which meant to convey the notion of a fast electronic process in which the excited state plays an important role. ESP is closely related to RSA, but as we shall see, is far from identical. A simplification of the nomenclature would occur if one were simply to distinguish between chemical photochromism and electronic photochromism, and this is what we propose at least for the purpose of this paper.

The main area of application of electronic photochromism is of course sensor, including eye protection [9] and pulse shaping in laser technology [10]. Fairly comprehensive references to the various schemes are given in the paper of Tutt and McCahon [7].

There are various phenomena which can lead to electronic photochromism, all of them leading to a nonlinear response of the material. However, the source of the nonlinearity may reside in field dependent polarizabilities of the material or more simply in the kinetics governed by populations and rate constants of a system of levels. In this paper we explore only this second possibility for an inorganic solid namely bismuth germanate ($Bi_4Ge_3O_{12}$).

[1] On leave from Institute of Physics, N. Copernicus University, Toruń, Poland.

0022-2313/91/$03.50

2. Basic principles

The simplest form of electronic photochromism is provided by the singlet–triplet structure of the energy levels of an organic molecule illustrated in fig. 1 and discussed fully in refs. [4–7]. The principal conditions for the occurrence of effective photochromism is that the separation of the singlet and triplet levels be essentially the same, and that the cross-section for the triplet–triplet absorption be sufficiently larger than the singlet–singlet cross-section. This is necessary to compensate for the difference in population of levels S_0 and T_0. If these conditions are met then the system can indeed provide a purely *passive* photochromic response since the same radiation is involved in the excitation $S_0 \rightarrow S_1$ as is being absorbed by the $T_0 \rightarrow T_1$ process.

In photochemical parlance the ground state absorption must overlap the triplet–triplet absorption, the latter having a substantially larger extinction coefficient. Chemical research points to organo-metallics as the source compounds. Note, however, that in the great majority of systems, the triplet–triplet absorption spectra are at *lower* energy than the ground state (singlet–singlet) absorption. If this is the case then the material can still be photochromic but is no longer passive (hence it is active), since it requires "pumping" to the first excited singlet S_1 by more energetic radiation. Thus, the search for passive materials is a search for the exception rather than the rule.

Once we leave the world of organic molecules and enter the world of inorganic solids, things become far more complicated. In the extreme case of pure semiconductors the singlet–singlet absorptions are replaced by inter-band transitions and triplet–triplet absorptions by intra-band, or free electron absorptions. The general behavior of the system can be very dependent on how close to the absorption edge is the wavelength of the incident light. In the vicinity of the absorption edge the light-induced absorption can be caused by such mechanisms as excitonic effects [11], formation of electron–hole plasma [12] or even simple thermal red shift of absorption edge [13]. In the case of doped solids the situation is different since the electronic identity of the defect and its coupling to the lattice play an essential role. The same concerns the molecular complexes in solids and we see here very little in the way of guidance leading to new passive photochromic devices based on kinetic nonlinearities.

3. Case of bismuth germanate

Motivated by the desire to develop tunable solid state lasers in the blue-green part of the spectrum and pumped in the UV by an excimer laser, we have been looking at a number of phosphor-type compounds. More specifically, we concentrated on excited state absorption (ESA) under excimer laser pumping [14,15]. One of the materials of interest was bismuth germanate (BGO – $Bi_4Ge_3O_{12}$), well known for its high luminescence yield. The ESA characteristics of BGO have been reported previously (we refer to ESA both as a phenomenon as well as a magnitude of excited state absorption in the range $0 \leq \text{ESA} \leq 1$). Aside from

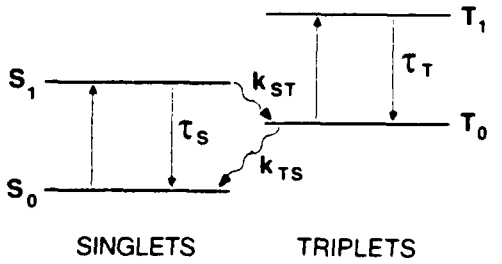

Fig. 1. The simple singlet–triplet scheme used to describe the RSA effect [7].

the extremely broad spectrum of ESA, covering most of the visible, we have identified its dependence on probe beam intensity I, which we called excited state photochromism (ESP). In the context of this paper ESP is an example of electronic photochromism, of the active kind since it requires the presence of a UV pumping beam. As we shall see, the simple models describing passive photochromism in organic molecules are no longer applicable.

4. Experimental

The BGO samples, obtained from Bicron Corp., were clearly transparent cubes of typically 0.8 cm long edges. They have been additionally polished on the excited side to prevent possible dielectric breakdown and consequent damage of the surface [16]. For the same reason we used an unfocused excimer laser beam as excitation, covering the whole face area.

Our ESA measurements have been described in detail in ref. [14]. They were carried out using excite-and-probe beam technique, utilizing an excimer laser beam (308 nm) as excitation (in transverse geometry) and He–Ne and argon ion lasers or a pulsed Xe lamp light as a probe beam. The setup which used the monochromatic probe beams had a fast photodiode and two-channel boxcar system in the detection branch. The other setup, with a polychromatic probe beam (Xe pulsed lamp) used a reticon detector and a synchronously working optical multichannel analyzer (OMA-III) system as an output device. We compared the results from both setups for their consistency. The laser-boxcar setup served also to measure the temporal behavior of ESA.

An additional arrangement was used to measure the temporal behavior of ESA during a single shot. It was arranged in the same optical geometry as the other setups, but with a fast transient recorder in the detecting branch. As a source of probe beam we used a He–Ne laser. Before recording by the digitizer, the electric noise (originating from the excimer) was subtracted from the measured signal and the resulting signal was preamplified. This procedure did not eliminate noise entirely but improved the signal quality.

The results of our measurements are expressed in terms of directly measurable excited state transmission (EST) defined as follows

$$\mathrm{EST} = I_p/I_u, \tag{1}$$

where I_p and I_u are the probe beam intensities measured after passing the pumped and unpumped medium. In other words,

$$\mathrm{EST} = (I_u \pm \Delta I)/I_u, \tag{2}$$

where ΔI is the change of transmission caused by pumping (positive for gain, negative for excited state absorption). EST can also be expressed as

$$\mathrm{EST} = \exp\{-(\sigma_{\mathrm{ESA}} - \sigma_e - \sigma_0)n_2 L\}, \tag{3}$$

where σ_{ESA} is the cross-section for the ESA, σ_0 denotes cross-section for ground state absorption (GSA), σ_e is the stimulated emission cross-section, n_2 denotes the population of the first excited state, and L is the length of the medium. The difference $[\sigma_{\mathrm{ESA}}(\lambda) - \sigma_0(\lambda)]n_2$ occurring in (3) is sometimes called an excited state difference spectrum [17,18]. It is seen in (3) that the ground state absorption can influence the EST but in clearly transparent BGO crystals σ_0 is negligible in the visible (less than 5×10^{-24} cm^2, at least four orders of magnitude smaller than both other σs).

Figure 2 illustrates the excited state transmission spectrum of crystals of BGO and GSGG : Cr^{3+} – the well known laser medium [19] – for comparison. Both spectra were measured by the OMA system. The EST spectrum of BGO, though very flat and extending over the whole measured spectral range, has very distinct features of the probe beam spectrum, provided here by the highly structured Xe pulsed lamp. One

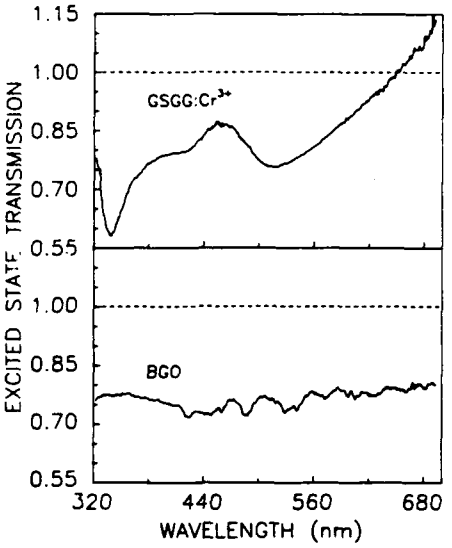

Fig. 2. The comparison of excited state transmission spectra of BGO and GSGG: Cr^{3+} crystals taken with the OMA system. Dashed lines denote a boundary between ESA and net gain (see eq. (3)).

can see a pronounced modulation of the spectrum which causes EST of BGO to look like a sort of distorted reflection of the Xe lamp spectrum. The EST spectrum of GSGG measured exactly in the same conditions does not reveal these features at all, and instead displays previously known EST features [17], including presence of gain (EST ≥ 1) in the red region. The observation of the strange behavior of ESA in BGO can be easily explained by its dependence on intensity I. Indeed, this was confirmed by direct measurements, results of which are shown in fig. 3. The dependence of EST on I was measured for three excitation levels (1–3) and using as probe beams the output of a He–Ne (1, 2) or Ar laser (476.5 nm) (3).

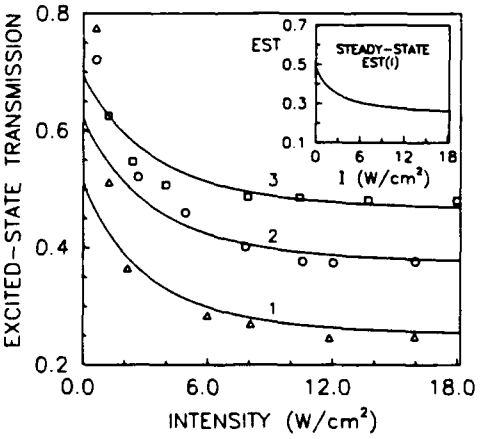

Fig. 3. The dependence of EST on probe beam intensity I. The dependences 1 (triangles) and 2 (circles) were measured at $\lambda = 632.8$ nm for excimer laser output: 140 and 90 mJ/pulse, respectively, 3 (squares) measured for $\lambda = 476.5$ nm (excimer: 60 mJ/pulse). Solid lines represent the theoretical fit by solutions (7) of the set (6) with the following parameters: $N_2 = 4.5\times10^{18}$ cm^{-3} (1), $N_2 = 3.2\times10^{18}$ cm^{-3} (2), $N_2 = 1.9\times10^{18}$ cm^{-3} (3), and $N_4 = 0$, $a_{21} = 4\times10^{6}$ s^{-1}, $a_{41} = 5\times10^{6}$ s^{-1}, $k_{34} = 10^{8}$ s^{-1}, $B_{21} = 1.75\times10^{23}$ cm^3/(Ws^3), $B_{23} = 10^{25}$ cm^3/(Ws^3), $g_{23} = 2\times10^{-15}$ Hz^{-1} $B_{45} = 6\times10^{27}$ cm^3/(Ws^3), and $g_{45} = 3.3\times10^{-12}$ Hz^{-1}. All curves were calculated at a fixed point of time: $t = 2\times10^{-7}$ s. Inset: stationary EST(I) dependence, calculated for the same parameters but with $W = 4.5\times10^{2}$ s^{-1}.

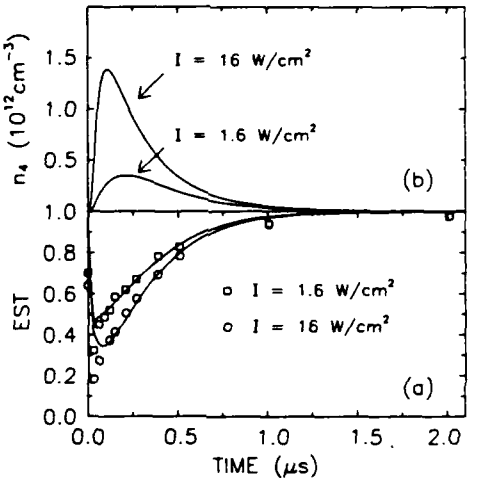

Fig. 4(a). Temporal EST evolution for two different intensities of the probe beam: $I = 1.6$ (squares) and 16 W/cm^2 (circles). Solid lines represent theoretical fit by solutions of (6) via the Runge–Kutta routine, with the same parameters as above and with $W = 4.4 \times 10^3$ s^{-1} ($W(t)$ square function of 30 ns duration). (b). Theoretical temporal evolutions of trap population $n_4(t)$ corresponding to situation (a).

Solid lines are theoretical fits provided by the model described further on. A distinct drop in EST (increase of ESA) is seen here, especially for small value of probe beam intensity, followed by a sort of saturation for higher values of I. Figure 4(a) presents the temporal behavior of EST measured by the laser-boxcar system for two probe beam intensities, both fitted by theoretical curves. Practically the same decay of ESA and luminescence [20] proves that both are governed by the kinetics of the luminescing state.

The results of single shot experiments, essential for further considerations are presented in fig. 5. The single-shot results are compared with corresponding measurements carried out at a 14 Hz repetition rate, averaged over 100 pulses. The time dependence of EST was measured for two probe beam intensities, a

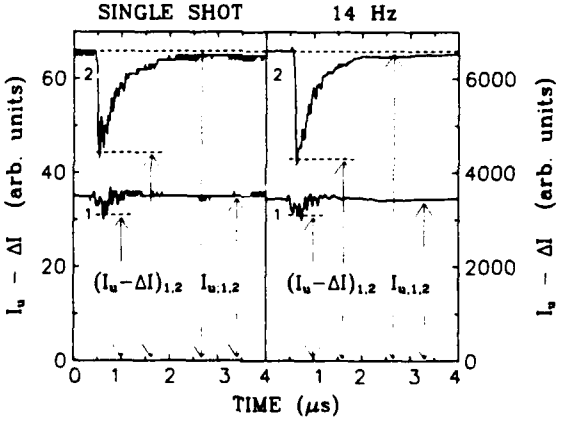

Fig. 5. The result of a single-shot experiment in comparison with 100 shots at a repetition rate of 14 pps. The negative pulses are "dark holes" in the constant background of probe beam light. EST was measured here for two probe beam intensities: I_1 (lower) and I_2 (higher). $I_{u,1,2}$ denote the intensities after passing the sample. The arrows indicate the intensity values used in EST formula (2) and serving to calculate the experimental EST (t_{min}). For single shot: EST(I_2) = 0.67, EST(I_1) = 0.89. For 14 pps respective values are: EST(I_2) = 0.65 and EST(I_1) = 0.89.

Fig. 6. Simple, three-level model (a) and "free carrier absorption" model (b), both providing qualitatively reasonable ESP behavior but with unphysically large I ($\sim$ MW/cm^2).

lower (1) and a higher (2) intensity. The temporal behavior of EST is measured here by means of the ratio $(I_u - \Delta I)/I_u$. We observe a practical identity of the results for single shot and 14 Hz. On the other hand, one can see a distinct dependence of EST on the probe beam intensity, which occurs in both cases, giving EST $\simeq 0.9$ for the lower I and EST $\simeq 0.7$ for the higher one. (The ΔI signals for lower I are rather noisy, nevertheless their depths were very repeatable). The fact that the dependence of ESA on I occurs even in single shot experiments is of great importance for the choice of our model.

5. Theoretical

Let us begin by making the following remarks:

(a) It is immediately obvious that for active photochromic materials (pump beam and probe beam at different frequencies), the scheme based on fig. 1 cannot lead to any nonlinearity on probe beam intensity. For a constant pump the transmission of the probe will be strictly determined by triplet–triplet absorption cross-section and the triplet population. Hence although the energy levels of BGO have sometimes been classified as singlets and triplets, we must depart from the simple picture of fig. 1.

(b) Because of the pulsed nature of the excimer laser, we must consider nonstationary solutions of the rate equations. Some models allow for the existence of stationary ESP, but these cannot be experimentally tested with our present setup.

(c) It appeared that the transient behavior of ESA and ESP could be formally reproduced by the simplest of all models, involving only three states, as illustrated in fig. 6(a). All that is necessary is the postulation of a fast non radiative path between levels 3 and 2. This model can be described by the following set of rate equations:

$$\begin{aligned} \dot{n}_1 &= -Wn_1 + (a_{21} + b_{21}I)n_2, \\ \dot{n}_2 &= Wn_1 - (a_{21} + b_{21}I + b_{23}I)n_2 + kn_3, \\ \dot{n}_3 &= b_{23}In_2 - kn_3, \end{aligned} \tag{4}$$

where n_i are populations of ith states, W denotes pumping rate, a_{21} is the spontaneous transition rate, $b_{ij}I$ are stimulated transition rates and k is the rate of radiationless transitions. One can see, that if I increases, it populates level 3 and in turn, for sufficiently high k, it may slow down the decay of the n_2 population. Hence, if n_2 decays more slowly for higher I than for lower, one can expect that at a given point of time ESA(lower I) < ESA(higher I) because: ESA $\sim 1 - e^{-\sigma_{23}n_2 L}$ and n_2(lower I) < n_2(higher I). However, to make this mechanism efficient, the probe beam should cause a severe depletion of the n_2

population (a situation which is sometimes identified with saturation). Indeed, our detailed calculations showed that probe beam intensities of the order of megawatts/cm^2 are needed to cause such a depletion and, in consequence, an ESP effect. The basic reason for this is the very large homogeneous bandwidth of the ESA spectrum ($\gtrsim$ 300 nm). Since the cross-section for absorption is inversely proportional to this band width, its small value would have to be compensated by an extraordinary large probe beam flux.

Moreover, in this case ESP occurs only as a transient, being a sort of a lack of equilibrium between the excitation and the changes of populations. Thus, this model, though providing qualitatively good solutions, failed from a quantitative point of view.

A similar difficulty arises in a model illustrated in fig. 6(b). It assumes the existence of some efficient free-electron absorption if the higher excited state is a part of a "conduction band" [21]. Thus, apart from conventional ESA (transitions $|2\rangle \rightarrow |3\rangle$), a "free-electron" ESA would occur, being strictly dependent on probe beam intensity. This model produced good fits to experimental data, but also for unrealistic probe beam intensities.

The failure of the simple models to account *quantitatively* for the observed photochromism suggest that we have to introduce another system of levels connected to the first by some nonradiative "intersystem crossing". The essential departure from the simple case of an organic molecule shown in fig. 1, is that the "intersystem crossing" takes place from a second excited state, reachable only in the presence of the probe beam I. This is shown in fig. 7(a). The model involves five levels with populations $n_1, \ldots, n_5$. According to known models of BGO [22,23] the state $|1\rangle$ is a totally symmetrical ^{1}A ground state, the luminescing $|2\rangle$ state should be a triplet ^{T}E whereas $|3\rangle$ is supposedly a singlet state ^{1}E [23]. At this stage little can be said, with any degree of certainty, about the origin of levels 4 and 5. From the preceding arguments it is clear that the $|4\rangle \rightarrow |5\rangle$ absorption process cannot be homogeneously broadened, because we would then run into the same difficulty of a small cross-section. We have to postulate therefore that the right hand side system of levels in fig. 7(a) has an origin other than the luminescing Bi complex. It is likely that they are provided by a population of traps. The "intersystem crossing" would then be a nonradiative energy or charge transfer process occurring from the Bi complex to the traps. The existence of trap levels in crystals composed of molecular complexes is a rather common fact [24–26] and they are well known to exist also in BGO. The literature describes several kinds of traps in BGO. Moncorgé et al. [22,23] mentioned some metastable levels lying below the luminescing ^{T}E state and higher excited state ^{1}E. Both of them, however, having low temperatures of thermalization [22] should not be visible at room temperature. Other kinds of traps have been investigated by Melcher [27,28]. Melcher identified four trapping levels lying below the luminescing state and visible in a thermoluminescent experiment. Their depths correspond to 65, 115, 150 and 175°C. For the most pronounced, (115°C), Melcher proved a direct correlation between thermoluminescence intensity (proportional to the concentration of traps) and radiation damage, caused by UV, γ-radiation or even sunlight. What is especially interesting is that each of the traps seems to have different

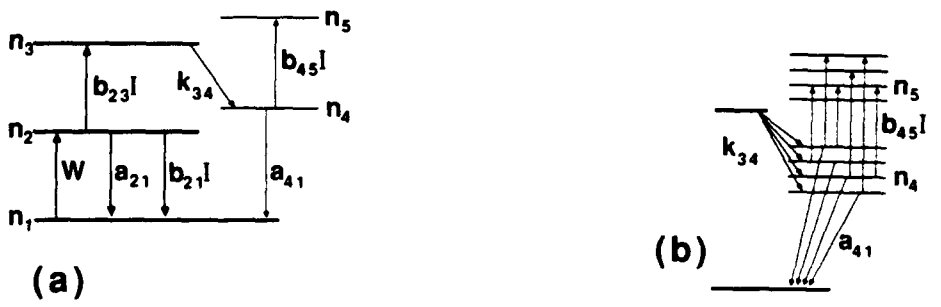

Fig. 7. Model of BGO, capable to reproduce the ESP effect. (a) model with one, specific trap level, taking part in the kinetics under the influence of a monochromatic probe beam. (b) detailed view of the right-hand side of (a).

properties. The 65 °C peak occurs only immediately after irradiation, decaying rapidly at room temperature, whereas the 115 °C peak has a lifetime of the order of hours. Moreover, their appearance and depth seems to depend on the wavelength of excitation [27].

In our experimental conditions we deal with very intense UV excitation of peak intensities of the order of megawatts/cm^2. Since even relatively weak UV exposure (e.g. sunlight) is capable of producing internal damage in BGO [27], our excitation must produce a great manifold of point defects distributed over various accidental sites, and revealing various slightly different energy levels. This is schematically represented in fig. 7(b) by the "ladder" of trap levels and their excited states.

The totality of traps may thus form a broad, inhomogeneous spectral distribution. This inhomogeneous broadening of the trap absorption spectrum is fundamental to the model. We postulate that these trap levels are fed by a kind of relatively efficient energy transfer from the higher excited state of the Bi complex. Thus, they are populated only via ESA transitions $|2\rangle \rightarrow |3\rangle$ and contribute no ground state absorption in the visible.

The probe beam is thus absorbed in two ways. The first "conventional" ESA occurs from $|2\rangle$ to $|3\rangle$ transitions and the spectrum is homogeneously broadened being a characteristic of the Bi complex. Another ESA appears as a result of the first one, (populated n_4), and occurs from the "ground" to the excited state of a given trap, selected by the probe beam frequency. The resulting EST is thus a "sum" of EST_{23} and EST_{45} by means of the following formula:

$$EST_{total} = EST_{23} \cdot EST_{45} = e^{-(\sigma_{23}-\sigma_{21})n_2 L}\, e^{-\sigma_{45} n_4 L}. \tag{5}$$

The resulting $EST_{total}(\lambda)$ spectrum is, of course, composed in the same manner.

Our model can be described by the following set of rate equations:

$$\begin{aligned}
\dot{n}_1 &= -Wn_1 + (a_{21} + b_{21}I)n_2 + a_{41}n_4,\\
\dot{n}_2 &= Wn_1 - Gn_2,\\
\dot{n}_3 &= b_{23}In_2 - k_{34}n_3,\\
\dot{n}_4 &= k_{34}n_3 - (a_{41} + b_{45}I)n_4,
\end{aligned} \tag{6}$$

where $G = a_{21} + b_{21}I + b_{23}I$, n_i is the population of the $|i\rangle$ state, W is the pumping rate. a_{ij} are spontaneous transition rates, $b_{ij}I$ are stimulated transition rates ($b_{ij} = B_{ij}\eta g(\nu)/c$, B_{ij} – the Einstein coefficient of the $|i\rangle \rightarrow |j\rangle$ transition, $g(\nu)$ is its line shape and η is the refractive index of the medium), I is the probe beam intensity affecting the medium, and k_{34} is a transfer rate between $|3\rangle$ and $|4\rangle$. For simplicity, the population n_5 is not taken into account since it plays no role in the final ESA expression (5). For the same reason, possible transitions from upper excited levels to lower ones are neglected to reduce the number of adjustable parameters.

The set of kinetic equations (6) can be solved by a Runge–Kutta fourth-order routine as well as analytically with the omission of the pumping process, using instead boundary conditions providing an initial population N_2 of the luminescing $|2\rangle$ state. We have done both and they serve equally well to fit the experimental data.

The analytical solutions of (6) with W omitted, and with the following boundary conditions: $t = 0 \Rightarrow n_1(0) = N_0 - N_2 - N_4$, $n_2(0) = N_2$, $n_3(0) = 0$ and $n_4(0) = N_4$ can be expressed as follows:

$$\begin{aligned}
n_2(t) &= N_2\, e^{-Gt},\\
n_3(t) &= \frac{b_{23}I}{k_{34} - G} N_2 \{e^{-Gt} - e^{-k_{34}t}\},\\
n_4(t) &= C_1\, e^{-k_{34}t} + C_2\, e^{-(a_{41}+b_{45}I)t} + \frac{k_{34}b_{23}I}{E - DG + G^2} N_2\, e^{-Gt},
\end{aligned} \tag{7}$$

and

$$n_1(t) = N_0 - \left[1 - \frac{a_{41}}{a_{41} + b_{45}I}\right]\left[N_4 + N_2\frac{b_{23}I}{G}\right] - \frac{F}{G}N_2\,e^{-Gt} - \frac{a_{41}}{k_{34}}C_1\,e^{-k_{34}t} - \frac{a_{41}}{a_{41} + b_{45}I}C_2\,e^{-(a_{41}+b_{45}I)t},$$

where $E = k_{34}(a_{41} + b_{45}I)$, $D = a_{41} + k_{34} + b_{45}I$,

$$C_1 = \frac{k_{34}b_{23}I(G - b_{45}I - a_{41})}{(a_{41} + b_{45}I - k_{34})(E - DG + G^2)}N_2,$$

$$C_2 = N_4 + \frac{k_{34}b_{23}I(k_{34} - G)}{(a_{41} + b_{45}I - k_{34})(E - DG + G^2)}N_2,$$

$$F = a_{21} + b_{21}I + \frac{a_{41}k_{34}b_{23}I}{E - DG + G^2},$$

and N_0 is the total number of atoms per cm^3. We should emphasize here that these solutions yield results identical with those solved numerically. The only difference is the lack of a 30 ns period of pumping time.

The results obtained from Runge–Kutta integration served to fit the measured temporal behavior of EST (fig. 4(a)) and to plot the trap population as a function of time: $n_4(t)$ (fig. 4(b)). To fit the EST(I) dependence (fig. 3) we used the analytical solutions (7) and EST formula (5). The parameters used to fit the experimental data are specified in the figure captions.

The cross-section value σ_{45}, being a critical point of our model (eq. (5)), is determined by the product of the Einstein coefficient and the line shape of the transition between the single trap and its excited state:

$$\sigma_{45}(\nu) = \frac{\eta h\nu}{c}B_{45}g_{45}(\nu). \tag{8}$$

Our fitting suggests that this product should be: $B_{45}g_{45}(\nu) \simeq 2 \times 10^{16}$ cm^3/(Ws^2) which gives: $\sigma_{45} \simeq 4 \times 10^{-13}$ cm^2. This is rather typical value for a homogeneous component of an inhomogeneously broadened spectrum [29]. Because our kinetics depends only on the product $B_{45}g_{45}(\nu)$, it provides freedom of balance between B_{45} and $g_{45}(\nu)$. Hence, assuming a "typical" spectral width of a point defect at room temperature $\simeq 10$ cm^{-1} [30], it would yield: $B_{45} \sim 6 \times 10^{27}$ cm^3/(Ws^3). Two orders of magnitude difference between B_{23} ($= 10^{25}$ cm^3/(Ws^3)) and B_{45} make sense if transitions $|2\rangle \rightarrow |3\rangle$ occurs with change of molecular spin, which is apparently the case [20], and $|4\rangle \rightarrow |5\rangle$ is spin allowed.

Stationary solutions of the set of rate equations (6) are:

$$\begin{aligned}
n_2 &= \frac{WN_0}{Wb_{23}IH/k_{34} + G},\\
n_3 &= \frac{WN_0b_{23}I}{Wb_{23}IH + Gk_{34}},\\
n_4 &= \frac{WN_0b_{23}Ik_{34}}{(a_{41} + b_{45}I)(Wb_{23}IH + Gk_{34})},\\
n_1 &= \frac{k_{34}N_0[(a_{21} + b_{21}I)(a_{41} + b_{45}I) + a_{41}b_{23}I]}{(a_{41} + b_{45}I)(Wb_{23}IH + Gk_{34})},
\end{aligned} \tag{9}$$

where

$$H = 1 + \frac{k_{34}}{b_{23}I} + \frac{k_{34}}{a_{41} + b_{45}I}.$$

The steady-state EST(I) dependence is plotted in the inset of fig. 3. It is striking that it has practically the same shape as nonstationary EST(I) solutions (measured and calculated at a given, fixed point of time). It

shows that the ESP effect in BGO is not of transient character (like in the model in fig. 6(a)) and should be also observable in a steady-state regime (with cw source of UV as pump).

6. Discussion

One of the crucial points of the proposed model is the lifetime of the trap state. As an alternative to a collection of traps contributing to the inhomogeneous width of the $|4\rangle \rightarrow |5\rangle$ ESA spectrum one could consider a single trap level, having a long lifetime ($a_{41} \sim 0$). This single trap would accumulate a large population over thousands (14 pps) of excimer laser pulses used in the experiment. Then, n_4 would be sufficiently high to produce a considerable contribution to the resulting $|4\rangle \rightarrow |5\rangle$ ESA (see (5)) (assuming that $\mathrm{ESA}_{45}(\lambda)$ is a homogeneously broadened, wide spectrum). Thus the observed ESP effect would be a result of such an accumulation in the trap level. To test this hypothesis we carried out the single-shot experiments. The results of these measurements preclude the possibility of n_4 accumulation, displaying no practical difference between single-shot and 14 Hz cases, hence a_{41} is at least $> 14\ \mathrm{s}^{-1}$. Moreover, the large background of n_4 should cause a distinct deviation from exponential-like ESA decay, which would be observed especially in the 14 Hz EST(t) measurement. This was not the case since, even after thousands of pulses, the decay of ESA is practically the same as that of luminescence [20]. What is most important, is that the ESP effect occurs even in a single shot. As we mentioned before, our traps are invisible to GSA measurements at least between 340 and 700 nm, whereas very long-living trap populations (like in ref. [27]) should manifest themselves in such measurements. Thus, we can state that n_4 accumulation does not take place. Without accumulation of n_4, the $|4\rangle \rightarrow |5\rangle$ transitions, if homogeneously broadened, cannot contribute markedly to the ESP effect. These experimental facts convinced us that we deal here with a rather large number of narrow absorption lines, where under illumination by a monochromatic probe-beam, only one of them (or some of them, in the case of Xe pulsed lamp) takes part in the ESP effect. Such narrow absorption lines, associated with very large σ_{45} can contribute to the final result (5). In this interpretation the $\mathrm{ESA}_{45}(\lambda)$ spectrum results then from a large inhomogeneous broadening of the trap absorption.

Returning to temporal ESA behavior, the fact that ESA(t) corresponds well to luminescence decay can be an implicit proof, within the assumptions of our model, that: (a) $k_{34} \gg 10^6\ \mathrm{s}^{-1}$ (luminescence decay time is $\sim 4 \times 10^{-7}$ s); and (b) $a_{41} > 10^6\ \mathrm{s}^{-1}$. Then, of course, the resulting ESA kinetics will follow $n_2(t)$. These high values of k_{34} and a_{41} parameters are also the reason why the steady state EST(I) dependence (inset of fig. 3) is practically of the same shape as the "transient" one.

It is perhaps of interest to describe the tendencies of solutions as we vary the parameters. First of all, if $a_{41} = 0$, the horizontal distance between the theoretical curves: EST(t) for 1.6 W/cm^2 and EST(t) for 16 W/cm^2 was always too large to fit experimental values properly. Also, only relatively high values of b_{45} and k_{34} are capable of producing a large enough vertical distance between the two minima of these curves.

The theoretical fit to experimental data is, of course, not perfect. One can see, e.g. in fig. 3, that for small values of I, the theoretical curves distinctly deviate from the experimental points. Also, in fig. 4(a), experimental EST(t) minima are deeper than obtained by theory. There are some possible causes of these discrepancies. First, rather trivial, may be connected with huge electric noise originating from the excimer laser, which tends to "add" some false peaks to actual EST(t); the other cause can be the simplicity of the model which does not cover all the mechanisms associated with the traps (e.g. transitions $|3\rangle \rightarrow |2\rangle$ and $|5\rangle \rightarrow |4\rangle$ are neglected). Nevertheless, the model reproduces the most important features of measured data reasonably.

7. Conclusions

We believe that we found the model which explains the observed effect of excited state photochromism in BGO. The observed ESP is then a result of the contributions from an intrinsic process, characteristic of the Bi complex and another one due to trap states. The first is homogeneously, the second inhomogeneously broadened. At this time we cannot produce direct proof of the existence of the described traps. One needs to realize, however, that they may be observable only in experiments of the type described here. In analogy to well established techniques we can call these as site selection of the excited state. As we have attempted to demonstrate, there are numerous reasons why other mechanisms do not explain the results. The proposed model is similar to that introduced by Macfarlane et al. [31,32] in the context of persistent spectral hole-burning. Unlike our model, however, the Macfarlane trap can be a single one, and is being fed by states corresponding to an inhomogeneous distribution.

Acknowledgements

We wish to thank M. Mayhew of Bicron Corp. for supplying the BGO crystals and Dr. L.J. Andrews for GSGG crystal sample. The support by the US Army Research Office under the Grant DAAL03-88-0103 is gratefully acknowledged.

References

[1] J. Hajtó and I. Jánossy, Phil. Mag. B 47 (1983) 347.
[2] F. Henneberger and H. Rossmann, Phys. Stat. Sol. (b) 121 (1984) 685.
[3] D.A.B. Miller, J. Opt. Soc. Am. B 1 (1984) 857.
[4] C.R. Giuliano and L.D. Hess, Appl. Phys. Lett. 12 (1968) 292.
[5] C.R. Giuliano and L.D. Hess, IEEE J. Quantum Electron. QE-3 (1967) 358.
[6] R.C. Hoffman, K.A. Stetyick, R.S. Potember and D.G. McLean, J. Opt. Soc. Am. B 6 (1989) 772.
[7] L.W. Tutt and S.W. McCahon, Opt. Lett. 15 (1990) 700.
[8] Cz. Koepke and A. Lempicki, Chem. Phys. Lett. 172 (1990) 224.
[9] R.C. Bertelson, in: Photochromism, Techniques of Chemistry, Vol. III, ed. G.H. Brown (Wiley Interscience, New York, London, Sydney, Toronto, 1971).
[10] A. Hordvik, IEEE J. Quantum Electron. QE-6 (1970) 199.
[11] F. Henneberger, Phys. Stat. Sol. (b) 137 (1986) 371.
[12] C. Klingshirn, H. Kalt, R. Renner and F. Fidorra, J. Cryst. Growth 72 (1985) 304.
[13] M. Lambsdorff, C. Dörnfeld and C. Klingshirn, Z. Phys. B 64 (1986) 409.
[14] Cz. Koepke, A.J. Wojtowicz and A. Lempicki, to be published.
[15] Cz. Koepke and A. Lempicki, J. Lumin. 47 (1991) 189.
[16] N. Bloembergen, Appl. Opt. 12 (1973) 661.
[17] L.J. Andrews, S.M. Hitelman, M. Kokta and D. Gabbe, J. Chem. Phys. 84 (1986) 5229.
[18] R. Moncorgé and T. Benyattou, Phys. Rev. B 37 (1988) 9177.
[19] B. Struve, G. Huber, V.V. Laptev, I.A. Shcherbakov and E.V. Zharikov, Appl. Phys. B 30 (1983) 117.
[20] Cz. Koepke and A. Lempicki, Chem. Phys. Lett., 172 (1990) 227.
[21] W.W. Piper and D.T.F. Marple, J. Appl. Phys. 32 (1961) 2237.
[22] R. Moncorgé, B. Jacquier and G. Boulon, J. Lumin. 14 (1976) 337.
[23] R. Moncorgé, B. Jacquier, G. Boulon, F. Gaume-Mahn and J. Janin, J. Lumin. 12 & 13 (1976) 467.
[24] G.B. Beard, W.H. Kelly and M.L. Mallory, J. Appl. Phys. 33 (1962) 144.
[25] M.J. Treadaway and R.C. Powell, J. Chem. Phys. 61 (1974) 4003.
[26] M. Böhm, B. Cord, A. Hofstaetter, A. Scharmann and P. Parot, J. Lumin. 17 (1978) 291.
[27] C.L. Melcher, IEEE Trans. Nucl. Sci. NS-32 (1985) 545.
[28] C.L. Melcher, Nature 313 (1985) 465.

[29] W.E. Moerner and M.D. Levenson, J. Opt. Soc. Am. B 2 (1985) 915.
[30] B. Di Bartolo. in: Optical Interactions in Solids, (Wiley, New York, London, Sydney, Toronto, 1968) p. 369.
[31] R.M. Macfarlane and R.M. Shelby, in: Persistent Spectral Hole-Burning: Science and Applications, ed. W.E. Moerner (Springer, Berlin, Heidelberg, New York, 1988) p. 127.
[32] A. Winnacker, R.M. Shelby and R.M. Macfarlane, Opt. Lett. 10 (1985) 350.

Thermal effects in excimer-excited bismuth germanate

C. Koepke,* A. J. Wojtowicz,* and A. Lempicki

Department of Chemistry, Boston University, 590 Commonwealth Avenue, Boston, Massachusetts 02215

Received October 12, 1990; revised manuscript received March 15, 1991

An interesting thermal effect associated with intense ultraviolet excitation of bismuth germanate ($Bi_4Ge_3O_{12}$) crystal is found to increase the excitation rate approximately 2 orders of magnitude beyond that determined from excitation intensity and absorption. The effect involves a nonlinear increase of absorption of thermal origin owing to a shift of the absorption edge and indicates the need to take this shift into account when dealing with excited-state absorption and gain measurements.

INTRODUCTION

In previous papers[1-3] we described excited-state absorption (ESA) and its peculiarities in bismuth germanate ($Bi_4Ge_3O_{12}$; BGO). In this paper we describe one more effect associated with the strong UV excitation used in those experiments. The excitation source was an excimer laser with an output energy of approximately 100–150 mJ/pulse. After passing through the optics the excitation fluence was ~ 30 mJ/cm^2 (without any focusing), and it entered the sample within ~ 30 ns. This gave an extraordinarily high transient power density of ~ 1 MW/cm^2, which caused some distinct effects in the crystal. Care was taken to use excimer-laser intensities just below dielectric breakdown on the sample surface. The exciting pulse converts into various forms of energy dissipated in the medium. One of them is direct excitation; another is used to create a manifold of point defects.[3,4] The rest must be converted into heat (lattice heating). As we show, this heat, deposited upon the surface of the sample, can dramatically influence the measured magnitude of excited-state absorption or possible gain in a material when the exciting-laser line falls within the steep absorption edge.

RESULTS AND DISCUSSION

As we mentioned above, the exciting-pulse energy falling on the sample was ~ 30 mJ/cm^2. Taking the measured ground-state absorption coefficient of BGO [$\alpha(308\text{ nm}) = 1.89$ cm^{-1}] and the number of absorbing atoms, one can estimate an excitation parameter expressed as $p = n^*/n_0$ (n^* is the number of excited centers per cubic centimeter, n_0 is the total number of centers per cubic centimeter), which leads to $p \approx 5.7 \times 10^{-6}$. From measured ESA $= 1 - \exp(-\alpha_{ESA}L)$ and the definition of the cross section

$$\alpha_{ESA} = \sigma_{ESA} p n_0, \tag{1}$$

one can obtain the σ_{ESA} value. With the value of p above, expression (1) gives $\sigma_{ESA} = 1.95 \times 10^{-17}$ cm^2. We have good reason to suspect that the actual σ_{ESA} is smaller. A source of this suspicion is the temperature dependence of the absorption coefficient at the pumping wavelength of 308 nm, which would lead to a serious underestimate of p in expression (1).

In transmission experiments the transmitted excimer-laser beam (308 nm) was detected by a photomultiplier coupled to a grating monochromator and a boxcar averager. The boxcar gate (30 ns) was adjusted to the time directly following the excitation. The excimer flashed with a repetition rate of 14 pulses/s.

We carried out two kinds of transmission measurement. The first took place over a shorter time scale (in a fixed period of time) and averaged 100 pulses for each laser energy; the second took place over a longer time scale and used a fixed laser energy but was a function of the number of pulses and hence of time. The first measurement, because of the gate position, yielded a transient transmission, whereas the latter one displayed the same transient transmission but superimposed upon long time changes of the transmission. We also measured the dependence of excited-state transmission (EST $= 1 -$ ESA) on the time (i.e., the number of pulses) on a long time scale and compared this with 308-nm transmission. The results are illustrated in Figs. 1 and 2.

The transmission $\mathcal{T}$ of the exciting-laser beam versus laser pulse energy E_p drops severely and displays a pronounced deviation from linearity, as shown in Fig. 1. Furthermore, the transmitted intensity decreases with repetition rate, showing an inertia that is characteristic of thermal effects.

The increase of ground-state absorption with the pulse energy could be attributed to electronic effects such as two-photon absorption (TPA) and formation of a hierarchy of excitonic species (free excitons, biexcitons, exciton gas, and electron–hole plasma) or to electronic photochromism,[5] with the essential contribution of some traps, unintentional impurities, or defect states, fed from the first excited state of BGO or from a conduction band. The contribution of the conduction band is quite unlikely because the 308-nm energy does not reach this band (which itself is not well defined in BGO) and, instead, corresponds to an efficient charge-transfer process.[6] The conduction band could be reached only by TPA. However, the TPA is known to modify distinctly the excitation and emission spectra,[7] which we do not observe. For the same reason we also exclude such phenomena as formation of biexcitons by TPA and formation of an electron–hole plasma (Mott transition) from an exciton gas,[8,9] which potentially might shift the absorption edge to the red. The

0740-3224/91/091831-04$05.00

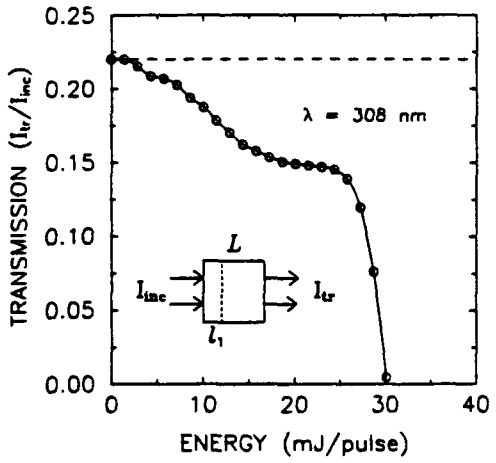

Fig. 1. Transmission of the excimer-laser beam as a function of the energy of the pulse entering the sample. The insert illustrates a two-layer model of the medium. The dashed line shows the linear transmission level.

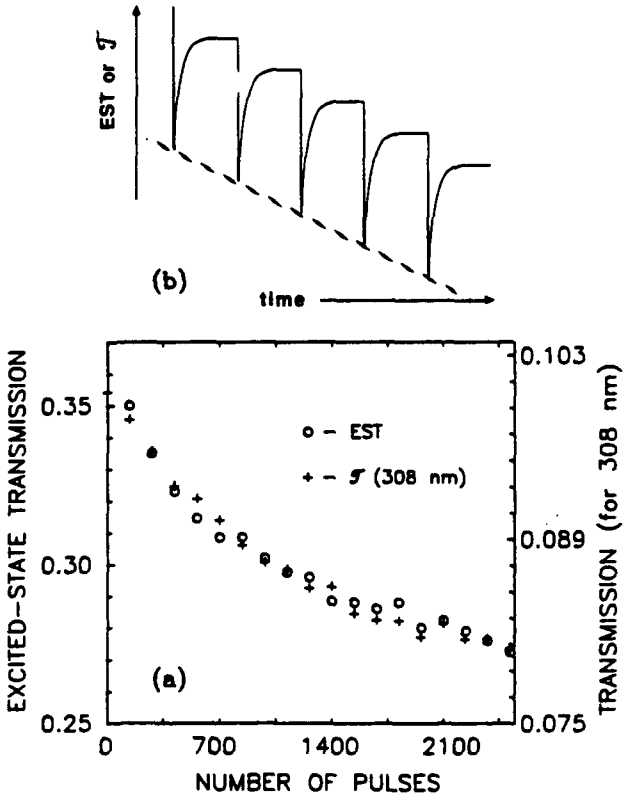

Fig. 2. (a) EST (circles) and $\mathcal{T}$ for the 308-nm line of the excimer laser (crosses) working at 14 pulses/s as a function of number of pulses. (b) Schematic illustration of how the transmissions of (a) were measured.

photochromism caused by traps or other species seems also to be an unlikely explanation, even though there are some thermoluminescent traps in BGO.[4] The energies of these traps lie, however, in the IR. Hence, in view of the distinct dependence of the absorption edge on temperature, we believe that the observed changes in transmission are of purely thermal origin.

Indeed, with our pumping energy, low quantum efficiency, and larg Stokes shift, one can expect a substantial increase of temperature T on the pumped side of the sample. From pumping energy, heat capacity, and neglect of thermal diffusion, we estimate a temperature increase of approximately 3 K after a single excitation pulse. Thus, after a series of pulses an increase of a few tens of degrees seems likely. Actually, the temperature, being limited by thermal diffusion, builds up for thousands of pulses with a characteristic time constant of the order of minutes.

Figure 2 shows EST (circles) and transmission for a 308-nm line (crosses) versus the number of excimer laser pulses (operating at a repetition rate of 14 pulses/s). The identity of results shows that the cause of the decrease of 308-nm transmission is the same as the decrease of EST (increase of ESA). This is the red shift of the absorption edge and the consequent increase of ground-state absorption, caused by the rising temperature. In this experiment EST was measured with a He–Ne laser, which provided a probe beam, and a fast photodiode connected to a two-channel boxcar averager was used as a detector. This setup was previously described in greater detail.[1,3] The decrease of $\mathcal{T}$ (308 nm) was measured by the same setup but without any probe beam; instead the excimer line (to be transmitted) and a normal transmission configuration were used.

The result, illustrated in Fig. 2(a), represents the slow background component of decreasing $\mathcal{T}$ and EST, as schematically shown by the dashed line in Fig. 2(b). A direct measurement of surface temperature T is not a simple task, because we deal here with a transient, short peak in T (following the excitation) localized at the surface and superimposed upon a slowly growing temperature background of the whole crystal. Such transient thermal responses of solid-state media are known, for example, in CdS,[10] and they can be as fast as the creation of phonons. Hence we could not measure this transient T directly but instead have measured the dependence of the position of the absorption edge on temperature. The results are shown in Fig. 3. The main part of this figure illustrates

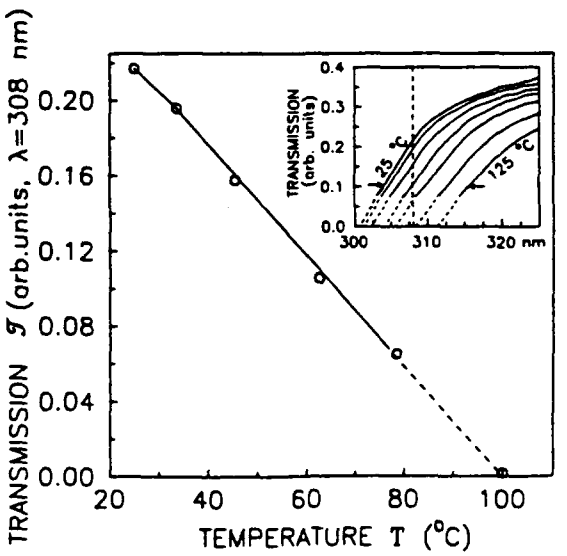

Fig. 3. Temperature dependence of the transmission of a 1.2-mm-thick sample at 308 nm. The inset shows the family of transmission edges measured at various temperatures. The temperatures corresponding to internal curves are, from left to right, 33.5, 45.5, 62.5, 78.5, and 100.0°C. The vertical dashed line indicates the position of the excimer-laser 308-nm line.

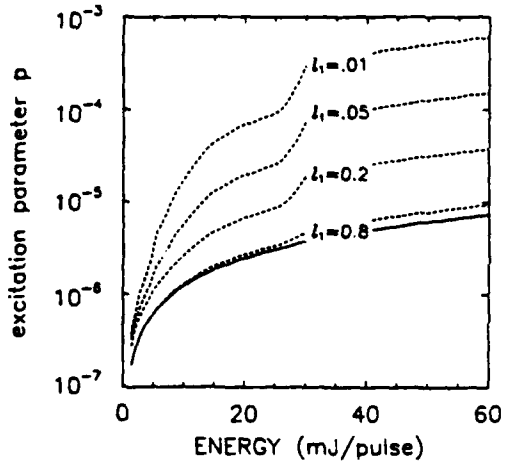

Fig. 4. Excitation parameter p versus pump-pulse energy [Eq. (2)] for different values of the hot layer thickness l_1 (in centimeters). The lowest p curve (solid) shows the excitation level calculated for linear transmission.

a thermal decrease of the transmission $\mathcal{T}$ for 308 nm. The data points are taken from the family of transmission spectra measured at various temperatures T, as shown in the insert. The measurements were carried out on a 1.2-mm-thick BGO sample, a simple heater (in which the sample was homogeneously heated in a hot-air bath), a Xe flash lamp, and an optical multichannel analyzer. Because of the rather thick sample we had to extrapolate the lower parts of the transmission spectra, as indicated by dashed curves. The vertical dashed line represents the 308-nm excimer-laser line location. The thermal red shift of the transmission edge is 12 nm/100 deg. This is in good agreement with the thermal shift of the luminescence excitation spectrum as reported by Moncorgé *et al.*[6] Since at room temperature the exciting line falls on the steep part of the absorption edge, the thermal absorption shift can cause a remarkable increase of absorption, even after a relatively small increase in temperature. This further increases the amount of energy deposited in the surface region of the sample, causing an even larger increase of temperature, which continues until equilibrium is established.

Thus there is an apparent positive feedback, leading to substantial nonlinearities in transmission such as are well known in other areas, for instance, in optical bistability.[10-13] However, unlike in optical bistability, where the most important and basic nonlinearity is seen in the s-shaped $\mathcal{T}$-versus-T function, our transmission temperature dependence is quite linear. In view of the results given in Fig. 1, we conclude that in our case the basic nonlinearity resides in $T(E_p)$ dependence, where E_p is the excimer-laser pulse fluence. Such a behavior has also been considered in optical bistability.[11,12] It is quite likely in our case, as it is a result of the positive feedback $\mathcal{T}(T) \rightleftharpoons T(\mathcal{T})$ and the complex character of sample pulse-by-pulse heating during excitation. As a result, a relatively thin hot layer characterized by enhanced excitation may be formed. The mechanism of this effect is complicated, and exact calculations are beyond the scope of this paper. Instead, we introduce a simple, two-layer model. The insert in Fig. 1 shows the model in which we assume that the temperature increase is confined to a layer of finite thickness l_1 whereas the entire thickness of the sample is L (=0.8 cm). The model makes sense only if an increase of the absorption coefficient in the hot layer is large enough ($\sim 1/l_1$) to reduce the intensity of the transmitted beam significantly. This is realistic since a temperature increase of only 75 K would cause an increase of the absorption coefficient from the room-temperature value of approximately 2 to ~100 cm^{-1}.

According to our model one can easily show that in the volume of the hot layer the dependence of excitation parameter p on pumping energy per pulse can be written as

$$p(E_p) = \frac{\{1 - \mathcal{T}(E_p)\exp[\alpha(L - l_1)]\}E_p}{h\nu n_0 l_1}, \qquad (2)$$

where $\mathcal{T}(E_p)$ is the nonlinear transmission of the whole sample and α is the room-temperature absorption coefficient. Equation (2) and the nonlinear transmission data of Fig. 1 were used to calculate $p(E_p)$ for different values of l_1 (in centimeters). The results are shown in Fig. 4. The dependence of p on the temperature profile below the pumped surface of the sample will be most pronounced when the thickness of the layer l_1 matches the probe-beam diameter (~200 μm). Assuming that is the case, we can see from Fig. 4 that an ~30-mJ pulse would correspond to an excitation parameter of the order of 10^{-4}. In view of expression (1), such an excitation parameter provides σ_{ESA} in a range from 10^{-19} to 10^{-15} cm^2, distinctly smaller than previously estimated.

CONCLUSION

We conclude that the measured ESA effect reveals an interesting thermal behavior because the line of the exciting excimer laser corresponds exactly to the steep absorption edge of BGO. The thermal red shift of the absorption edge and subsequent feedback between absorption and temperature can boost the excitation parameter p by some 2 orders of magnitude. As a result it increases the ESA coefficient α_{ESA} by the same factor. The effect described seems to be universal whenever intense laser excitation is used in the vicinity of an absorption edge. This pumping nonlinearity would be capable of increasing a possible gain in similar experimental conditions.

ACKNOWLEDGMENTS

We are indebted to M. Mayhew of Bicron Corporation for supplying the BGO samples. Support by the U.S. Army Research Office under grant DAAL03-88-0103 is also gratefully acknowledged.

*On leave from the Institute of Physics, N. Copernicus University, Toruń, Poland.

REFERENCES

1. C. Koepke and A. Lempicki, Chem. Phys. Lett. **172**, 224 (1990).
2. C. Koepke and A. Lempicki, Chem. Phys. Lett. **172**, 227 (1990).
3. C. Koepke and A. Lempicki, J. Lumin. **47**, 227 (1991).
4. C. L. Melcher, IEEE Trans. Nucl. Sci. **NS-32**, 545 (1985).
5. S. K. Deb and L. J. Forrestal, in *Photochromism*, Vol. III of Techniques of Chemistry, G. H. Brown, ed. (Wiley-Interscience, New York, 1971), p. 633.

6. R. Moncorgé, B. Jacquier, and G. Boulon, J. Lumin. **14**, 337 (1976).
7. M. Casalboni, R. Francini, U. M. Grassano, C. Musilli, and R. Pizzoferrato, J. Lumin. **31–32**, 93 (1984).
8. C. Klingshirn, H. Kalt, R. Renner, and F. Fiddora, J. Cryst. Growth **72**, 304 (1985).
9. F. Henneberger, Phys. Status Solidi B **137**, 371 (1986).
10. M. Dagenais and W. F. Sharfin, Appl. Phys. Lett. **45**, 210 (1984); M. Dagenais, Appl. Phys. Lett. **45**, 1267 (1984).
11. J. Hajtó and I. Jánossy, Philos. Mag. B **47**, 347 (1983).
12. F. Henneberger and H. Rossmann, Phys. Status Solidi B **121**, 685 (1984).
13. D. A. B. Miller, J. Opt. Soc. Am. B **1**, 857 (1984).

EXCITED-STATE ABSORPTION IN EXCIMER-PUMPED $CaWO_4$ CRYSTAL

Cz. Koepke*, A.J. Wojtowicz†, and A. Lempicki

Boston University, Chemistry Dept. 590 Commonwealth Ave., Boston, MA 02215

ABSTRACT

We report Excited State Absorption (ESA) in a $CaWO_4$ under excimer laser excitation (308 nm), whose spectrum proves to be very broad and intense. We also calculate a stimulated emission cross–section and show that it is at least one order of magnitude smaller than broad–band ESA cross–section, which precludes laser action in an excimer–excited, undoped $CaWO_4$ crystal. The WO_4^{2-} ESA spectra can be assigned to $2e \rightarrow 4t_2$ transitions and related to 10Dq energy in T_d symmetry. Using the spectroscopic parameters from measured emission and ESA, we construct a configuration coordinate diagram including a higher excited state. The diagram predicts that the initial and terminal states of ESA transition are characterized by different equilibrium positions and, consequently, different charge distribution. It is suggested that this effect can be explained by mixing of the t_2 symmetry d–type wave functions with p orbitals of the tungsten ion. The overall ESA is of a complex nature, being a combination of conventional ESA, decaying like luminescence and another, long lasting component possibly connected with phosphorescent traps. This behavior is reproduced by a simple kinetic model.

*On leave from Institute of Physics, N. Copernicus University, Toruń, Poland

†Present address: Institute of Physics, N. Copernicus University, 87–100 Toruń, Poland

I. INTRODUCTION

The enormous success of Ti:Sapphire lasers demonstrates that the solid state option is often preferred to dyes. This paper therefore describes an attempt at finding a tunable solid state laser in the blue–green region of the spectrum. If a primary laser source is to emit in the blue–green it has to be pumped in the UV. An excimer laser is the obvious pumping source. The materials can be chosen from a family loosely known as "phosphors" which play an important role in lighting, TV and X–ray detection [1]. Among the "phosphors", materials containing transition metal ions in d^0 configuration are particularly important [1] and have been suggested as potential laser candidates [2]. A typical example is $CaWO_4$, which is the subject of this paper.

The work we describe is <u>not</u> an attempt at extending the detailed knowledge of the spectroscopy of this material, which has been the subject of many publications [3–11]. Our <u>primary interest</u> is in the higher excited states which may be responsible for Excited–State Absorption, (ESA), and therefore will determine the feasibility of laser action.

Although excimer lasers are reliable and nowadays universally used for pumping dyes, they have their limitations for our present application. The main one is the discrete number of lines which may or may not fall in the most desirable absorption region of the "phosphor". The absorption of the d^0 – type materials is dominated by very intense, charge transfer† bands in the near UV. It is often the case that the excimer lines fall into unacceptably high absorption regions, providing insufficient penetration depth to conduct ESA (or gain) measurements. On the other hand, choosing the longest excimer line at

---

†this is a very simplified picture in view of the results of Ziegler et al.[12] which prove that an actual behavior is associated rather with redistribution of orbitals than with direct transfer of charge.

308 nm may result in an excitation in the tail of the absorption to which native or accidental defects, such as WO_3– Schottky defect, usually contribute. This may cause an inelegance of the results because the intrinsic process of charge transfer excitation and ionic emission may be accompanied by other processes. This is unfortunately the case in $CaWO_4$. Since we cannot tune the excimer pumping, one may resort to a limited tuning of the material's absorption by temperature. We found this of some utility in the present work. Again we wish to emphasize that our main objective was to ascertain the laser possibilities of the excimer – phosphor combination rather than detailed spectroscopy for which a different pumping source (tunable parametric or second harmonic generation) may be more suitable.

II. MATERIAL

$CaWO_4$ is one of the best known luminophors, described in numerous papers (e.g. [3–11]) and popular because of its high luminescence yield, high quenching temperature, and very broad emission spectrum. In single crystal form $CaWO_4$ is transparent in the visible and has a strong absorption in UV, involving charge transfer processes. The absorption edge starts below 300 nm [13], which leaves us the choice of using the 248 nm excimer radiation and consequently, too small penetration depth, or 308 nm radiation which coincides with the absorption tail. To measure ESA we had to use the latter and face the consequences.

The tungsten ion is in $5d^0$ configuration and fourfold coordination. All of the modern work on tetroxo ions [7,14] recognize the fact that the T_d symmetry is not maintained. Crystallographic data indicate that the symmetry is D_{2d} (e.g. [8]) and site symmetry S_4 (e.g.[10]). Moreover, in the excited state the T_d symmetry (if ever there was one) can distort due to a static Jahn–Teller effect to C_{3v} [15]. Nevertheless it is useful

(and most authors follow this [7,14,16]) to start with the T_d symmetry to classify the terms. This is shown in Fig. 1.

Since in the ground state $1t_2$, $1a_1$, 1e, $2t_2$, $2a_1$, $3t_2$ and t_1 one–electron molecular orbitals are occupied (see Fig. 1a), the WO_4^{2-} molecular complex can be excited via $t_1 \rightarrow 2e$ transition to the following molecular terms: $^3T_1$, $^1T_1$ and $^1T_2$ due to the $(t_1^5,2e)$ configuration. The lower lying triplet is believed to be a source of the luminescence [6,8,17]. The next excited state originates in $(t_1^5,4t_2^1)$ configuration, resulting in four singlet terms: $^1T_2$, $^1T_1$, $^1E_1$, and $^1A_2$ [1]. The transition between one–electron states, $2e \rightarrow 4t_2$, corresponds to 10Dq energy in T_d symmetry. This is a parity forbidden d–d transition whereas absorption occurring between t_1 and 2e, being a charge transfer transition, should have a large oscillator strength. The electronic structure of the WO_4^{2-} complex is illustrated in Fig. 1a,b where (a) results from one–electron molecular–orbital calculations (after Kebabcioglu and Müller [18]), and (b) from semiempirical assignments and calculations of total electronic energy (after Butler [1]). The confirmation of the triplet nature of the excited state of tetroxo anions (first proposed by Ronde and Blasse [19]) has been provided by Van der Waals and his collaborators [20,21,14]. We shall come back to this aspect later. To the extent that the splittings are roughly correct Fig. 1 illustrates the point that on the basis of one–electron energy levels (Fig. 1a) one would expect the system to produce an optical gain since ESA occurs at low (infrared) energies. On the other hand, the diagram (b) seems to extend the range of ESA transitions, which would terminate on higher energy terms of $(t_1^5,4t_2)$ configuration.

As we shall see, the measured ESA spectrum is very broad, overlapping the luminescence and dominating the stimulated emission. The time dependence of ESA indicates that it is not of simple nature and consists of several components having widely different decay times. The short (μs range) components, which decay like luminescence, are due to the W complexes. The long component, is so slow that it is not changing at all during the time of the measurement (being possibly of the order of hours). Assuming that

it originates from different centers it can be described by a kinetic treatment, (see Appendix). The existence of well known phosphorescent traps is a likely source of this long ESA component.

The interpretation of the short components leads us to a distinction between the intrinsic WO_4^{2-} complex and a Schottky defect WO_3.

In general the spectroscopic measurements of the ESA provide little information, other than position, width and intensity of a rather structureless and broad band.

III. EXPERIMENTAL

We shall refer to ESA both as the name of a phenomenon and as the dimensionless value of absorption: $ESA = 1 - \exp(-\alpha_{ESA}L)$, where α_{ESA} is the excited state absorption coefficient and L is the medium length.

Our measurements yield directly Excited State Transmission (EST) which is related to ESA by

$$EST = 1 - ESA = I_p/I_u \qquad (1)$$

where I_p is probe beam intensity measured <u>after</u> passing through the pumped medium and I_u is the intensity <u>after</u> passing through the unpumped medium. The ratio (1) contains also a contribution from ground state absorption (GSA), because [22]

$$EST = \exp[-(\sigma_{ESA} - \sigma_{GSA})n_2 L] \qquad (2)$$

where σ_{ESA} is the ESA crossection, σ_{GSA} the GSA crossection, and n_2 is the population of the first excited state. The term $[\sigma_{ESA}(\lambda) - \sigma_{GSA}(\lambda)]n_2$ is sometimes called as the Excited State Difference Spectrum, [23], and a positive contribution of $\sigma_{GSA}n_2$ corresponds to absorption bleaching. For our crystals there appears to be a flat absorption extending throughout the visible region, with an absorption constant (measured at

632.8 nm) $\alpha \simeq 0.17\ cm^{-1}$. Some of this may be due to light scattering. This value translates into a crossection $\sigma_{GSA} \simeq 1.3 \times 10^{-23} cm^2$. Since, as will be shown, σ_{ESA} is of the order of $\simeq 10^{-19} cm^2$, the crossection σ_{GSA} in expression (2) can be neglected.

The sample used in our measurements was 7.8 mm long crystal, carefully polished on entrance, exit, and pumped faces. The sample could be heated to $\sim 200 - 220\ ^{o}C$ in a hot air bath using a simple heater. Experiments were carried out with two different kinds of apparatus, both using transverse pumping geometry (Fig. 2 a,b). The excitation was provided by an excimer laser (Questek 2240) with a lightly focused beam covering the whole face area (308 nm, pulse duration $\simeq$ 30 ns, energy falling on the sample $\lesssim$ 120 mJ/pulse/cm^2, repetition rate 14 or 10 pps). The limited focusing avoided dielectric breakdown on the sample surface and consequent damage [24]. The two different experimental setups of Fig. 2a and b while using the same excitation, differed in the sources of the probe beam and the detection electronics. Setup (a) was used to detect a temporal evolution of ESA following pulsed excitation and utilized a monochromatic CW beam from a krypton laser with a waist of $\simeq 250\ \mu m$ in the region of the sample. For detection we used an ultra fast silicon photodiode (EG&G Electro–Optics FND–100), connected to a fast transient recorder (DSP 2001 S) controlled by computer. The luminescence level was reduced practically to zero by a system of diaphragms and far–field geometry. No directional deviation of the probe beam was observed as well as possible transverse beam distortions were absent after passing the sample. Measurements were averaged over 450 pulses.

The setup (b) was designed to provide ESA spectra and utilized a pulsed Xenon lamp (EG&G Electro–Optics FX–504) serving as a polychromatic probe beam. The diameter of the lamp beam was $\simeq 500\ \mu m$. The detector was an OMA III (EG&G Princeton Applied Research) coupled to spectrograph (Jarrell–Ash MonoSpec 27). In these experiments every other pulse of the excimer laser was adjusted in time to the maximum of the Xe–lamp probe beam pulse (of repetition rate 7 pps and pulse duration

$\simeq 0.5\ \mu s$), whereas the other excimer pulses caused only luminescence of the sample, the probe beam being absent. The probe beam pulses passing through the excited sample were detected by the gated OMA reticon (set up to register a spectrum from 320 nm to 690 nm) and averaged in one of the memories of the OMA computer controller. Sample luminescence pulses (without the probe beam) were averaged in another memory. As a result we could obtain the following difference: $I_{pL}(\lambda)-I_L(\lambda)$, where $I_{pL}(\lambda)$ is the probe beam spectrum after passing through the pumped sample plus the luminescence spectrum, and $I_L(\lambda)$ is the luminescence spectrum only, in the absence of the probe beam. In other words, $I_{pL}-I_L = (I_u-\delta I + I_L)-I_L = I_u-\delta I$, where I_u is the measured probe beam intensity for the unpumped medium and δI is a decrease of the probe beam due to excited state absorption. Thus we measured both terms of this difference simultaneously, avoiding the influence of long–time drifts of the excimer laser intensity. In a subsequent measurement $I_u(\lambda)$ was measured (for an unpumped sample). In both of the above measurements a background signal was automatically subtracted in real time. Eventually, we obtained the spectrum expressed by the formula: $EST(\lambda) = [I_u(\lambda)-\delta I(\lambda)]/I_u(\lambda)$.

In our measurements we used the 308 nm excimer line, falling into the absorption tail at room temperature (RT), but corresponding to distinctly higher absorption at elevated temperatures (thermal red shift of the absorption edge). At RT the absorption coefficient of about 0.9 cm^{-1} is too small to provide sufficient excitation rates and distinct effects. We therefore performed experiments at 220 ^{o}C where the absorption increased to $\sim 1.6\ cm^{-1}$, and is very close to the steep rise of the absorption edge. Small changes in temperature which may be caused by excimer laser excitation, especially at high repetition rates, can also cause an additional increase of absorption. The effects of absorption increase (and their consequences) are common whenever monochromatic excitation falls close to the absorption edge [25].

IV. RESULTS

IVa. Temperature dependence of luminescence

We measured the temperature dependence (between RT and ~ 200 °C) of the luminescence decay and respective emission spectra. For decay experiments we used the photodiode coupled to the transient recorder. This measurement recorded the time dependence of the total output. Emission spectra were acquired by the ungated (time integrating) OMA system under exactly the same conditions. There are several literature reports on the temperature dependence of the decay [9,11] but our attention was focused on effects caused by the particular conditions of excimer excitation. At RT the luminescence decay is composed of at least two exponentials having the time constants 0.6 μs and 9.2 μs. At higher temperatures ($T \gtrsim 200$ °C) the decay reduces to a single–exponential component. The overall light yield of $CaWO_4$ is governed by the 9.2 μs component. Eventually this component shortens with temperature and at 469 K it is ~ 0.5 μs. The shorter component entirely disappears. The longer component can be ascribed to the decay of WO_4^{2-} emission. The shorter component is probably connected with a WO_3 defect, whose emission will be described later. Figure 3 illustrates the dependence of WO_4^{2-} decay time on the temperature. The experimental points were fitted to the familiar formula:

$$\phi = \tau / \tau_r = 1/(1 + s\, \tau_r \exp[-\Delta E/kT]) \qquad (3)$$

where τ_r is the radiative lifetime. We estimate it to be ~ 15 μs, from our data of decay time at RT and quantum efficiency of ~ 0.6 (an average from: [9,13,26]), assuming that ϕ at T = 0 K is unity. s is a frequency factor, and ΔE is the thermal activation energy of the first excited state. The best fit has been obtained with $s = 5.35 \times 10^9\ s^{-1}$ and $\Delta E = 300$ meV. The value ΔE is in a good agreement with reported values [9,11].

Figure 4 shows the emission spectra for the same temperature range. The striking

feature is the non–monotonic behavior of the temperature dependence. The curves taken 296 K – 343 K clearly display thermal quenching (and blue shift), which occurs as long as the excimer line falls on the flat portion of the absorption spectrum. For higher temperatures, because of the thermal red shift of the absorption edge, higher excitation overcomes the thermal quenching and intensity of the luminescence increases despite of the increase of temperature. Also, note a distinct narrowing of the HT (high temperature) spectrum and a blue shift of its maximum.

The observed changes in spectral shapes suggest that there are at least two emission centers. The excimer pumping on the red side of the absorption edge tends to excite them both. It is known that excitation in the absorption tail favors green emission ascribed to a WO_3 complex (Schottky defect) [8,27]. For shorter wavelength excitation, the blue emission of the WO_4^{2-} predominates. Because of the red shift of the absorption edge with temperature, excitation at a fixed excimer frequency mimics shorter wavelength excitation. Thus we observe a changing balance of $WO_3 - WO_4^{2-}$ emissions, until above 350 K the WO_3 green emission practically disappears. The HT spectrum, peaking around 440 nm is undoubtedly the spectrum of WO_4^{2-} complex [8,28]. Since the RT spectrum contains the mixed emission of WO_4^{2-} and WO_3, we can obtain the WO_3 spectrum by subtracting the HT from the RT spectrum. In this subtraction we have to introduce a scale factor F which takes into account the increase of excitation with temperature. Fig. 5 shows both room– and high temperature spectra and the Schottky (SCH) defect emission extracted from them. It peaks at around 540 nm in good agreement with known data [8]. It is interesting to note that also the temperature dependence of decay favors this interpretation, indicating that the longer decay is due to the WO_4^{2-} complex.

The existence of WO_3 emission in $CaWO_4$ may have some consequences for the observed ESA. At RT some ESA contribution from the WO_3 complex may exist. However, because the WO_4^{2-} luminescence dominates at RT, we assume that it also dominates the observed ESA.

IVb. Excited–State Absorption Measurements.

Figure 6 presents the ESA and luminescence decays and their logarithms (in insert) measured at room temperature. The ESA measurement was performed with a krypton laser probe beam at 520.8 nm. The dashed line shows the zero level from which the ESA/luminescence pulses start. Clearly luminescence intensity returns to this level whereas ESA does not. The same is seen in the insert as manifested by different slopes of the logarithmic decays. The HT decays of luminescence and ESA measured at T = 496 K are illustrated in Fig. 7. One can see here an even more distinct, long ESA component, reflected also in the insert by a smaller slope. We explain this behavior in the Appendix. The ESA spectra have been measured using a gated OMA detector with a 300 ns gate set directly after excitation. Thus, the system detected the transient ESA at a time when the contribution of trap–related ESA is small. Hence, the obtained spectra characterize the ESA of tungsten complexes rather than the long–lived traps. Fig. 8a illustrates the ESA crossections. The $\sigma_{ESA}(\tilde{\nu})$ was derived from measured EST using the number of excited complexes n_2 calculated from the excimer laser fluence and absorption characteristics of the crystal. The appropriate excitation parameters: $p = n_2/n_1$ (n_1 is the number of the complexes in the ground state) were 7.4×10^{-5} at RT and 1.2×10^{-4} at HT.

The most important finding is that the ESA spectrum is very broad, structureless, overlapping the luminescence range and spreading even further.

V. STIMULATED EMISSION

We can now return to the chances of $CaWO_4$ as a possible laser material. First of all if we observe EST < 1, it means that no net gain can take place. The proper way to evaluate the magnitude of ESA–to–gain ratio is to compare their crossections. As it is seen in Fig. 8a, σ_{ESA} is of the order of $\sim 10^{-19}$ cm^2. On the other hand, the stimulated emission crossection σ_{ST} can be evaluated from McCumber's theory of phonon–terminated

lasers, [29], which, after some simple manipulations, [30], provides the following expression:

$$\sigma_{ST}(\nu) = \frac{S(\nu)}{8\pi\tau_r \int_0^\infty S(\nu)d\nu} \left[\frac{c}{\eta\,\nu}\right]^2 \qquad (4)$$

where $S(\nu)$ is the measured luminescence spectrum , τ_r is the radiative lifetime (estimated earlier to be $\sim 15\ \mu s$), and η is the refractive index of the medium. Results are illustrated in Fig. 8b. One can see here, that σ_{ST} is at least one order of magnitude smaller than σ_{ESA}. This, of course, precludes possible lasing in $CaWO_4$.

VI. CONFIGURATION COORDINATE MODEL

We wish to emphasize the effects which have to be taken into account. First of all, there is an enormous electron–lattice coupling which makes the luminescence spectrum featureless and broad. On the other hand, because $CaWO_4$ luminesces from a triplet state and the ground state is a singlet, there must be a considerable mixing in the excited state caused by spin–orbit coupling and/or J–T effect. Spin–orbit coupling is expected to be considerable in this 5d material, and also may increase in the excited state due to the mixing of the p– and d–orbitals. We cannot see any direct evidence of J–T effect. However, the J–T effect, being possibly different in the 2e and $4t_2$ states (electron–lattice coupling to the different modes) can contribute to the spectral width of the ESA transition. Thus, both effects can increase the probability of the ESA transition and broaden its spectrum. Having such a variety of effects, but observing only evidence of strong electron–lattice coupling, we can either renounce further interpretation (in view of lack of any quantitative data on J–T effect and SOC) or take the simplest assumption of linear coupling to one, full symmetry mode, and see how far it leads and where it fails. It has at

least this advantage that the configuration coordinate diagram can be plotted on a quantitative energy scale which is directly related to the experimental data.

With some additional assumptions, parameters deduced from luminescence spectra presented in previous sections allow us to construct the one–configurational coordinate diagram, of the WO_4^{2-} and WO_3 complexes. For construction of the diagram we need maxima of the emission lineshapes (19470 cm^{-1} for WO_4^{2-} and 15850 cm^{-1} for WO_3 obtained from the experiment) and Stokes shifts. In order to determine Stokes shifts one has to know the positions of absorption lineshape maxima. Since absorption (and reflection) spectra are dominated by strong, parity and spin allowed singlet – singlet transitions, while emission comes from the parity allowed but spin forbidden triplet – singlet transition, this proves to be difficult. The absorption peaks are simply not known. However, coupling to one full symmetry mode results in equal contributions to the Stokes shift from emission and absorption. Therefore, since the emission lineshape maxima are known, it would be sufficient to know the positions of zero–phonon lines (ZPL) if these were observable. Since they are not in view of the strong coupling, we have to resort to values estimated on the basis of an approximate analysis of the emission lineshapes. This gives ZPL lines at about 28000 cm^{-1} for WO_4^{2-} and 22000 cm^{-1} for WO_3. The maxima of absorption lineshapes would then be 36530 cm^{-1} and 28150 cm^{-1} for WO_4^{2-} and WO_3 respectively. For the WO_4^{2-} complex this agrees with values obtained by Butler [1, p. 296], on the basis of excitation spectra and semiempirical molecular orbital calculations. Butler gives about 37000 cm^{-1} for the lowest energy, spin forbidden transition $(t_1^6) \longrightarrow (t_1^5,2e)$.

In harmonic approximation the total energy (electronic and vibrational) for the ground, singlet state, due to the (t_1^6) configuration, will be:

$$E_1(Q) = A \cdot Q^2 \qquad (5)$$

and for the first excited triplet state due to $(t_1^5,2e)$:

$$E_2(Q) = A \cdot (Q - Q_o)^2 + E_{ZPL} \cdot \qquad (6)$$

where E_{ZPL} is zero–phonon line energy for the $(t_1^5) \rightarrow (t_1^5,2e)$ transition, Q_o is the equilibrium position of the complex in the first excited state, 2e, and $2 \cdot A \cdot Q_o^2$ is equal to the Stokes shift. If we choose coordinate units so that $Q_o = 1.0$ for WO_4^{2-} in the 2e state then the Stokes shift for the WO_4^{2-} complex will determine the shape of all the parabolas. With this convention and using the same form of equations as (5) and (6), the equilibrium position for WO_3 in the first excited state is equal to 0.85.

To include the ESA process one should remember that the initial state for ESA transition is the same as the luminescing state i.e. the lowest $(t_1^5,2e)$ triplet. We assume that the final state of ESA transition is one of the $(t_1^5,4t_2)$ singlet terms. Since the energy difference between $(t_1^5,4t_2)$ and $(t_1^5,2e)$ is 10Dq(Q), the corresponding excited state parabola can be expressed as

$$E_3(Q) = A \cdot (Q - Q_o)^2 + E_{ZPL} + 10Dq(Q) \qquad (7)$$

where two first terms describe the first excited state parabola. In a linear coupling model:

$$10Dq(Q) = 10Dq + BQ \qquad (8)$$

where 10Dq(0) is the pure electronic contribution to the total energy of the complex (9120 cm^{-1} calculated by Kebabcioglu and Müller [18]), while the parameter B describes the contribution of the electron–lattice interaction. For increasing Q the energy separation between 2e and $4t_2$ parabolas would grow, reaching at Q = 1 the experimental value of maximum of ESA transition lineshape: $E_{ESA} = 20500\ cm^{-1}$, $10Dq(Q=1) = E_{ESA}$. Hence, at Q=1, $BQ = E_{ESA} - 10Dq(0) = 11380\ cm^{-1}$. We thus obtained all the parameters: A, E_{ZPL}, 10Dq(0), and B needed to construct the energy diagram. It is shown in Fig.9. The first excited state parabola of the WO_3 complex was found using the same value of A, $E_{ZPL} = 22000\ cm^{-1}$ and $Q_o = 0.85$ (from the Stokes shift). Since 10Dq(0) for WO_3 is not

known and there in no good experimental data on ESA available we were not able to calculate its higher excited state parabola.

It is interesting to note that an equilibrium position of the lattice for the WO_4^{2-} complex in $(t_1^5,4t_2)$ state, which can be calculated from (7) and (8), is 0.33. This value is between 0 (ground state equilibrium position) and 1 (first excited state equilibrium position). Finally, we can note that the resulting barrier between ground and first excited state is much higher that the thermal activation energy ($\sim 1730\ cm^{-1}$) derived from measured thermal dependence of luminescence decay. This is quite understandable in view of a single–coordinate model [31,32]).

VII. DISCUSSION

As we mentioned in the Introduction, materials containing transition metal ions in d^0 configuration have been proposed as media for new solid state lasers. This possibility was based on two intuitive but highly misleading arguments: (a) to the extent that charge transfer processes may be pictured as resulting in d^1 configuration of the metal ion, there should be no ESA (like in Ti^{3+}); (b) single–electron, molecular orbital calculations (Fig. 1a) indicate that $2e \rightarrow 4t_2$ transitions which may lead to ESA are in the infrared. None of these proved to be correct upon a first time ESA measurement in a d^0 complex. What we have found is a very intense and broad ESA band totally excluding laser action. Using measured emission spectra we calculated stimulated emission cross–sections which are at least an order of magnitude smaller than respective $\sigma_{ESA}(\tilde{\nu})$. The same is true for transition metal ions other than W^{6+} [33]. These observed facts could not easily be deduced from previous knowledge about $CaWO_4$, namely the triplet nature of the excited state and the combined effects of a Jahn–Teller distortion and spin–orbit coupling. The reason is that the magnitude of the splittings introduced by these effects is simply not

known. Since additionally the ESA measurements reported here provide no further clue how to account for them, we have chosen the simplest route to ignore them. We have used the parameters of the measured ESA and certain reasonable guesses as to the position of ZP lines to create a one–configuration coordinate model of the crystal. The model reveals various aspects of a strongly lattice–coupled ESA transitions and, in particular, displacements of the consecutive parabolas. There displacements account for the large bandwidth of luminescence and ESA spectra.

Since for lack of additional information we have decided to use the single configuration coordinate model, we must for the sake of consistency interpret these displacements in terms of that model. Thus the displacement of the $4t_2$ parabola with respect to the luminescent one (2e) indicates a degree of charge redistribution upon the ESA transition. If the $4t_2$ one–electron wavefunctions were exclusively of d–character, we would expect only negligibly small relaxation upon the $2e \longrightarrow 4t_2$ transition. Consequently the 2e and $4t_2$ parabolas would have almost the same equilibrium positions and the ESA spectrum, peaking at $\sim 9126\ cm^{-1}$ would be quite narrow. However, since the d–wavefunctions of t_2 symmetry do mix with p states of the metal ion, a change in charge distribution can occur. The p–orbitals of the central ion, being penetrating ones, can contribute to spin–orbit coupling (SOC), especially in view of the heavy tungsten atom ($Z = 74$) increasing SOC in the higher ($4t_2$) excited state.

We can now speculate on the meaning of these results obtained with the simplest of all possible models, while we recall what has been neglected. It is known [15] that for $3d^0$ crystals, such as YVO_4, the spin–orbit coupling (SOC) is very small, and is dominated by the crystal field anisotropy, and first of all, by a very strong, static Jahn–Teller (J–T) effect. However, in $4d^0$ ($CaMoO_4$) tetroxo–anions, SOC becomes larger and there are indications [15,34] that SOC plays some role in view of heavier central atom, but the hierarchy:

$$J\text{–}T > CFA > SOC >> SSC \qquad (9)$$

still holds. $CaWO_4$, being $5d^0$– type crystal and having even heavier central atom (Z = 74), should reveal distinctly larger SOC. Judging from the simplest assumptions ($\zeta \sim Z^4$): SOC should be about 10 times larger than for $CaMoO_4$. This may be an overestimation in view of work of van der Waals [16], who states that going from $3d^0$ to $4d^0$ etc. one can observe a smaller increase in SOC than expected. However, it seems likely that in a particular case of tungstates ($CaWO_4$) the hierarchy (9) might have not been satisfied, and the SOC could be of the order of J–T effect (i.e.
J–T ≃ SOC > CFA >> SSC).

There is an interesting confirmation of van der Waals estimates of the importance of SOC from ESA measurements in $CaMoO_4$ [33,35]. In this case the simple single–configuration coordinate model fails completely because it predicts a narrow ESA spectrum (no displacement of the $4t_2$ and 2e parabolas), whereas the spectrum is quite broad, similar to that of $CaWO_4$. Thus, the simple model provides no evidence for large SOC and its failure suggests the dominance of a J–T distortion. This conclusion convinces us that there is some merit in applying a very simple and obviously inadequate model to a very complicated situation.

It is to be hoped that a much better understanding of the ESA processes, and the nature of the states can eventually be obtained. It may however require ESA measurements to be carried out at low temperatures and with adequately tunable pumping sources.

ACKNOWLEDGMENTS

We are grateful to Dr. L.H. Brixner of E.I. du Pont de Nemours and Co. for supplying the $CaWO_4$ sample. The support of the U.S. Army Research Office under Grant DAAL03–88–0103 is also gratefully acknowledged.

Appendix: KINETICS OF ESA

The presence of a slow component of ESA forces us to postulate the existence of an additional ESA process, originating from a level other than the luminescence level.

The simplest kinetic model capable to reproduce the observed decay of ESA is shown in Fig.10 and can be described by the following set of decay equations:

$$\begin{aligned} \dot{n}_1 &= a_{21}n_2 + a_{31}n_3 \\ \dot{n}_2 &= -Gn_2 \\ \dot{n}_3 &= kn_2 - (a_{31} + b_3I)n_3 \end{aligned} \tag{1}$$

and

$$EST = e^{-(\sigma_2 n_2 + \sigma_3 n_3)L} \tag{2}$$

where $G = a_{21} + b_2I + k$, n_i are populations of i–th states, a_{ij} – rates of spontaneous $i \longrightarrow j$ transitions, $b_{2,3}I$ are the rates of ESA transitions from 2–nd and 3–rd level, k is an "intersystem" crossing rate, σ_2 and σ_3 are components of total crossection σ_{ESA}, and L is the length of the medium. For simplicity we neglected the pumping process, instead assuming the boundary conditions: $n_1(0) = N - N_2 - N_3$, $n_2(0) = N_2$, and $n_3(0) = N_3$, where N_2 and N_3 are initial populations estimated from excitation strength and N is the total number of centers in cm^3. The solutions are following:

$$\begin{aligned} n_2(t) &= N_2 e^{-Gt} \\ n_3(t) &= Ce^{-(a_{31} + b_3I)t} + \frac{k}{a_{31} + b_3I - G} N_2 e^{-Gt} \\ n_1(t) &= N - N_2\left[1 + \frac{k}{a_{31} + b_3I - G}\right]e^{-Gt} - Ce^{-(a_{31} + b_3I)t} \end{aligned} \tag{3}$$

and $$C = N_3 - \frac{k}{a_{31} + b_3I - G} N_2$$

The solutions expressed in the form of ESA = 1 – EST, (see (2)) and luminescence intensity $\propto n_2$ are plotted in Fig. 7 (dotted lines) for parameters specified in the caption. The fit is not very sensitive to the precise values of parameters. The results suggest that the long lasting component of ESA decay is connected with some background population $n_3 \simeq N_3$ which partakes in ESA but does not contribute to luminescence. We believe that it is a population of well known phosphorescent traps [3–5]. Their phosphorescence is very weak in comparison to WO_4^{2-}/WO_3 luminescence and its decay time is of the order of hours (according to [3,4] and our own observations). Our results show that N_3 may be five orders of magnitude smaller than N_2 and still contribute to ESA, but it is observable only at long times.

References

[1] K.H. Butler, *Fluorescent Lamp Phosphors, Technology and Theory*, (The Pensylvania University Press, University Park and London, 1980)

[2] W. Krupke and M.J. Weber, *Prospects for New Dielectric Solid State Lasers*, at Topical Meeting on Tunable Solid State Lasers, October 26 – 28, 1987, Williamsburg, Virginia, Technical Digest, vol. 20

[3] R.H. Gillette, Rev. Sci. Instrum. 21 (1950) 294

[4] J.R. Cook, Proc. Phys. Soc. (London) 71 (1958) 422

[5] J.R. Cook, Proc. Phys. Soc. B 68 (1955) 148

[6] W. Walter and K.H. Butler, J. Electrochem. Soc. 116 (1969) 1245

[7] R. Grasser, E. Pitt, A. Scharmann, and G. Zimmerer, Phys. Stat. Sol. (b) 69 (1975) 359

[8] R. Grasser and A. Scharmann, J. Luminescence, 12/13 (1976) 473

[9] G. Beard, W.H. Kelly, and M.L. Mallory, J. Appl. Phys. 33 (1962) 144

[10] R. Biederbick, G. Born, A. Hofstaetter, and A. Scharmann, Phys. Stat. Sol. B 69 (1975) 55

[11] V. Schäfer, Z. Physik, 166 (1962) 429

[12] T. Ziegler, A. Rauk, and E.J. Baerends, Chem. Phys. 16 (1976) 209

[13] R.G. Peterson and R.C. Powell, J. Luminescence, 16 (1978) 285

[14] J.H. van der Waals, Acta Phys. Polon. A 71, (1987) 809

[15] W. Barendswaard, R.T. Weber, and J.H. van der Waals, J. Chem. Phys. 87 (1987) 3731

[16] J.H. van der Waals, Int. Rev. Phys. Chem. 5 (1986) 219

[17] G. Blasse, Structure and Bonding, 42 (1980) 1

[18] R. Kebabcioglu and A. Müller, Chem. Phys. Lett. 8 (1971) 59

[19] H. Ronde and G. Blasse, J. Inorg. Nucl. Chem. 40 (1978) 215

[20] W.A.J.A. van der Poel, M. Noort, J. Herbich, C.J.M. Coremans, and J.H. van der Waals, Chem. Phys. Lett. 103 (1984) 245

[21] W.A.J.A. van der Poel, J. Herbich, and J.H. van der Waals, Chem. Phys. Lett. 103 (1984) 253

[22] B. Di Bartolo, *Optical Interactions in Solids*, (John Wiley & Sons, Inc., New York, London, Sydney, Toronto, 1968)

[23] L.J. Andrews, S.M. Hitelman, M. Kokta, and D. Gabbe, J. Chem. Phys. 84 (1986) 5229

[24] N. Bloembergen, Appl. Opt. 12 (1973) 661

[25] Cz. Koepke, A.J. Wojtowicz, and A. Lempicki, J. Opt. Soc. Amer. B 8, (1991), in press

[26] C.E. Tyner and H.G. Drickamer, J. Chem. Phys. 67 (1977) 4103

[27] G. Blasse and W.J. Schipper, Phys. Stat. Sol. (a) 25 (1974) K163

[28] M.J. Treadaway and R.C. Powell, J. Chem. Phys. 61 (1974) 4003

[29] D.E. McCumber, Phys. Rev. 134 (1964) A299

[30] A.J. Wojtowicz, W. Meng, A. Lempicki, G.H. Beall, D.W. Hall, and T.C. Chin, IEEE J. Quantum Electron. QE–24 (1988) 1109

[31] L.J. Andrews, A. Lempicki, B.C. McCollum, C.J. Giunta, R.H. Bartram, and J.F. Dolan, Phys. Rev. B 34 (1986) 2735;

[32] R.H. Bartram, J.C. Charpie, L.J. Andrews, and A. Lempicki, Phys. Rev. B 34 (1986) 2741

[33] Cz. Koepke and A. Lempicki, J. Luminescence, 47 (1991) 189

[34] W. Barendswaard and J.H. van der Waals, Molec. Phys. 59, (1986) 337

[35] Cz. Koepke and A. Lempicki, to be published

Figure captions

Fig. 1 (a) One–electron MO theoretical energies (after [18]) and, (b) semiempirical calculations of the total electronic energy and term assignments for WO_4^{2-} complex, (after [1]). Each circle in (a) corresponds to a pair of different–spin electrons.

Fig. 2 Experimental setups used in excitation–and–probe beam measurements. Both arrangements use transverse pumping provided by an excimer laser. Setup (a) uses single wavelength probe beam and fast transient recorder detection. Setup (b) uses broad band probe beam and an OMA detection system. The letters denote as follows:
PD–s – photodiodes, S – sample, BB – beam blockers,
UVF–s – ultraviolet filters, OF – optic fiber, $\omega/2$ – repetition rate divider.

Fig. 3 Dependence of the governing (WO_4^{2-}) luminescence decay time on temperature (circles). Solid line is theoretical curve calculated with equation (3) for the activation energy $\Delta E = 300$ meV and frequency factor $s = 5.35 \times 10^9\ s^{-1}$. Measurements performed for total luminescence output.

Fig. 4 Family of emission spectra measured at various temperatures under excimer excitation ($\lambda = 308$ nm).

Fig. 5 RT and HT spectra and WO_3 center emission spectrum extracted from them. To do this, we used the following recipe: SCH = RT – F·HT, where F=0.62 is a factor implicitly describing the increase of excitation under heating.

Fig. 6 Excited–state absorption and luminescence decays at room temperature. Dashed line shows zero level for both decays. An actual scale of ESA is from 0 (zero level) to ~ 8 % in the peak. Insert presents logarithms of these decays.

Fig. 7 ESA and luminescence decays at high temperature (solid lines) fitted with kinetic model described in appendix (dotted lines). The parameters used are: $N_2 = 4.8 \times 10^{17}$ cm^{-3}, $N_3 = 10^{12}$ cm^{-3}, $a_{21} = 10^6$ s^{-1}, $a_{31} = 2 \times 10^{-4}$ s^{-1}, $b_2 = 1.3$ cm^2/(Ws), $b_3 = 0.4$ cm^2/(Ws), $k = 10^6$ s^{-1}.Dashed line is zero level for both decays, insert shows logarithmic decays. ESA range: 0 – 13 % .

Fig. 8 ESA crossection spectra (a) and stimulated emission spectra (b) calculated from McCumber theory using measured luminescence spectra, both measured at RT and HT. The excitation parameters corresponding to ESA measurements were: $p = 7.4 \times 10^{-5}$ for RT and $p = 1.2 \times 10^{-4}$ for HT. Stimulated emission crossections were calculated with radiative lifetime $\tau = 1.5 \times 10^{-5}$ sec.

Fig. 9 Quantitative single–configuration–coordinate model of $CaWO_4$ constructed on the basis of measured emission and ESA spectra and 10 Dq value taken from [8]. Dashed line represents the first excited state of WO_3 complex.

Fig. 10 Kinetic model explaining ESA in $CaWO_4$ crystal.

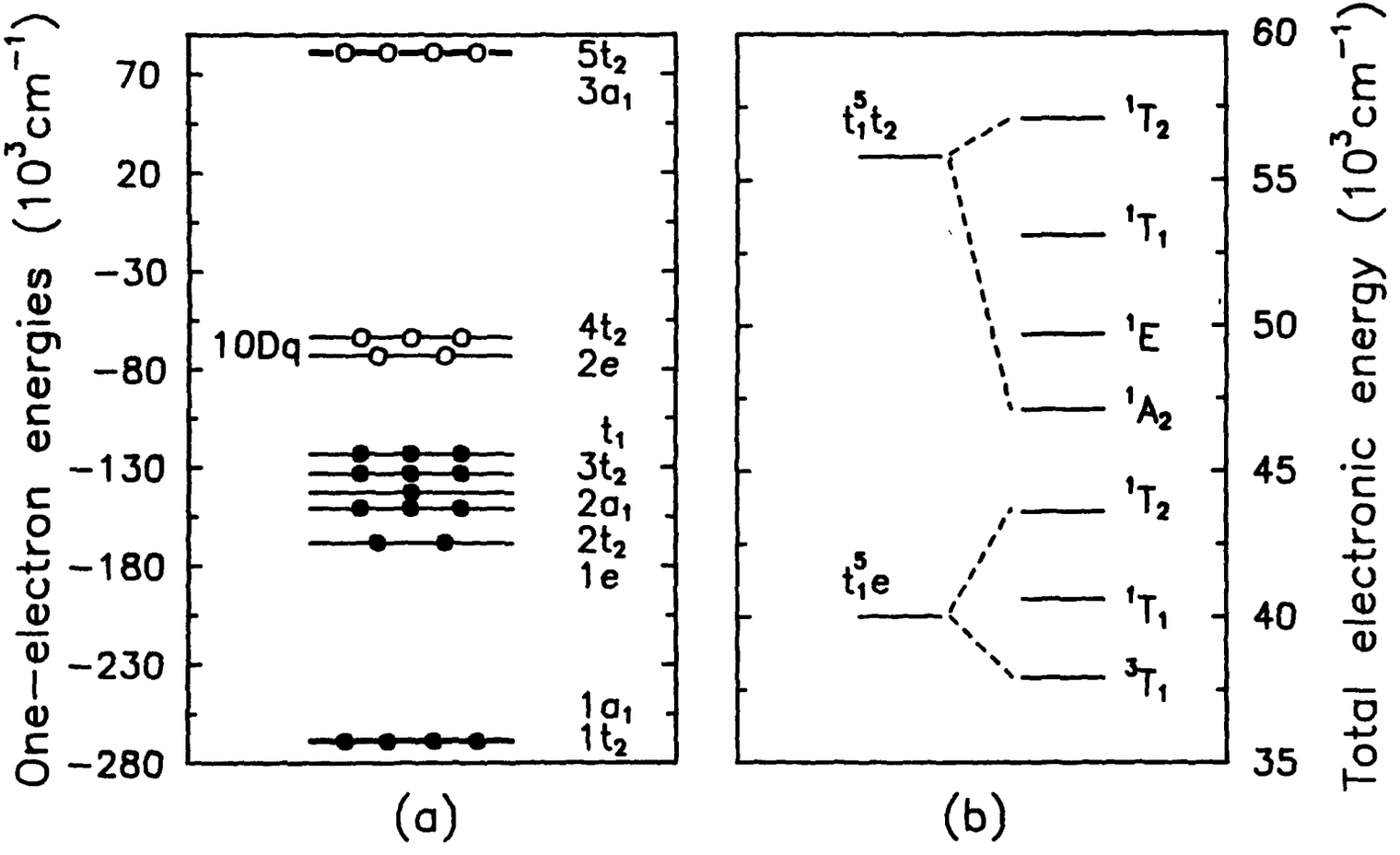
One-electron energies ($10^3 cm^{-1}$)
70
20
-30
-80
-130
-180
-230
-280
10Dq
$5t_2$
$3a_1$
$4t_2$
$2e$
t_1
$3t_2$
$2a_1$
$2t_2$
$1e$
$1a_1$
$1t_2$
(a)
$t_1^5t_2$
t_1^5e
$^1T_2$
$^1T_1$
^1E
$^1A_2$
$^1T_2$
$^1T_1$
$^3T_1$
(b)
60
55
50
45
40
35
Total electronic energy ($10^3 cm^{-1}$)

Fig. 1 [illegible]

(a)

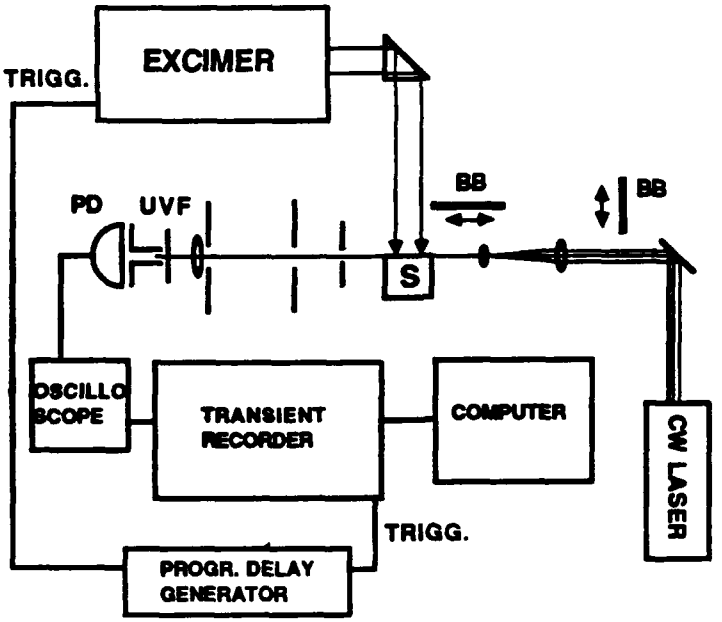
TRIGG.
EXCIMER
PD
UVF
BB
BB
S
OSCILLO SCOPE
TRANSIENT RECORDER
COMPUTER
CW LASER
TRIGG.
PROGR. DELAY GENERATOR

(b)

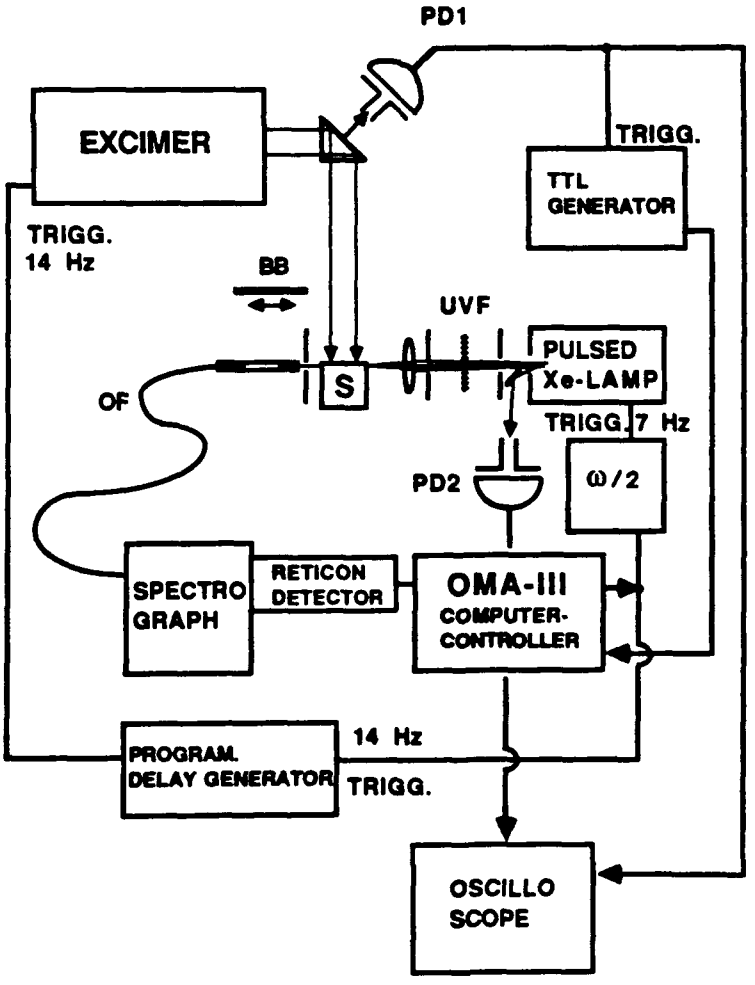
PD1
EXCIMER
TRIGG.
TTL GENERATOR
TRIGG. 14 Hz
BB
UVF
PULSED Xe-LAMP
S
OF
TRIGG. 7 Hz
PD2
ω/2
SPECTRO GRAPH
RETICON DETECTOR
OMA-III COMPUTER-CONTROLLER
PROGRAM. DELAY GENERATOR
14 Hz
TRIGG.
OSCILLO SCOPE

Fig. 2

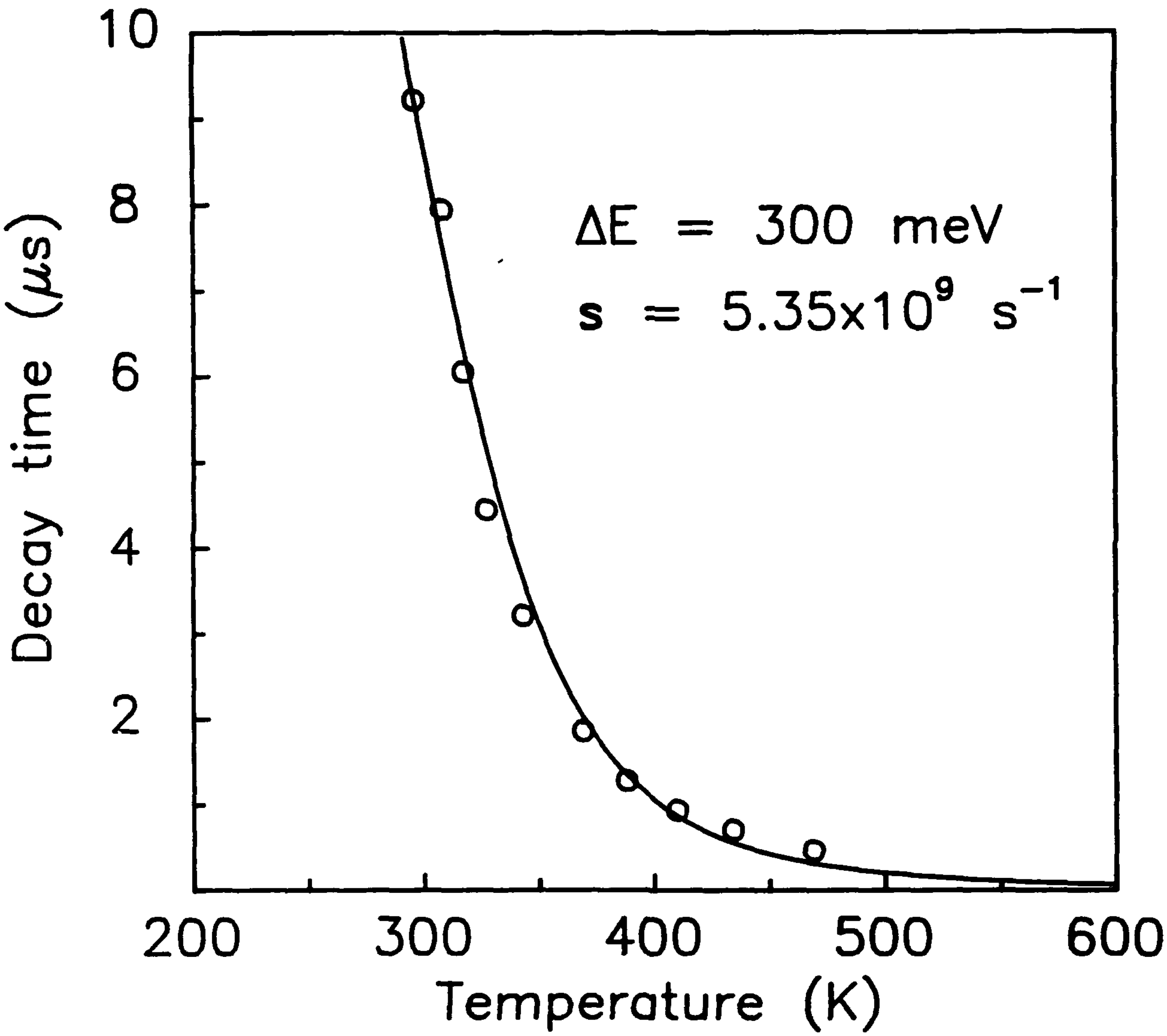

10
8
6
4
2
200
300
400
500
600
Decay time (μs)
Temperature (K)
ΔE = 300 meV
s = 5.35x10^9 s^-1

Fig. 3

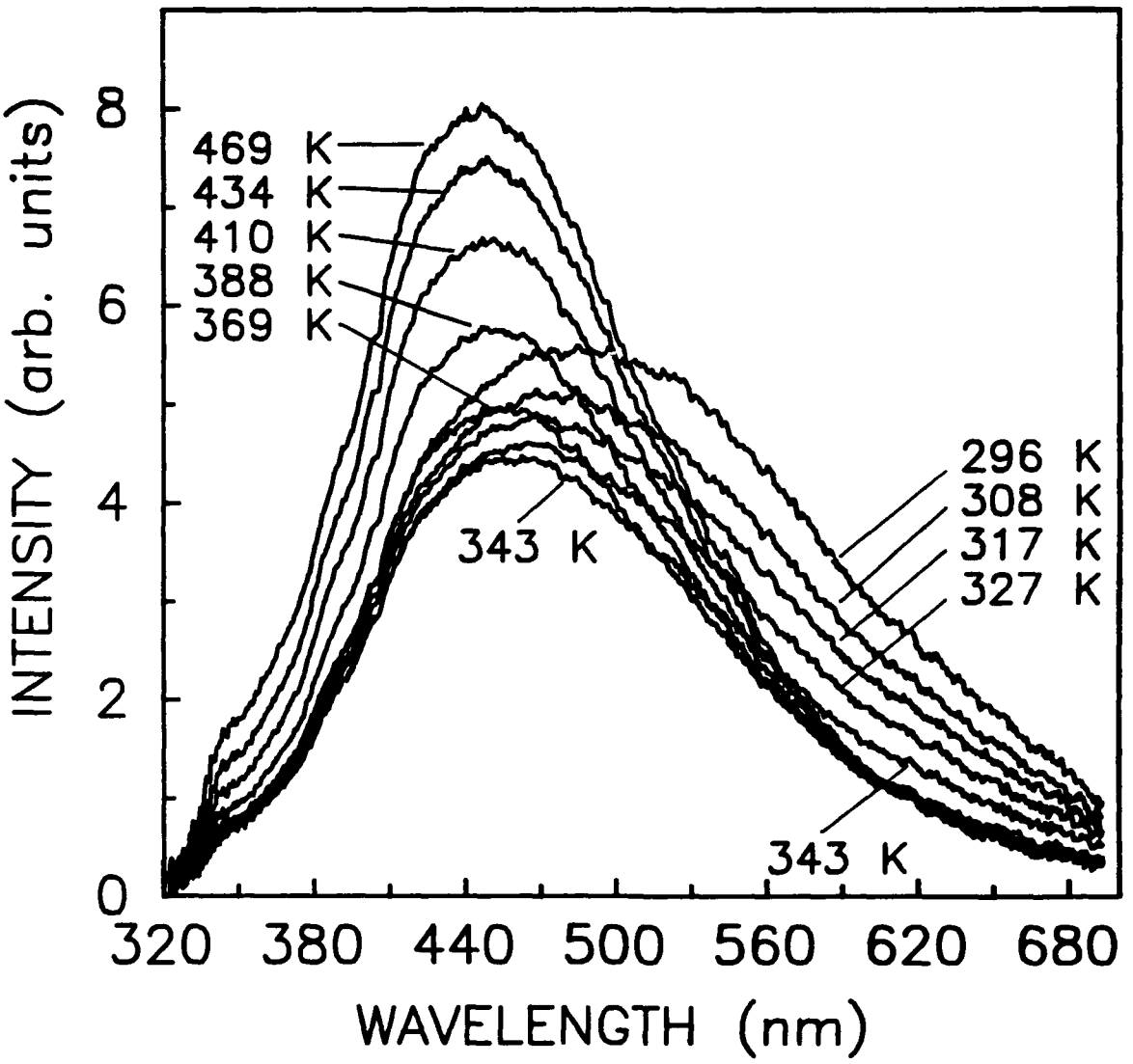
INTENSITY (arb. units)
0
2
4
6
8
469 K
434 K
410 K
388 K
369 K
343 K
296 K
308 K
317 K
327 K
343 K
320
380
440
500
560
620
680
WAVELENGTH (nm)

Fig. 4

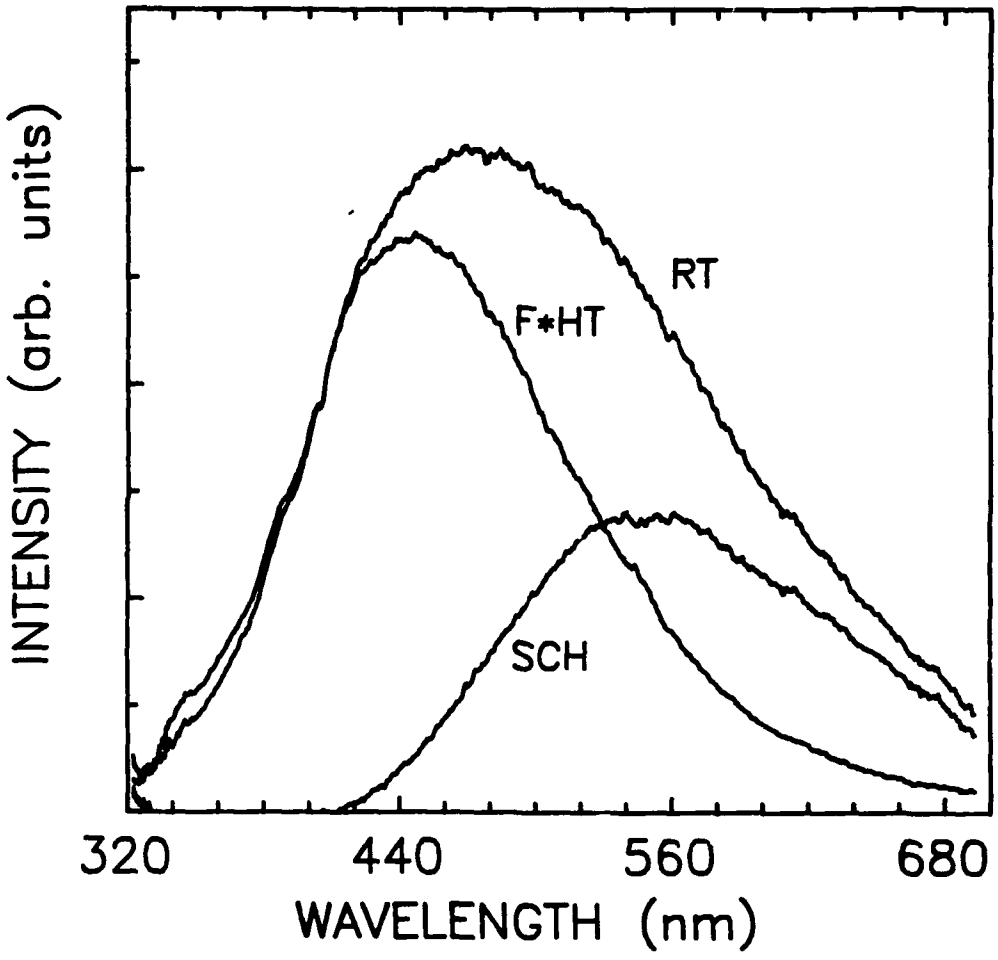

Fig. 5

G. Kopine et al. "Excited-State Absorption in Ex... Fungicol

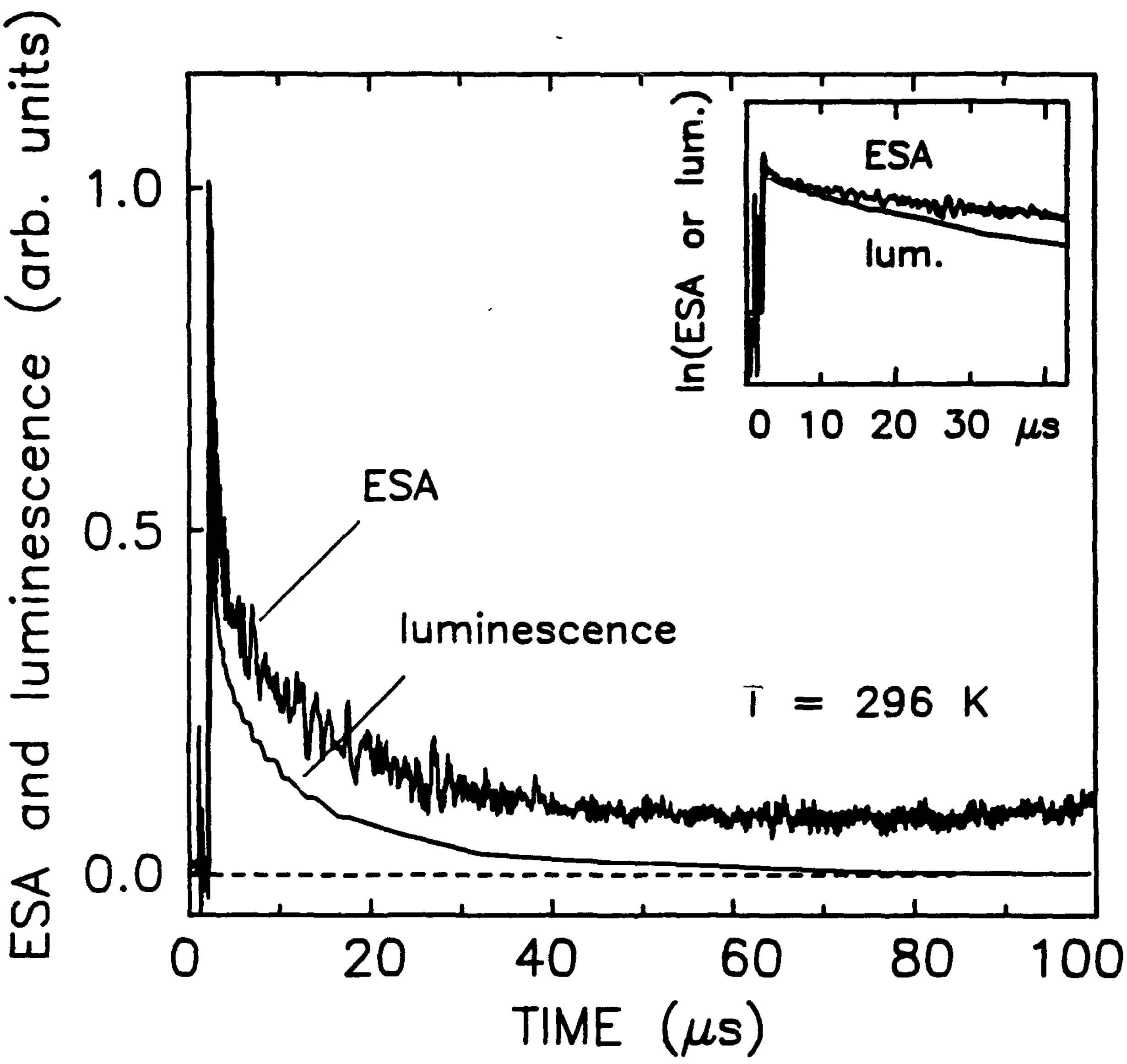

Fig. 6

G. Koepke et al, Excited-State Absorption in [illegible] [illegible] Cr:GSGG

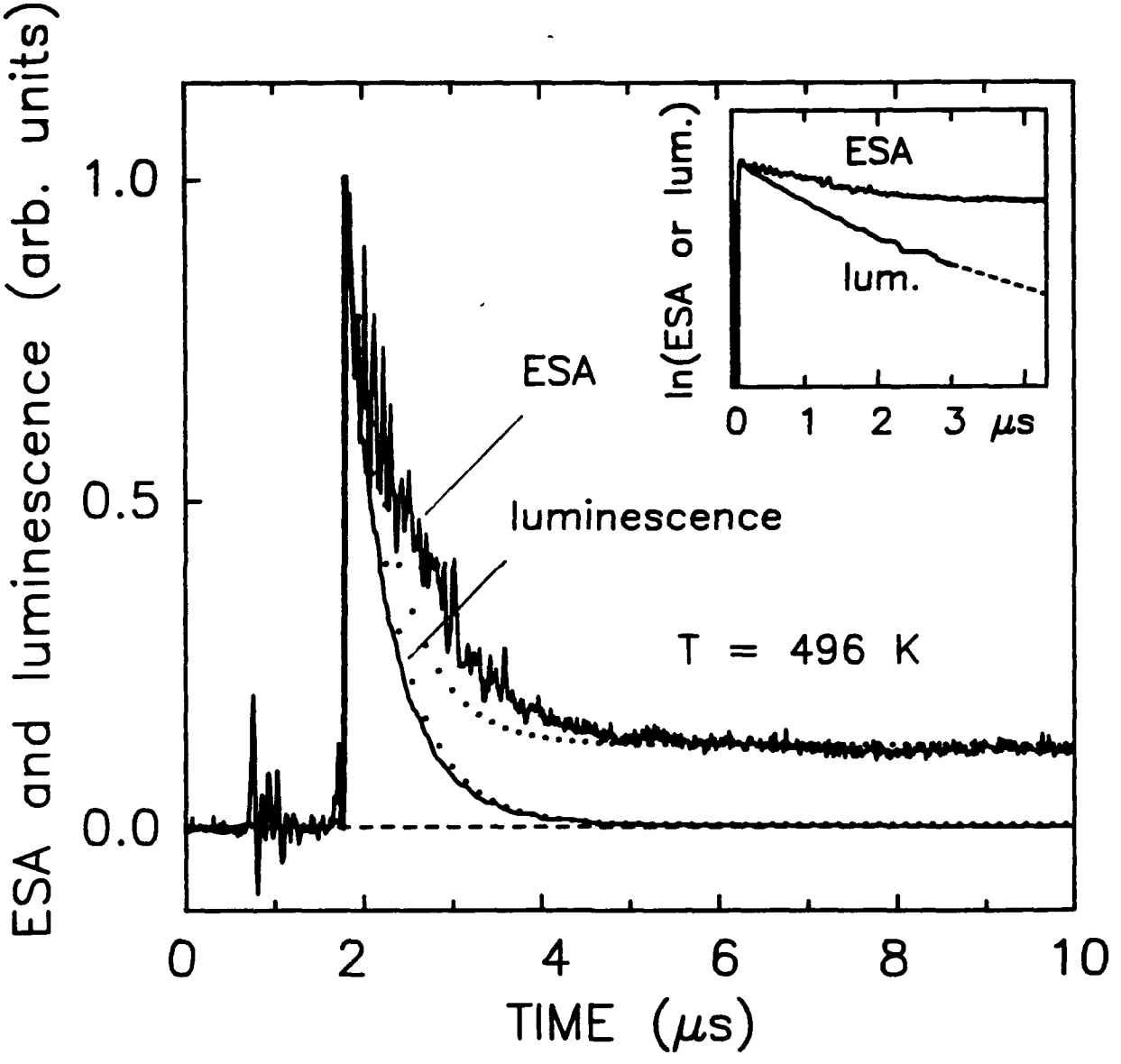

Fig. 7

C. Koepke et al. "Excited-State Absorption in Excimer-Pumped $Tm:WO_4$"

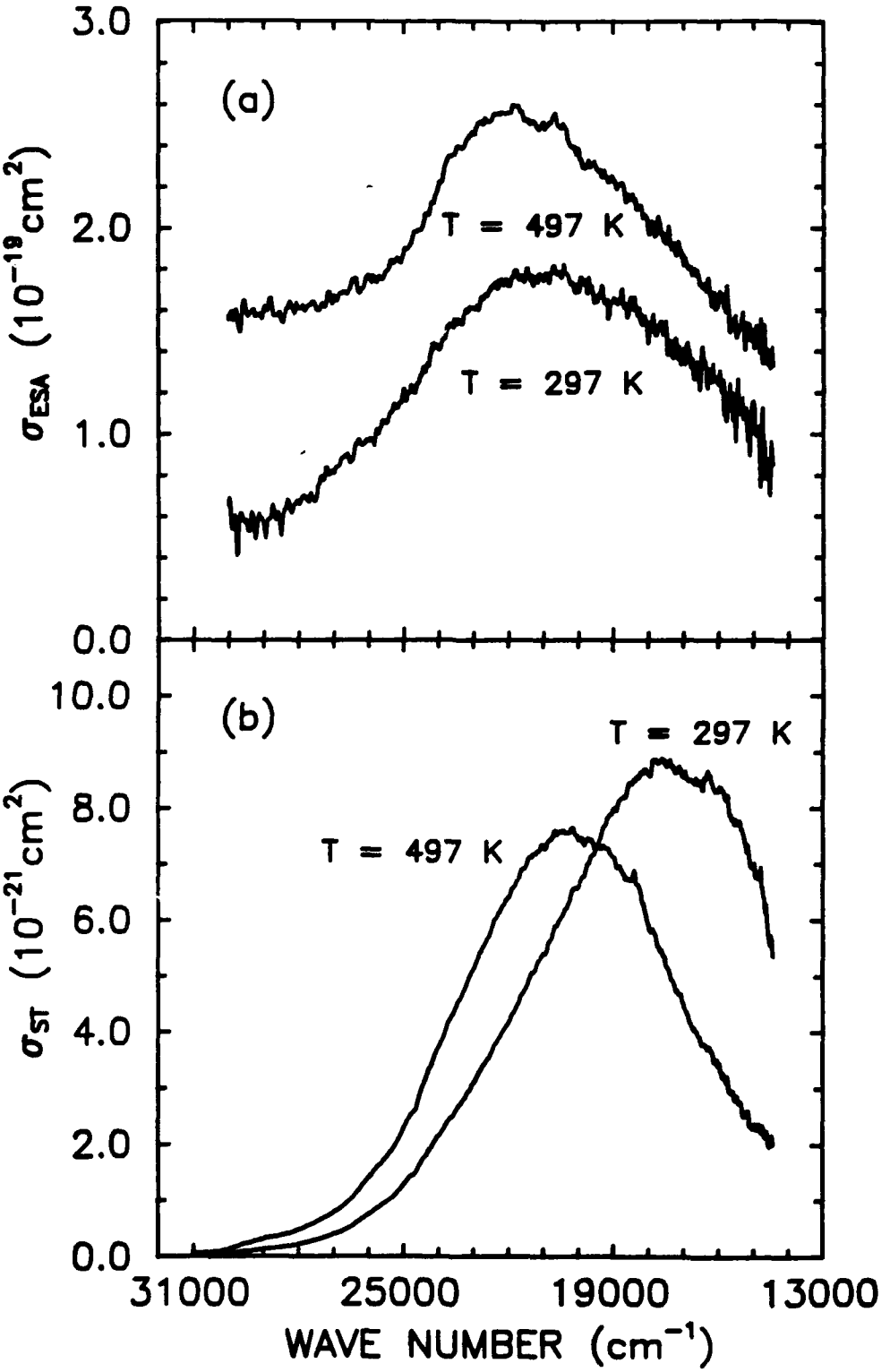

Fig. 8 C. Vaughn et al., "Excited-State ... in Erbium-Doped ..."

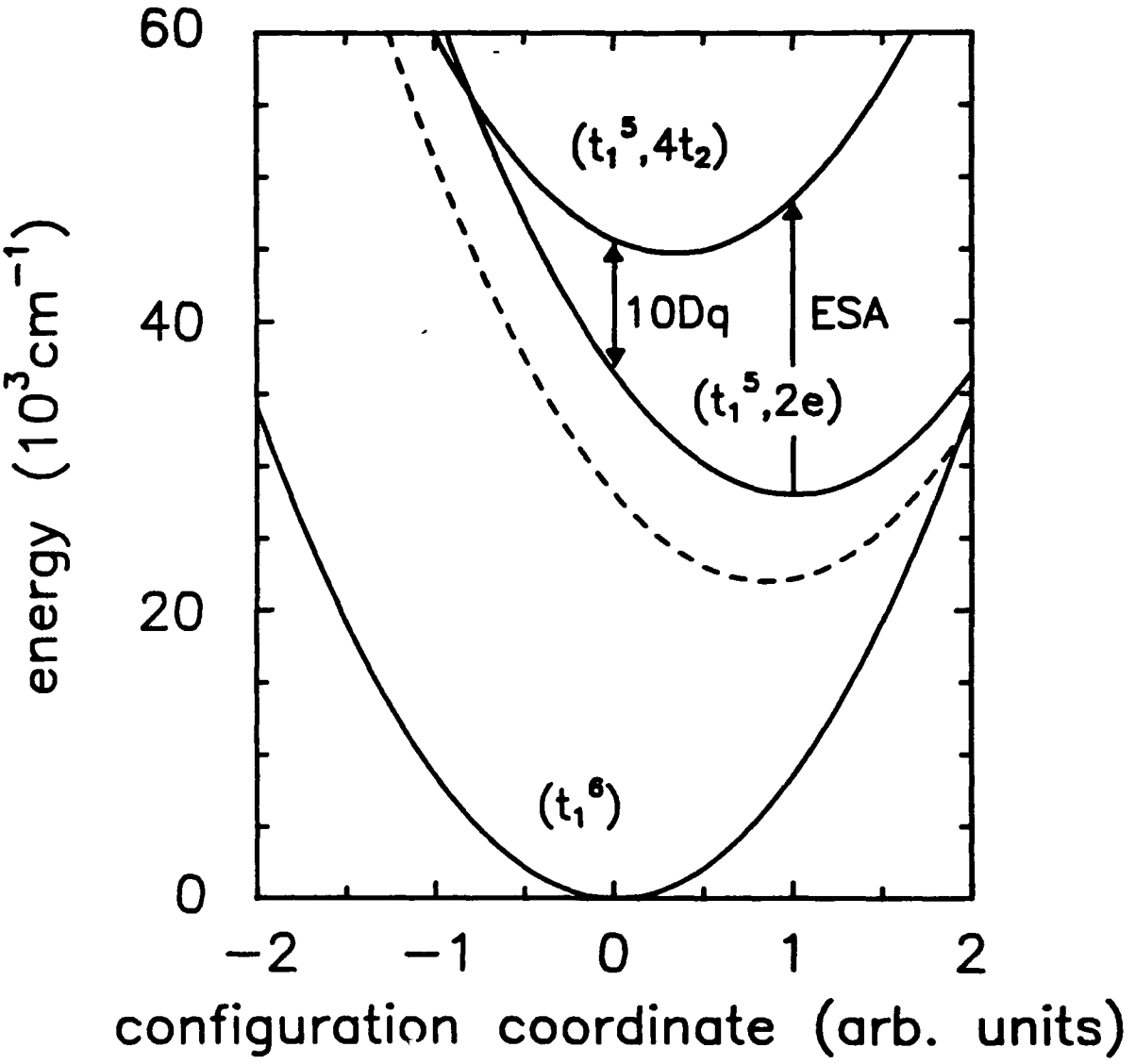

Fig. 9

C. Keeple et al. "Excited-State Absorption in Excimer-Pumped $CaWO_4$"

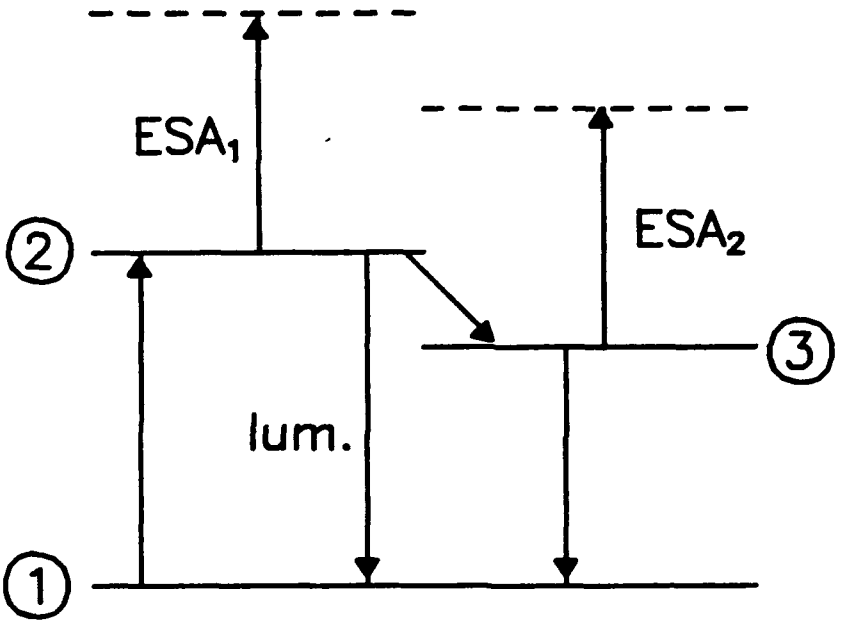

Fig. 10

Co Koephe et al., Excited-State Absorption in Excimer-Pumped C...

EXCITED-STATE ABSORPTION IN $ZnWO_4$ CRYSTAL

Cz. Koepke* and A. Lempicki

Boston University, Chemistry Department, 590 Commonwealth Ave., Boston, MA 02215

Abstract

We report the first time measurement of Excited–State Absorption (ESA) in a zinc tungstate ($ZnWO_4$) crystal. The ESA is assigned to the $2e \rightarrow 4t_2$ transitions and can be related to the 10Dq energy in T_d symmetry. The breadth and height of the ESA spectrum, compared with stimulated emission spectrum, precludes any possibility of laser action in this material. Using measured spectroscopic parameters we create a single–configuration–coordinate model, employing measured ESA. Judging from this diagram, the terminal state of ESA transitions, is likely to be affected by an admixture of p–orbitals of the tungsten ion into its d–orbitals. Together with a large internal heavy atom effect, p–orbitals can contribute to spin–orbit coupling which, in turn, causes a triplet character of the higher excited state.

*On leave from Institute of Physics, N. Copernicus University, Toruń, Poland

1. Introduction.

$ZnWO_4$ is a well known phosphor, often used as a host for various dopants. Recently doped with Cr^{3+} it became a broad–band tunable laser around ~ 1 μm [1]. There is a rather small number of papers dealing with optical properties of undoped $ZnWO_4$. The crystal has a monoclinic structure [1,2]. Its optical properties are mostly determined by the WO_4^{2-} molecular complex and are strongly affected by charge transfer processes [3]. The fourfold coordinated tungsten ion, of T_d symmetry, is in $5d^0$ electronic configuration. According to known one–electron molecular orbital energy diagrams [4,5] the WO_4^{2-} complex can be excited via $t_1 \rightarrow 2e$ transition. The next, higher transition can occur between the 2e and $4t_2$ states, split by 10Dq (d–d transition) (Fig. 1 of ref. [6]).

Undoped $ZnWO_4$ has been considered as a promising scintillator [2,7–10], but has never been suggested as a possible candidate for a tunable laser. Its broad luminescence spectrum (in the very desirable blue–green region) and high absorption in the ultraviolet (UV), together with the availability of UV pumping sources as excimer lasers, made this crystal of interest as a potential, optically pumped, tunable laser.

In this paper we report on the strong Excited–State Absorption (ESA) in $ZnWO_4$ which, compared with stimulated emission, precludes laser action, but is itself interesting and, we believe, contributes something new to the spectroscopy of tetra–oxo ions in crystals.

2. Experiment.

The sample used in our experiments was carefully polished on entrance, exit, and pumped faces. $ZnWO_4$, because of its monoclinic structure has a very distinct cleavage direction which makes this crystal difficult to machine. We have chosen the pumped

face to be polished along the cleavage plane (010), since the entrance and exit faces, perpendicular to this plane, are thus easier to polish and obtain mirror–like surface quality. The resulting sample was 1.1 cm long and 1.5 mm thick.

The excite–and–probe–beam experiments were carried out in transverse geometry, using two sources of excitation: an excimer laser (XeCl) working at 308 nm or a nitrogen laser working at 337.1 nm. The excimer laser was used in the measurements of ESA and luminescence decays and the luminescence spectra , whereas a N_2 laser was chosen for taking the ESA spectrum. In ESA measurements the probe beams were provided by an krypton laser (excimer pumping) and by a Xe flash lamp (with the nitrogen pumping). The temporal behaviors of the ESA and luminescence were detected by a fast photodiode coupled to a transient recorder and to a computer acquiring the data. Both, luminescence and ESA spectra were detected and acquired by an OMA–III system, for ESA measurements working in specially customized, synchronous mode [6]. Because OMA utilizes a polychromatic source as a probe beam (pulsed Xe lamp) which is hard to focus to less than ~ 500 μm, and while $ZnWO_4$ has a very shallow excitation depth, (about 30 μm), when using an excimer laser, we were forced to switch to a nitrogen laser (excitation depth ~ 250 μm at 331.7 nm) to provide a sufficient overlap of excited and probe beam volume and thus, obtain a measurable ESA effect. The changes in Excited–State Transmission {EST = I(pumped medium)/I(unpumped medium), I – probe beam intensity after passing the sample} although very small (up to 3 percent), were nevertheless sufficient to obtain a distinct ESA spectrum. The problem of the very thin excited layer with excimer laser as the pump, was not that critical, because the Kr ion laser probe beam can be focused to tens of μm–s. All these details of excitation were taken into account in deriving the ESA crossection.

In order to determine the parameters needed to calculate the stimulated emission crossection spectrum, specifically the quantum efficiency, we have carried out additional measurements of the dependence of luminescence on temperature between 23 and 450 K,

using a hi–temp, closed–cycle helium refrigerator.

3. Results.

Figure 1 shows the temperature dependence of light yield and decay for the luminescence produced by excimer laser excitation. Fig. 1a illustrates the temperature dependence of the total light output obtained by integration of luminescence spectra over the energy, the spectra having been intergated before over the time by ungated OMA. Fig. 1b gives the temperature dependence of the total light output decay. Both, light $I(T)$ and $\tau(T)$ are fitted by the familiar formula, suitable for nonradiative decays in strongly coupled systems [e.g. 11]:

$$\eta = \tau(T)/\tau(0) = I(T)/I(0) = \frac{1}{1 + \tau_r s \exp(-\Delta E/kT)} \qquad (1)$$

where $\tau_r = \tau(0)$ is the radiative lifetime, s is frequency factor, and ΔE is energy barrier for thermal activation of the excited state. Identification of $\tau(0)$ with radiative lifetime is equivalent to the assumption that at T = 0 the quantum efficiency $\eta(0)$ is 100 %. Although there are exceptions to this, it is an assumption often made in absence of absolute measurements. The expression (1) fits the experimental dependencies with ΔE = 450 meV (~ 3630 cm^{-1}) and $\tau_r s = 2.5 \times 10^7$ which for τ_r = 36 μs gives $s = 6.94 \times 10^{11}$ s^{-1}. The similar procedure was used by Grassman et al. [9], but for excitation by cosmic muons, and by Furtak et al. [12] with X–ray excitation.

The curve (1) fits the experimental data reasonably well, but room–temperature quantum efficiency of our sample, derived from these data and (1) is ~ 60 %, considerably smaller than in [9,12].

The comparison of the luminescence decay to that of ESA is presented in Fig. 2. We have been taken very special care to register the luminescence decay exactly in the same geometry as ESA decay. Otherwise both decays can differ considerably. This is caused by thermal effects in thin excited layer of the sample, that with very intense excimer beam fluence is especially effective [13]. The ESA and luminescence, decay apparently in the same manner, which is seen additionally in the inset on a logarithmic scale. This proves that both ESA and luminescence occur from the same state. Since both decays are single–exponential, we can also state that just one site is responsible for optical properties of $ZnWO_4$. This incidentally is simpler than the case of $CaWO_4$, [6], which shows an additional, long component of ESA.

Figure 3 presents the ESA crossection spectrum $\sigma_{ESA}(\lambda)$ compared to stimulated emission crossection spectrum $\sigma_{ST}(\lambda)$. $\sigma_{ESA}(\lambda)$ was derived from excitation conditions (laser energy, sample absorption, and geometry) and with the following recipe [e.g. 14]:

$$\sigma_{ESA}(\lambda) = -\frac{\ln\ EST(\lambda)}{n^{*}L} + \sigma_{GSA}(\lambda) \qquad (2)$$

where EST is the directly measured Excited–State Transmission:
$EST = \exp(-\alpha_{ESA}L)$, n^{*} is the concentration of excited complexes per cm^3, σ_{GSA} is the ground–state absorption crossection and L is the length of the medium. To calculate $\sigma_{ESA}(\lambda)$ we used $n^{*} = 4.5\times10^{16}\ cm^{-3}$ which corresponds to the excitation strength $p = n^{*}/n_0 \simeq 3\times10^{-6}$ (n_0 is total number of complexes in the ground state). The stimulated emission crossection $\sigma_{ST}(\lambda)$ was calculated from the measured room–temperature (RT) emission spectrum, with the McCumber theory of phonon–terminated lasers [15,16], RT decay time, and quantum efficiency determined before. These parameters were: $\eta(RT) = 0.6$ and $\tau(RT) = 20.9\ \mu s$. It is seen that $\sigma_{ESA}(\lambda)$ is at least two orders of magnitude greater than $\sigma_{ST}(\lambda)$ and vastly overlaps the region of emission. This, of course, precludes

any lasing in undoped $ZnWO_4$ crystals.

4. Configuration coordinate model.

Looking at typical one–electron energy diagrams for tetra–oxo ions, derived from molecular orbital calculations [4,5], it is very hard to predict if a given system would reveal optical gain or ESA. Because the 10Dq energy corresponding to ESA transitions, falls usually into the infrared [4], one could easily state that while the emission occurs in blue–green region, thus ESA should not interfere and as a result a net gain should be observed. But to handle this problem properly we must take into account the strong electron–lattice coupling which is the source of the large luminescence bandwidth. The traditional way to deal with this problem is to construct a configuration coordinate model. Using the measured spectroscopic parameters including the ESA spectrum, we created a single–configuration coordinate (SCC) diagram, which includes the higher excited state ($4t_2$). We do not write specific molecular terms in this diagram, but we strongly believe that, like in others crystals with tetra–oxo ions, such as $CaMoO_4$ and $CaWO_4$, the ground state is a totally symmetric singlet ($^1A_1$) and the luminescing state, as we know from our results – being also the source of ESA, is a triplet state [3,17,18]. Also, as shown by Butler [22], the higher excited state $4t_2$ has a singlet character. Our model is based on the following assumptions: a) harmonic approximation, the energy curves are strictly parabolic, and b) linear electron–lattice coupling – all the parabolas have the same curvature.

To construct the SCC diagram we used the following spectroscopic parameters: a) ZPL taken from emission lineshape, b) maximum of the emission lineshape, c) maximum of the ESA lineshape and, d) 10Dq energy taken from MO calculations [4]. The 10Dq value determines the distance between 2e and $4t_2$ states at the equilibrium point of the ground state parabola ($Q = 0$). Because of very strong electron–phonon coupling, the ZPL is quite

invisible, even at 4 K [19], hence we had to rely on an approximate estimation. Judging from emission lineshape, ZPL should be placed somewhere between 24600 and 26200 cm^{-1}. The emission lineshape maximum is at 18980 cm^{-1}. The maximum of absorption lineshape, quite unmeasurable in our case because of very strong allowedness of GSA transitions, should be somewhere around 300 nm (Ref.[8] and our own data). Having this in mind we took the higher value for ZPL: 26200 cm^{-1} as the most probable, which corresponds to a Stokes Shift ~ 14440 cm^{-1} and gives reasonable value for absorption maximum: ~ 33420 cm^{-1}. The ESA lineshape maximum occurs at ~ 20870 cm^{-1}.

The energies of the three states are obtained by using the following set of equations:

$$\begin{aligned} E_1 &= A\,Q^2 \\ E_2 &= A(Q - Q_o)^2 + ZPL \\ E_3 &= E_2 + 10Dq + C\,Q \end{aligned} \qquad (3)$$

where Q is the configuration coordinate expressed in arbitrary units, Q_o is the equilibrium position of the first excited state (2e), and $C = \tilde{\nu}(ESA_{max}) - 10Dq = -2AQ_oQ_1$ with Q_1 designating the equilibrium position of the higher excited state ($4t_2$) in respect to that of the lower excited state (2e) (in such a convention Q_1 is negative).

The SCC diagram was calculated with the convenient normalization: $Q_o = 1$.

The result is illustrated in Fig. 4. Note that the first excited–state parabola is shifted to the right if one adopts the sign convention of eqs. (3). This shift undoubtedly is related to $t_1 \rightarrow 2e$ charge redistribution accompanying the charge transfer transition. It is interesting that the second excited–state parabola (terminal state of the $2e \rightarrow 4t_2$ ESA transition) is shifted in the opposite direction. Interpretation of these shifts in terms of changes of ionic size (Blasse [20]) is at best risky, but consistency in interpreting the SCC model would indicate a charge redistribution back to the ligands.

To the extend that the luminescing state has a predominantly triplet character and

terminal ESA state is supposed to be a singlet [22], the strength of the ESA transition in comparison with that of the luminescence, indicates that the terminal state of ESA must have a decidedly mixed singlet–triplet character. Existence of strong luminescence proves itself that such a mixing occurs and is very efficient. This mixing can occur via spin–orbit interaction or e.g. as a consequence of the Jahn–Teller effect [23,24]. Because so far there is no report about Jahn–Teller effect in $ZnWO_4$, we assume that spin–orbit coupling is mostly responsible for the mixing of singlet and triplet terms of 2e and $4t_2$ states. This is very likely, especially in view of the internal heavy atom effect [25], which with large tungsten atomic number (Z = 74) must be quite substantial.

The observation of the large width of the ESA spectra is consistent with the displacement of the second excited state parabola with respect to the first excited state, as measured by the quantity Q_1. The charge redistribution indicated by this displacement is likely to be connected with a contribution of p–orbitals of the central ion to the higher ($4t_2$) excited state [21], and possibly also with the additional contribution of $2p_\sigma$– ligands orbitals to this state (eg.[26]). The contribution of "penetrating" p–orbitals can also increase the spin–orbit coupling through their specific commutation properties with the orbital angular momentum [27,28]. The value of $|Q_1|$ can serve here as a qualitative measure of the p–orbital contribution. $|Q_1|$ is a considerable percentage of Q_o (82 %) and this fact results in very broad ESA spectrum. Thus, one can make a tentative hypothesis that in this case, the large internal heavy atom effect is the main cause responsible for the high strength of ESA transitions, whereas the contribution of p–orbitals (originated both, from the central ion and from ligands) is the cause of their broad spectrum, having itself some influence on SOC and hence on ESA strength. Our hypothesis is of course a rough simplification and a deeper insight into this problem could be provided by detailed calculations of the same type as those of Ziegler et al. [29] but addressed to the "10Dq" transitions. To our knowledge such calculations have not yet been made.

Finally, one can note that the barrier between ground and first excited state determined

from the SCC model ($\sim 12300\ cm^{-1}$) is much larger than that determined from the temperature fits of eq.(1) ($\sim 3630\ cm^{-1}$, Fig. 1). This is quite common within the SCC model, as shown before [30,31].

5. Conclusions

We have measured Excited–State Absorption (ESA) in an undoped $ZnWO_4$ crystal. Since is much stronger than the calculated stimulated emission it precludes any laser action in this material. However, the measured ESA spectrum allowed us to construct a single–configuration coordinate diagram involving the higher excited state. The shift of the equilibrium position of this state is as high as -81.4 % of that of the lower (luminescing) excited state and, hence, indicates an essential change of charge distribution in the terminal state of the ESA transitions. This is likely to be connected with the considerable admixture of p–orbitals of the central ion and of the ligands to the higher excited state. The spin–orbit coupling, which we attribute principally to the internal influence of the W^{6+} ion, can be still further increased by the p–orbitals admixture to the d–states. Spin–orbit coupling, in turn, mixes the states of different multiplicity, which in view of the triplet character of the lower excited state, makes ESA transitions much more allowed than pure, luminescence, $T - S$ transitions. We can see this in the σ_{ESA}/σ_{ST} ratio, and in the σ_{ESA} value itself. We hope that these results may give an incentive to calculations similar to ref. [29], but for the transitions between excited states.

Acknowledgments

The crystal samples of $ZnWO_4$ were supplied by Dr. Kurt Nassau. We are grateful to Dr. A.J. Wojtowicz for numerous and valuable discussions. The support of U.S. Army Research Office under Grant DAAL03–88–0103 is gratefully appreciated.

References

[1] W. Kolbe, K. Petermann, and G. Huber, IEEE J. Quantum. Electron. QE–21, (1985) 1596

[2] B.C. Grabmaier, IEEE Trans. Nucl. Sci. NS–31, (1984) 372

[3] G. Blasse, Structure and Bonding, 42, (1980) 1

[4] R. Kebabcioglu and A. Müller, Chem. Phys. Lett. 8, (1971) 59

[5] R. Grasser, E. Pitt, A. Scharmann, and G. Zimmerer, Phys. Stat. Sol. (b) 69, (1975) 359

[6] Cz. Koepke, A.J. Wojtowicz, and A. Lempicki, "Excited–State Absorption in Excimer–Pumped $CaWO_4$ Crystal", to be published

[7] T. Oi, K. Takagi, and T. Fukazawa, Appl. Phys. Lett. 36, (1980) 278

[8] P.J. Born, D.S. Robertson, P.W. Smith, G. Hames, J. Reed, and J. Telfor, J. Luminescence, 24/25, (1981) 131

[9] H. Grassmann, H.G. Moser, and E. Lorenz, J. Luminescence, 33, (1985) 109

[10] Y.C. Zhu, J.G. Lu, Y.Y. Shao, H.S. Sun, J. Li, S.Y. Wang, B.Z. Dong, Z.P. Zheng, and Y.D. Zhou, Nucl. Instr. Meth. Phys. Res. A244, (1986) 579

[11] F. Williams, in *Luminescence of Inorganic Solids*, ed. by P. Goldberg (Academic Press, New York and London, 1966)

[12] S.P. Furtak and M.V. Pashkovskii, Phys. Stat. Sol. 33, (1969) 555

[13] Cz. Koepke, A.J. Wojtowicz, and A. Lempicki, "Thermal Effects in Excimer–Excited Bismuth Germanate", J. Opt. Soc. Amer. B (1991) in press

[14] W.M. Fairbank, Jr., G.K. Klauminzer, and A.L. Schawlow, Phys. Rev. B 11, (1975) 60

[15] D.E. McCumber, Phys. Rev. 134, (1964) A299

[16] A.J. Wojtowicz, W. Meng, A. Lempicki, G.H. Beall, D.W. Hall, and T.C. Chin, IEEE J. Quantum Electron. QE–24, (1988) 1109

[17] W. Walter and K.H. Butler, J. Electrochem. Soc. 116, (1969) 1245

[18] R. Grasser and A. Scharmann, J. Luminescence, 12/13, (1976) 473

[19] C.C. Klick, J. Opt. Soc. Amer. 41, (1951) 816

[20] G. Blasse and A. Bril, "Characteristic luminescence", Philips. Tech. Rev. 31 (1970) p.317

[21] C.J. Ballhausen, *Molecular Electronic Structures of Transition Metal Complexes*, (McGraw–Hill, New York, London, Toronto, 1979)

[22] K.H. Butler, *Fluorescent Lamp Phosphors, Technology and Theory*, (The Pennsylvania State University Press, University Park and London, 1980)

[23] W. Barendswaard and J.H. van der Waals, Molec. Phys. 59, (1986) 337

[24] W. Barendswaard, R.T. Weber, and J.H. van der Waals, J. Chem. Phys. 87 (1987) 3731

[25] D.S. McClure, J. Chem. Phys. 17, (1949) 905

[26] M. Karplus and R.N. Porter, *Atoms and Molecules; an introduction for students of physical chemistry*, (W.A. Benjamin, New York, 1970)

[27] S.P. McGlynn, T. Azumi, and M. Kinoshita, *Molecular Spectroscopy of the Triplet State*, (Prentice–Hall, Englewood Cliffs, New Jersey, 1969)

[28] N.J. Turro, *Modern Molecular Photochemistry*, (The Benjamin/Cummings Publishing Co., Inc. Menlo Park, California; Reading, Massachusetts; London, Amsterdam, 1978)

[29] T. Ziegler, A. Rauk, and E.J. Baerends, Chem. Phys. 16, (1976) 209

[30] L.J. Andrews, A. Lempicki, B.C. McCollum, C.J. Giunta, R.H. Bartram, and J.F. Dolan, Phys. Rev. B 34, (1986) 2735

[31] R.H. Bartram, J.C. Charpie, L.J. Andrews, and A. Lempicki, Phys. Rev. B 34, (1986) 2741

Figures captions

Fig. 1 (a) Dependence of total luminescence light yield on temperature;
(b) dependence of decay time of total luminescence output on temperature.
Both experimental data (circles) are fitted by theoretical curve (eq.1)

Fig. 2 Comparison of ESA and luminescence decays. Insert shows them on a logarithmic scale.

Fig. 3 Comparison of ESA crossection (dashed line) with stimulated emission crossection (solid line).

Fig. 4 Single–configuration coordinate diagram of $ZnWO_4$ crystal.

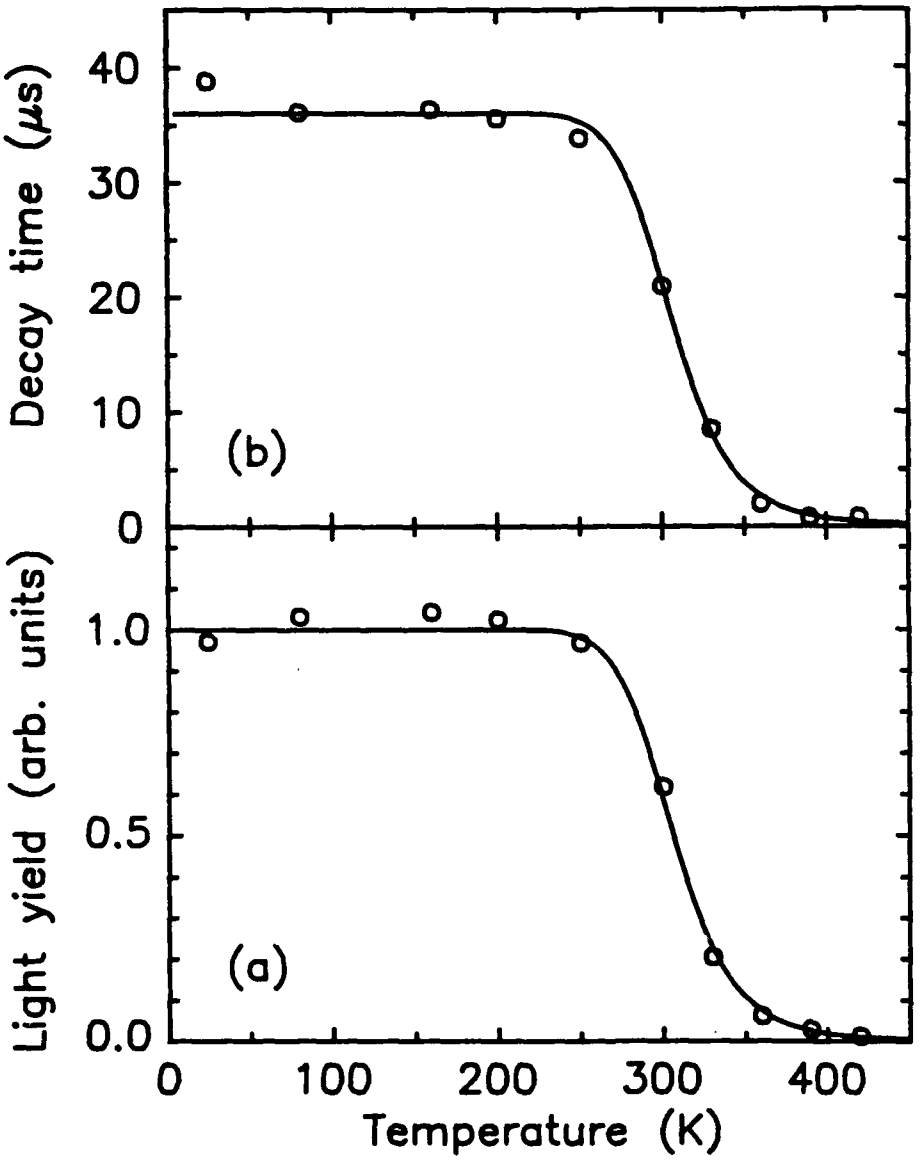

Fig. 1

G. Kispert and A. Lempicki
"Excited-State Absorption in Ti:Sapphire Crystal"

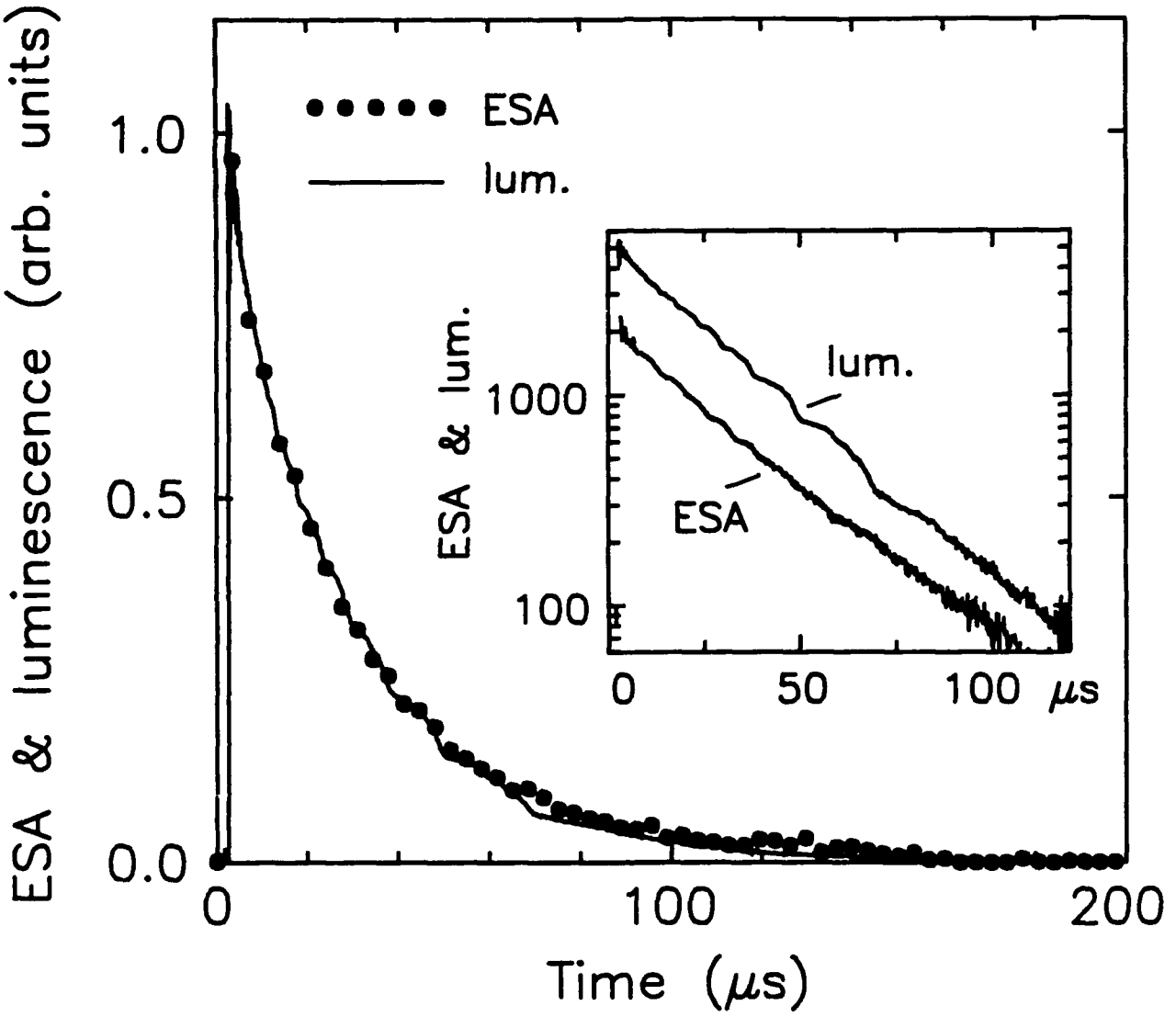

Fig. 2

C. Lempicki and A. Lempicki
"Excited State Kinetics in $ZnWO_4$ crystal"

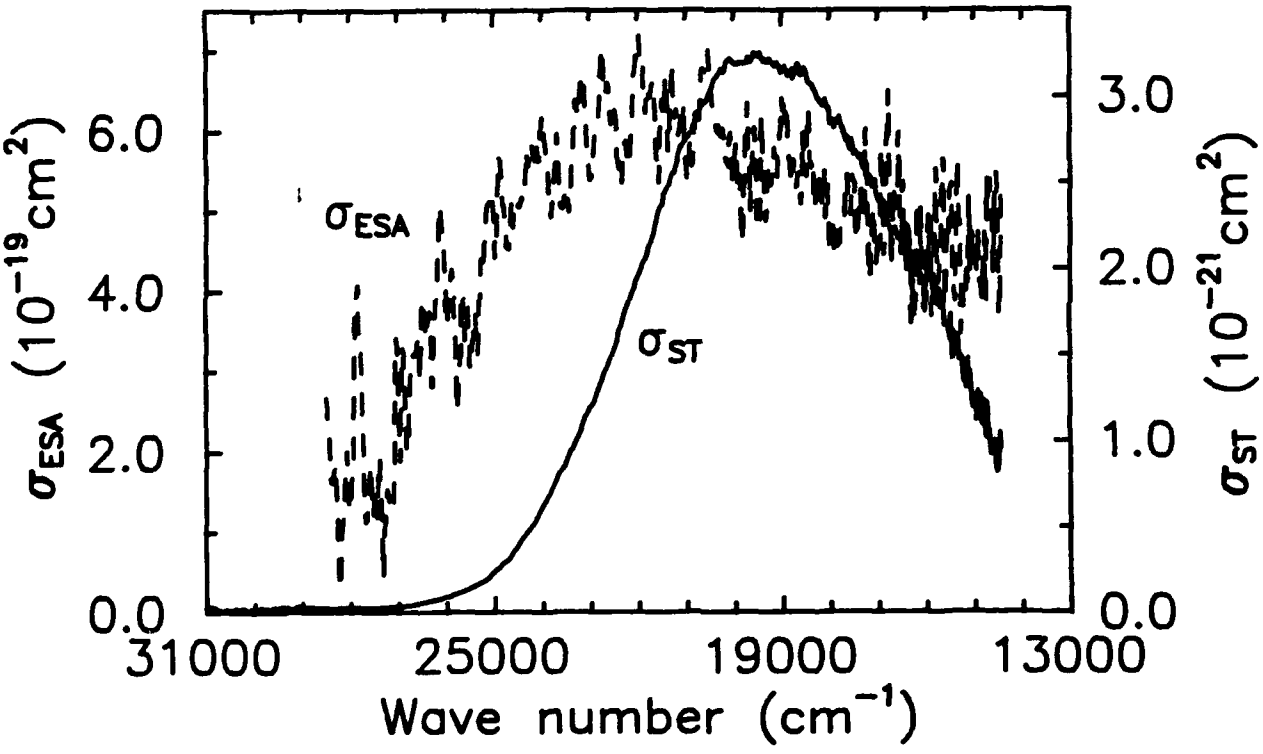

Fig. 3

Cz. Koepke and A. Lempicki
"Excited State Absorption in $PrWO_4$ crystal"

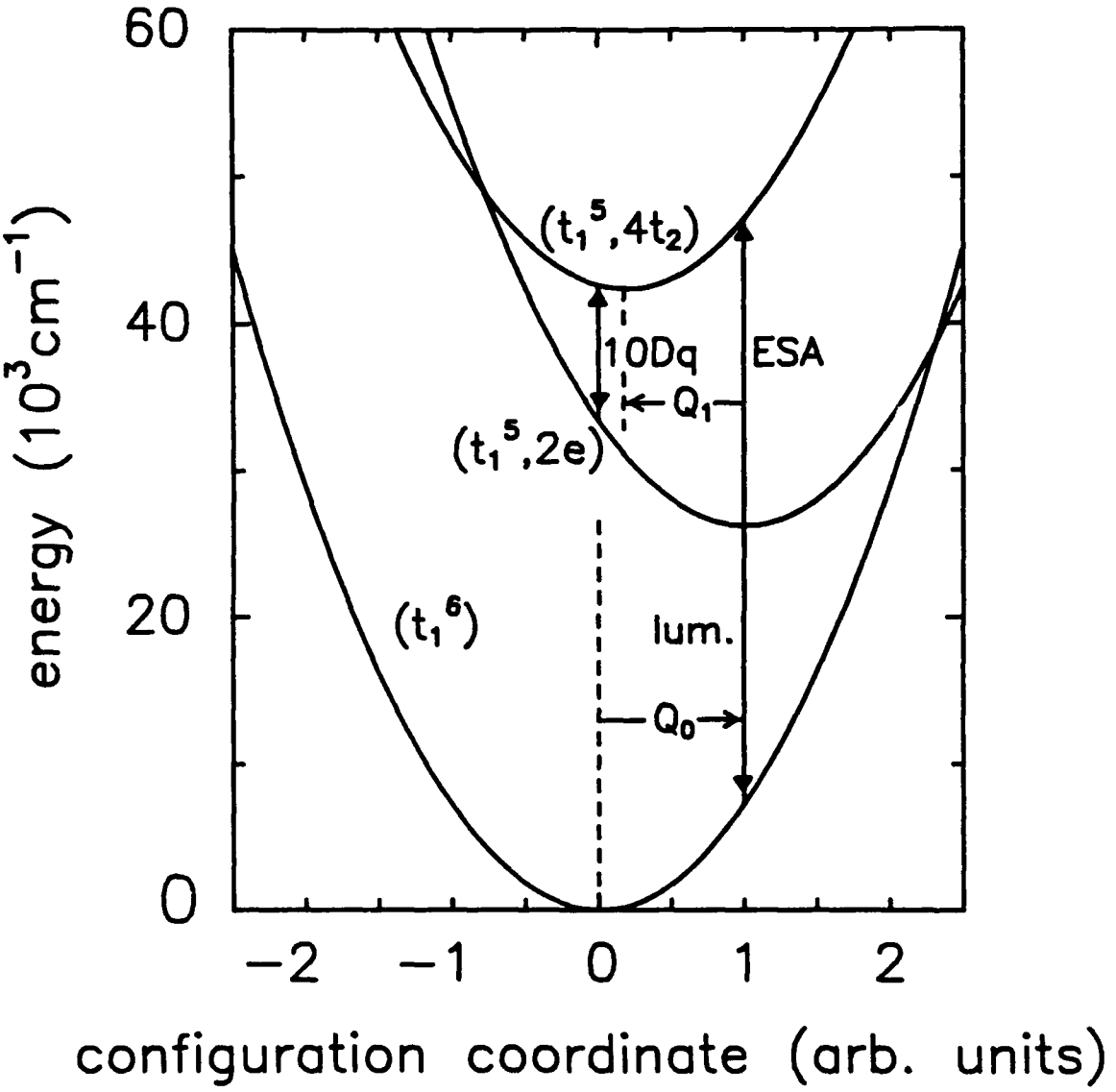

Fig. 4

Cr Knapke and A. Lempicki
"Excited-State Absorption in $ZnWO_4$ crystal"

GLASSES CONTAINING CLOSED-SHELL MOLECULAR COMPLEXES, I: LUMINESCENCE

Cz. Koepke* and A. Lempicki

Boston University, Chemistry Dept. 590 Commonwealth Ave., Boston, MA 02215

and

G.H. Beall

Corning Incorporated, Corning, New York 14831

Abstract

We report the first spectroscopic evaluation of several new glasses, containing molecular complexes of transition metal ions. Under 308 nm excitation these glasses show broad and efficient luminescence, peaking in the blue and green. We have measured the temperature dependence of the total light yield and decay time. The room–temperature quantum efficiency derived from them, appears to be quite high (e.g. ~ 88 % for zirconate glasses). The additional interesting parameters derived from fits to the temperature dependence, are the thermal activation energy ΔE and the frequency factor s. ΔE–s are relatively low but still confined to the common range. The frequency factor, however, appears unusually low.

---

*On leave from Institute of Physics, N. Copernicus University, Toruń, Poland

1. Introduction.

Luminescent glasses have always been a subject of great interest, particularly because of their laser application. To date, however, only glasses doped with Rare Earth ions have been found useful in laser technology. The ever present interest in tunable sources has directed our attention to glasses showing broad–band luminescence.

There is a whole branch of luminescence concerned with crystalline materials made of molecular complexes: central metal anion – surrounded by e.g. oxygen ligand cations [1]. These materials, sometimes loosely referred to as "phosphors", have played a dominant role in lighting and cathodo–luminescent displays. One particular group, namely crystals containing transition metal ions in d^0 configuration, has been the subject of recent study for possible laser application [2–5]. As it turned out [2–5] in some of these materials (such as $CaWO_4$, $CaMoO_4$ and $ZnWO_4$) Excited–State Absorption (ESA) was too large and precluded laser action. It was nevertheless interesting to investigate the same type of complexes in glasses, since their luminescent properties were not studied at all. Thus we have synthesized and investigated glasses containing ZrO_2 (in three concentrations), Nb_2O_5 and WO_3 groups. All these glasses have very broad luminescence spectra and some of them (Zr glasses) have quantum efficiency as high as 87 % .

2. Material

The compositions of the ZrO_2– and WO_3–containing glasses are given in Table I. The Nb_2O_5–doped composition is a proprietary Corning, Inc. glass, which is basically a pyrophosphate (~ 33 mole % P_2O_5) containing zinc and mixed alkali as the key modifiers.

It is difficult to properly asses oxygen coordination to Zr^{4+}, Nb^{5+}, and W^{6+}, the predominant ions, in these glasses. However, based on a recent EXAFS study of Zr

coordination in simple alkali silicate and fully polymerized alkali aluminosilicate compositions (Farges et al. [6]), it is expected that Zr will be 8–fold coordinated by oxygen. It is also probable that Zr polyhedra may be grouped into edge and/or corner–shared clusters. Even less is known about the coordination of Nb^{5+} and W^{6+}. Raman spectroscopy of Nb in simple alkali silicates show features similar to Ti bearing glasses, suggesting a similar structural role (Ellison and Hess [7]). The suggested coordination is a highly distorted 5– or 6–coordinated site. W^{6+}, on the other hand, shows a Raman spectrum with a band at nearly the same frequency as the aqueous ion, suggesting nearly perfect tetrahedral coordination.

It should be kept in mind, however, that the conclusions for Nb and W are based on data from simple compositions in which there are non–bridging oxygens available for the establishment of coordination polyhedra. The tungsten–containing silicate glass composition listed here is not expected to contain abundant (if any) non–bridging oxygens, because the alumina to modifier ratio is greater than unity. As a consequence, it is possible that the coordination geometry could be modified. For the niobium–doped phosphate glass, on the other hand, which is based on mixed alkali and zinc as major modifiers, non–bridging oxygens are expected to be abundant.

3. Experimental.

The samples, 1 cm^3 colorless cubes, were attached to the cold finger of a closed–cycle helium refrigerator. For excitation we used a 308 nm line of an excimer laser. Absorption and emission spectra were measured with OMA III system, utilizing an ungated reticon detector, whereas decay times were obtained with a fast photodiode coupled to a transient recorder.

4. Results

The absorption and emission spectra of three zirconate glasses of 4%, 6%, and 8% concentration of ZrO_2 group, are presented in Fig. 1. The emission spectra are quite broad, peaking in the blue (~ 440 nm). The absorption is small over the luminescence region and rises steeply in the ultraviolet. Figure 2 illustrates absorption and emission spectra for tungstate and niobate glasses. The luminescence of tungstate glass peaks in the green (~ 520 nm) whereas that of niobate has a maximum in the blue–green (~ 470 nm). Both tungstate and niobate emissions reveal even broader spectra than those of zirconate glasses.

The luminescence decays are illustrated in Fig. 3. The luminescence of zirconate glasses decays mostly single–exponentially whereas that of tungstate and niobate glasses displays also shorter component, most pronounced for the tungstate glass. This two–exponential decay might possibly be connected with the relatively high concentration of tungstate group in the glass host.

Figure 4 presents the temperature dependence of light yield and decay time for three zirconate glasses (4,6,and 8%). Each point of the light yield (T) dependence represents an integral over the emission spectrum. Because the spectra were taken by the ungated, time–integrating OMA, the final result is the total light yield at a given temperature. The decay times were measured for total light output.

The experimental points for both luminescence and lifetime as a function of temperature are fitted by the simple Mott–Seitz theory of the radiationless transitions for the case of strongly lattice–coupled systems [8,9]:

$$\eta = I/I_o = \tau/\tau_r = 1/(1 + s\tau_r \exp[-\Delta E/kT]) \qquad (1)$$

where η is quantum efficiency, I is luminescence intensity (I_o – at T = 0), τ is the

observed lifetime, τ_r is the radiative lifetime, s is the frequency factor, and ΔE is thermal activation energy barrier between ground and excited state. We should emphasize that though we deal here with a two–parameter fit, the choice of the pair is highly restrained i.e. only one pair of parameters fits satisfactorily the experimental data; any other pair (e.g. both parameters scaled by some factor) does not provide a satisfactory fit. The temperature dependencies of the light yield and decay time for tungstate and niobate glasses are shown in Fig. 5. They are also fitted by the theoretical curve (1).

The quantum efficiencies η and RT time decays of the measured glasses are presented in Table II. It is assumed here that $\eta = 1$ at T = 0 K. It is ineresting that almost all of these glasses (except tungstate) show quite high RT quantum efficiency which indicates a relatively small strength of radiationless transitions.

5. Discussion

It appears that luminescent properties of glasses containing d^0 molecular complexes are quite comparable to crystalline, stoichiometric materials containing the same complexes [10]. The quantum efficiency of zirconate glasses is even higher than typical η for crystalline materials. Another typical and potentially useful feature is the large Stokes shift and lack of overlap between emission and absorption. Absorption, as in crystals, has its maximum in the UV. Though, one might not rule out a possibility that the absorption edge is connected with the glass host rather than with intrinsic features of the complex itself, the results obtained with 308 nm excitation seem to prove that we still excite the complex. This aspect is important in the excited state absorption measurements [11] which incidentally provide an additional, implicit confirmation of the coordination of these complexes in glasses.

It seems likely that the absorption and emission mechanisms in these glasses are

quite comparable to those in crystals. Absorption is somehow connected with the redistribution of d–orbitals [12], historically known as "charge transfer" and luminescence occurs from a triplet state [13,14]. The glass host can manifest itself in some statistic distribution of crystal field from site to site [15] which may contribute to the linewidth but this is probably insignificant compared to electron–lattice coupling.

The most informative are the results of temperature dependence of η and τ of these glasses. They seem to be in quite good agreement with the Mott–Seitz theory of nonradiative transitions in strongly electron–lattice coupled systems, which provides two very important parameters: the thermal activation energy ΔE and the frequency factor s. Table III specifies these parameters, providing a best fit of (1) to the experimental data. As can be seen, the frequency factor s derived from fitting the data points by the simple Mott–Seitz theory, can take the values as small as $\sim 10^4\ s^{-1}$. This is a very striking result in view of the almost universal belief that frequency factors should always be of the order of $10^{13} - 10^{14}\ s^{-1}$ [16,17].

Acknowledgment

This work was partially supported by the U.S. Army Research Office under Grant No. DAAL03–88–0103.

References

[1] F.A. Kröger, *Some Aspects of the Luminescence of Solids*, (Elsevier Publ. Co., Amsterdam 1948)

[2] Cz. Koepke, A.J. Wojtowicz, and A. Lempicki, "Excited–State Absorption in Excimer–Pumped $CaWO_4$", to be published

[3] Cz. Koepke and A. Lempicki, J. Luminescence. 47, (1991) 189

[4] Cz. Koepke and A. Lempicki, "Excited–State Absorption in $ZnWO_4$ Crystal", to be published

[5] Cz. Koepke and A. Lempicki, "Excited State Absorption in Solid State Molecular Complexes", in *OSA Annual Meeting Technical Digest 1990,* Vol.15 of the OSA Technical Digest Series (Optical Society of America, Washington, D.C., 1990) p. 192

[6] F. Farges, C.W. Ponader, and G.E. Brown, Geochem. Cosmochimica Acta, (1991) in press

[7] A. Ellison and P. Hess, J. Non. Cryst. Solids, (1991) in press

[8] N.F. Mott, Proc. Roy. Soc. (London), A 167, (1938) 384

[9] F. Seitz, J. Chem. Phys. 6, (1938) 150

[10] G. Blasse, Structure and Bonding, 42 (1980) 1

[11] Cz. Koepke, A. Lempicki, and G.H. Beall, "Glasses Containing Molecular Complexes, II: Excited–State Absorption", this issue

[12] T. Ziegler, A. Rauk, and E.J. Baerends, Chem. Phys. 16 (1976) 209

[13] H. Ronde and G. Blasse, J. Inorg. Nucl. Chem. 40 (1978) 215

[14] W.A.J.A. van der Poel, M. Noort, J. Herbich, C.J.M. Coremans, and J.H. van der Waals, Chem. Phys. Lett. 103 (1984) 245

[15] A.J. Wojtowicz and A. Lempicki, J. Luminescence. 39, (1988) 189

[16] R.H. Bartram, J.C. Charpie, L.J. Andrews, and A. Lempicki, Phys. Rev. B 34, (1986) 2741

[17] C.W. Struck and W.H. Fonger, J. Luminescence, 10 (1975) 1

Table I.

Percentages of the ZrO_2– and WO_3– containing glasses.

Sample ID:	EYQ (ZrO_2,4%)	EYU (ZrO_2,6%)	EYT (ZrO_2,8%)	EYY WO_3
SiO_2	74	72	70	52
Al_2O_3	19	18	20	23
Li_2O	2	4	–	–
MgO	5	6	5	–
CaO	–	–	–	5
ZnO	–	6	5	–
WO_3	–	–	–	20
ZrO_2	4	6	8	–

Table II.

Room–temperature quantum efficiencies and decay times of the investigated glasses.

Glass	η (RT) (%)	τ (RT) (μs)
Zirconate, 8 %	86.5	143.2
Zirconate, 6 %	87.6	146.0
Zirconate, 4 %	86.6	174.4
Tungstate, 20 %	8.2	7.1
Niobate, 1 %	65.0	23.2

Table III.

Thermal activation energies and frequency factors derived from the best fits of the formula (1) to the experimental data.

Material	ΔE (meV)	s (s^{-1})
Zirconate glass, 8%	110	6.7×10^{4}
Zirconate glass, 6%	125	1.1×10^{5}
Zirconate glass, 4%	130	1.0×10^{5}
Tungstate glass, 20%	45	7.4×10^{5}
Niobate glass, 1%	110	1.2×10^{6}

Captions to figures

Fig. 1 Absorption and emission spectra of three zirconate glasses under 308 nm excitation.

Fig. 2 Absorption and emission spectra of tungstate and niobate glasses under 308 nm excitation.

Fig. 3 Luminescence decays of tungstate (1) and niobate (2) glasses, and three zirconate glasses (3: 8 %, 4: 6 %, 5: 4 %).

Fig. 4 Temperature dependence of the light yield and decay time for three zirconate glasses. Solid lines represent theoretical fits to eq. (1).

Fig. 5 Temperature dependence of the light yield and decay time for tungstate and niobate glasses. Solid lines are the fits with the expression (1).

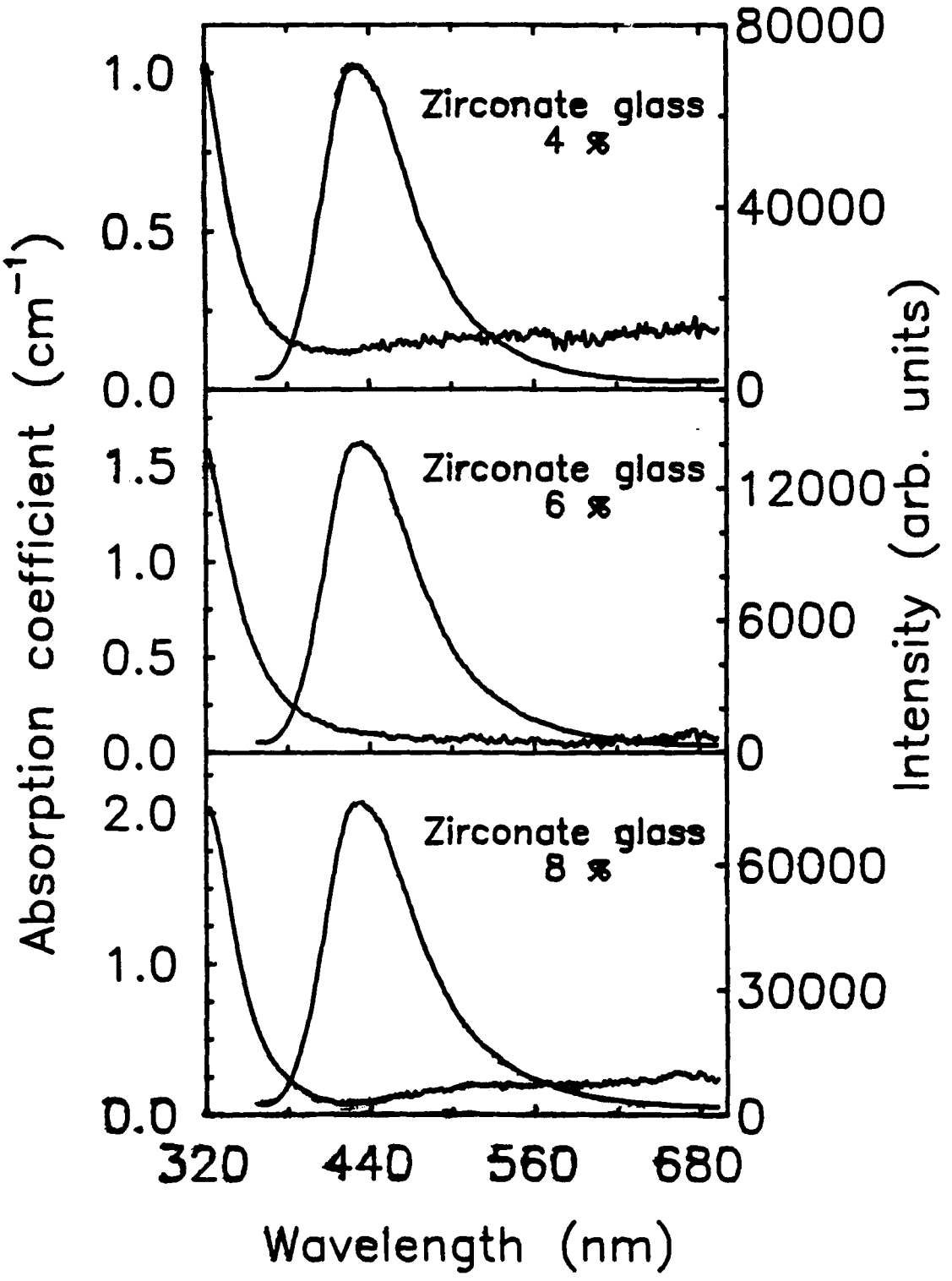

Fig. 1

O. Koepke, et al., „Glasses Containing... I: Luminescence

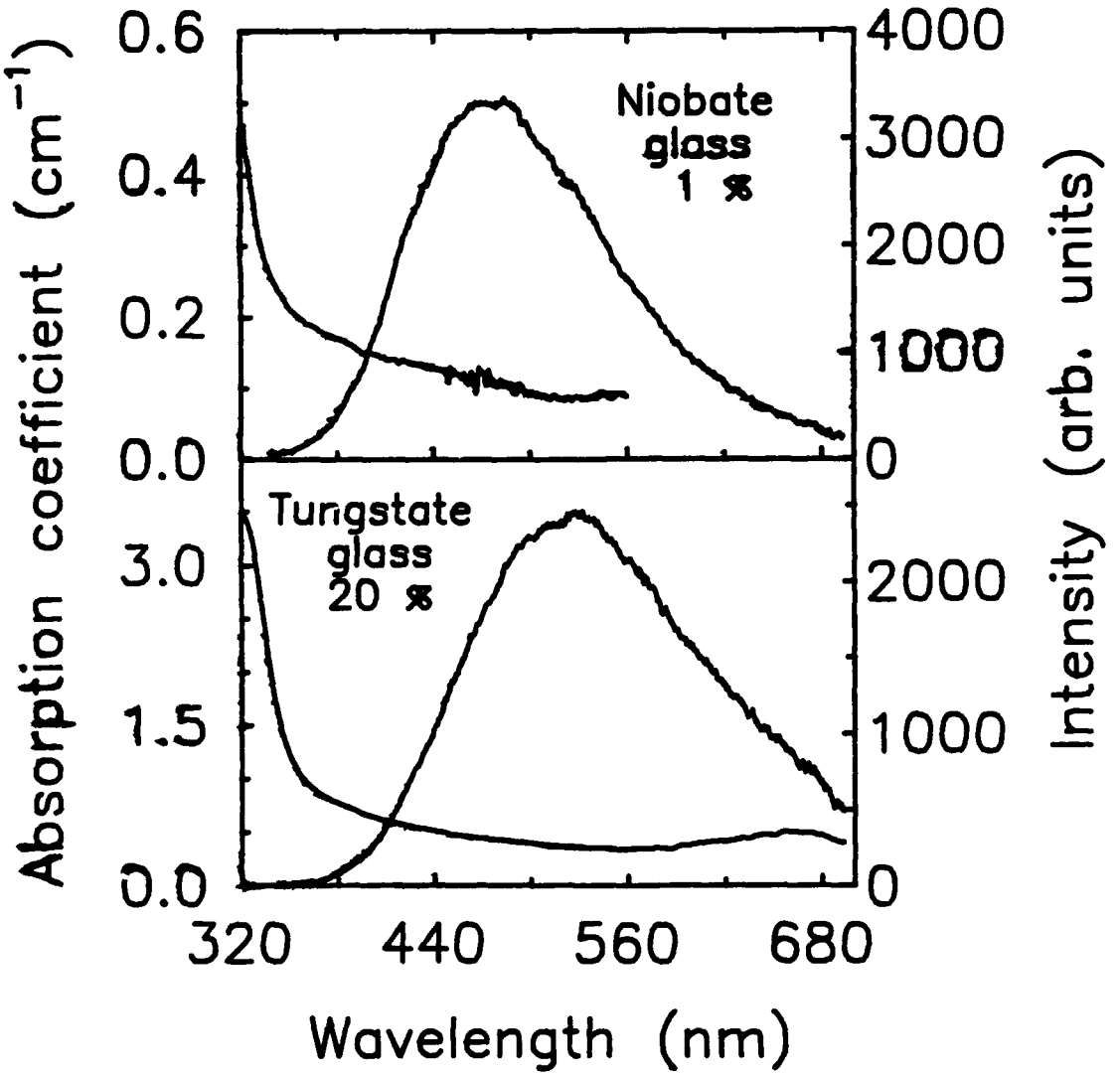
Niobate
glass
1 %
Tungstate
glass
20 %
Absorption coefficient (cm^{-1})
Intensity (arb. units)
0.6
0.4
0.2
0.0
3.0
1.5
0.0
4000
3000
2000
1000
0
2000
1000
0
320
440
560
680
Wavelength (nm)

Fig. 2

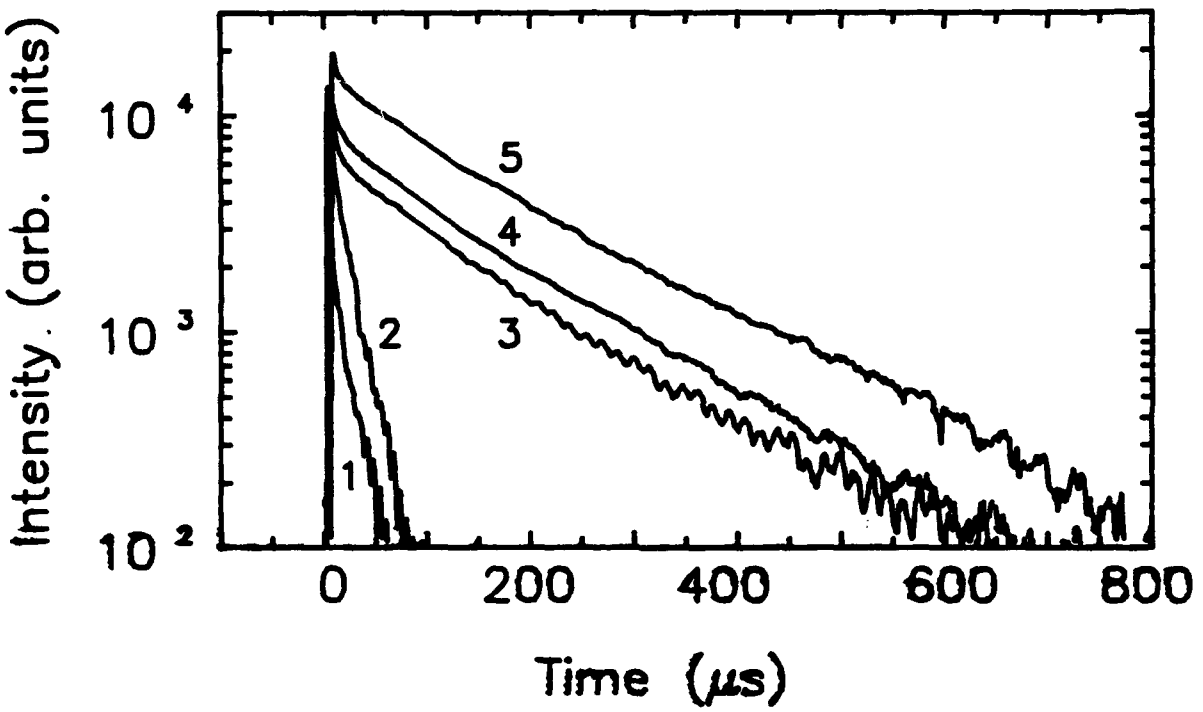

Fig. 3

Cz. Koepke et al. „Glasses Containing ... I: Luminescen

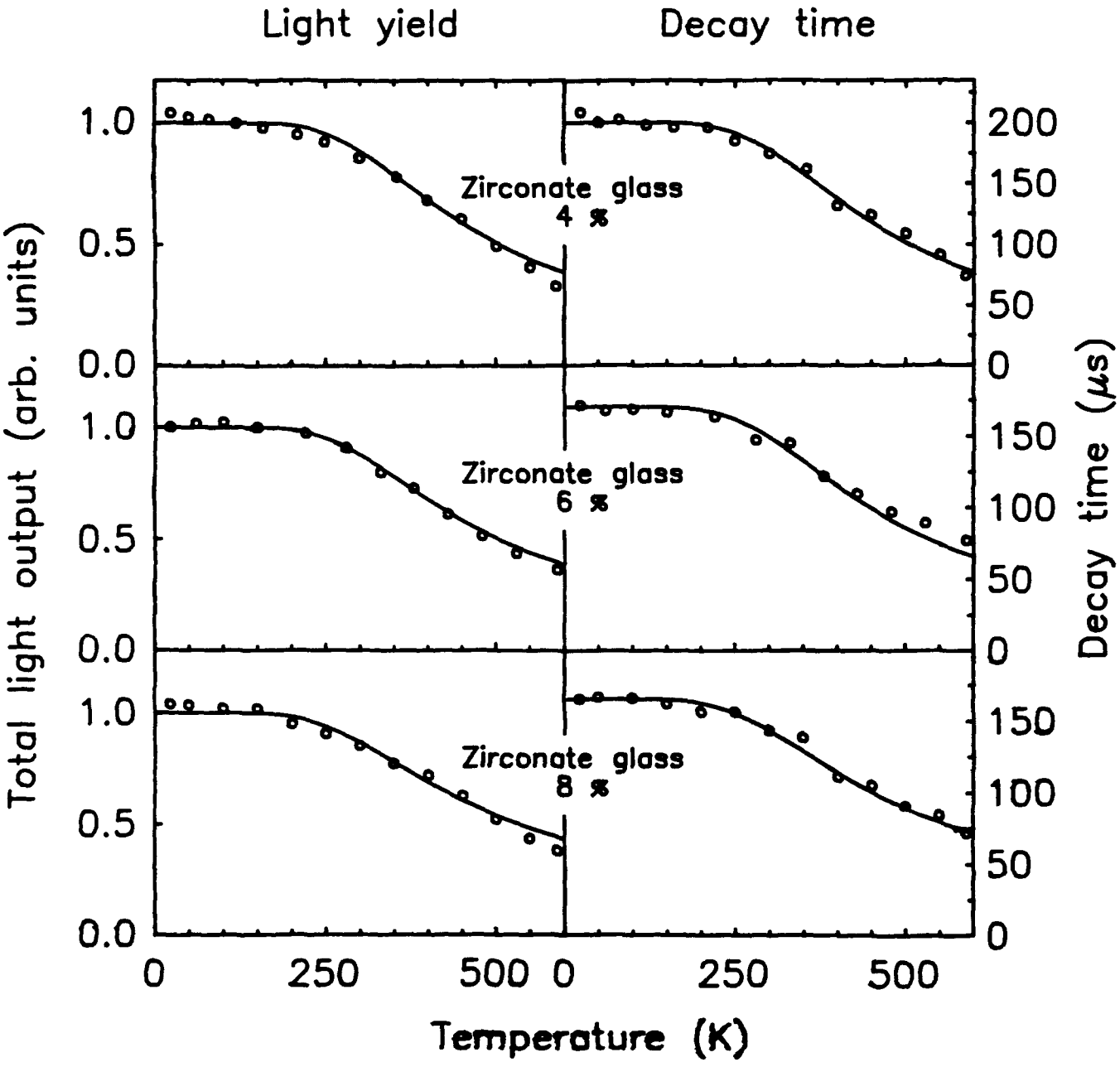

Fig. 4

Cz. Koepke et al. „Glasses Containing ... I: Luminescence

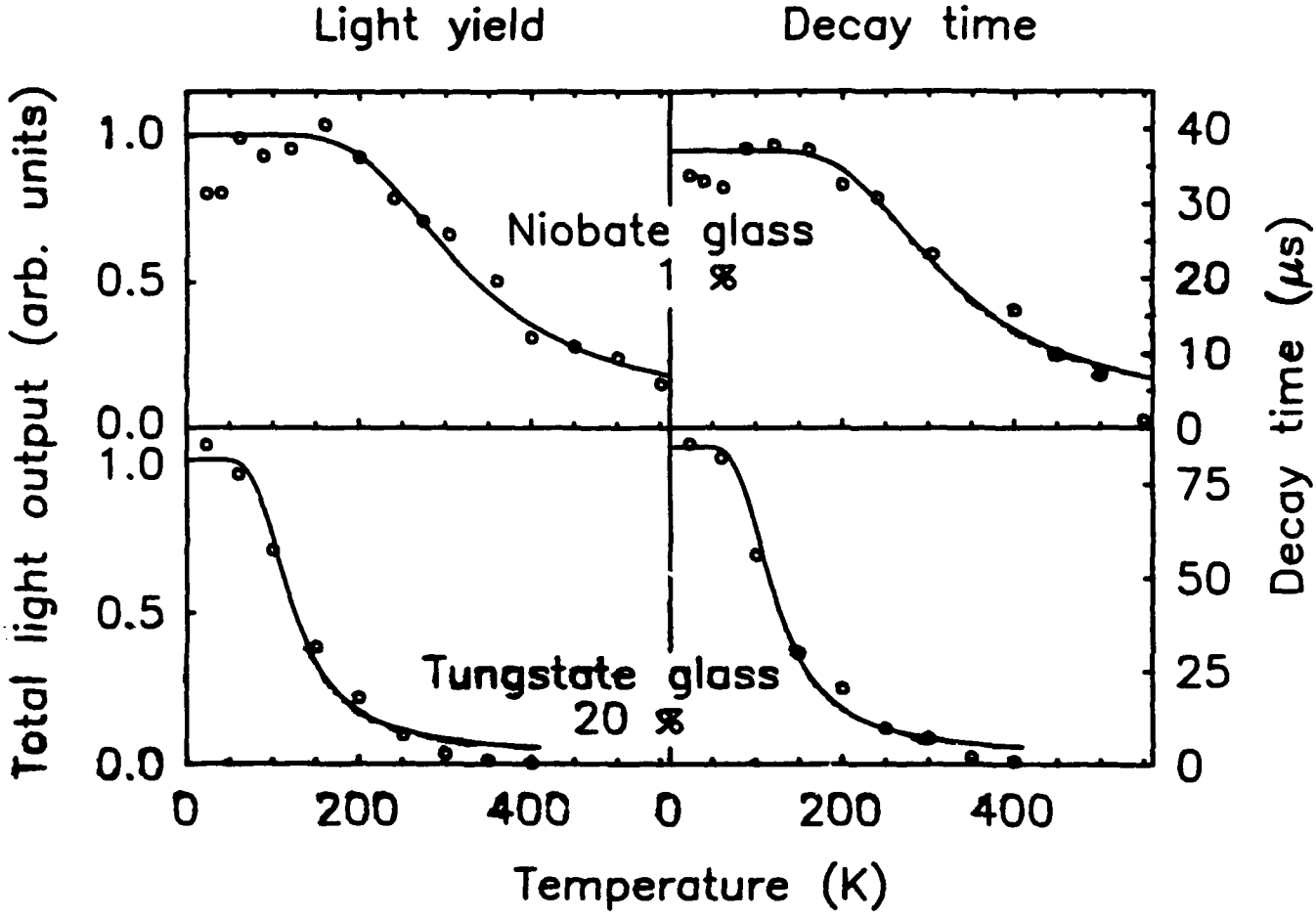

Fig. 5

Cz. Koepke et al. "Glasses Containing... I: Luminescen

GLASSES CONTAINING CLOSED-SHELL MOLECULAR COMPLEXES, II: EXCITED STATE ABSORPTION

Cz. Koepke* and A. Lempicki

Boston University, Chemistry Dept. 590 Commonwealth Ave., Boston, MA 02215

and

G.H. Beall

Corning Incorporated, Corning, New York 14831

Abstract

We have evaluated several new glasses, containing molecular complexes of d^0 transition metal ions, from the point of view of their suitability as possible tunable laser materials. Using as excitation source the 308 nm line of an excimer laser, we found that despite of the relatively large quantum efficiency, these glasses have very strong Excited-State Absorption (ESA) of crossections about three order of magnitude greater than the stimulated emission crossections. The ESA spectra are very broad and their maxima are shifted to the violet or ultraviolet region in comparison with luminescence, however in view of its high level, ESA still precludes any laser action in these materials. Nevertheless, one of these glasses (niobate-doped) suggest a direction for further development and possibly reduced ESA.

---

*On leave from Institute of Physics, N. Copernicus University, Toruń, Poland

1. Introduction.

In ref. [1], thereafter called I, we have reported on the luminescent properties of some new types of glasses containing transition metal ions in d^0 configuration. Since these materials exhibit high quantum yields and broad–band emissions in the blue–green, they are obvious candidates for tunable lasers in this region. Previous work on analogous crystalline materials ($CaWO_4$, $CaMoO_4$, $ZnWO_4$ [2–5]) led to the conclusion that excited state absorption (ESA) was dominant and precluded laser action. However, this does not necessarily hold true for glasses which may have different coordination of the metal ion. Moreover, among the available compositions (see I) there were niobate and zirconate glasses, of which we had no crystalline analogs. This paper is therefore devoted to ESA of these amorphous materials. The samples, were the same as reported in I.

2. Experimental.

Excited–State Absorption measurements were carried out using virtually the same arrangement as described in [3]. The ESA and luminescence decays were measured with a fast photodiode coupled to a transient recorder (1024 channels × 10 ns in the fastest mode) and to a computer collecting the data. An excimer laser (XeCl) working at 308 nm was our source of excitation (in transverse geometry) and as a probe beam in ESA measurements we used a violet line (415.4 nm) of a krypton laser. ESA was observed (and registered) as a hole (immediately following the excimer pulse) in the constant "background" of the probe beam light.

The ESA spectra were measured using the excimer laser as a pump, pulsed Xe lamp as a source of the probe beam and a gated OMA system, controlled by computer, for detection. Each spectrum was acquired with averaging over 1000 shots of the excimer laser

and with a reticon gate of 0.89 μs set at 0.2 μs delay. This setup was described in greater detail in [3]. For taking luminescence spectra we also used the OMA system, but working in an ungated mode [1].

3. Results and discussion.

Figure 1 presents the ESA decays compared to luminescence decays for zirconate glasses of three different concentrations (4%, 6% and 8% of ZrO_2). The ESA is here expressed as dimensionless absorption: $ESA = 1 - \exp(-\alpha_{ESA}L)$, and its height is normalized to the luminescence signal. The inserts illustrate the ESA and luminescence decays on a logarithmic scale. For all three cases the ESA and luminescence follow similar, mostly single–exponential decays. This indicates that there is just one luminescent site and both ESA and luminescence occur from the same state.

Figure 2 shows the comparison of ESA crossection $\sigma_{ESA}(\lambda)$ to stimulated emission crossection σ_{ST} for these three zirconate glasses. The stimulated emission crossections were calculated from McCumber theory of phonon–terminated lasers [6,7], using measured luminescence spectra and radiative lifetimes reported in I (exact values are written in the caption). σ_{ESA} was derived with the following formula (e.g. [8]):

$$\sigma_{ESA}(\lambda) = -\frac{\ln\ EST(\lambda)}{n^{\star}L} + \sigma_{GSA}(\lambda) \qquad (1)$$

where EST is the directly measured Excited–State Transmission:
$EST = I(\text{pumped medium})/I(\text{unpumped medium}) = \exp(-\alpha_{ESA}L)$, I is probe beam intensity after passing the sample, $n^{\star}$ is the concentration of excited complexes in cm^3, σ_{GSA} is ground–state absorption crossection and L is the length of the medium. The

concentration n^* was calculated from the excimer laser beam fluence and ground state absorption of the sample, the latter (and σ_{GSA} as well) obtained in a separate measurement. The values of n^* used in σ_{ESA} derivation are given in the caption. The most important feature of σ_{ESA} spectra is their breadth and very high level, at least three orders of magnitude greater than σ_{ST}. This, of course, precludes any possibility of lasing in these materials. It is also interesting that their maxima are shifted to shorter wavelengths in comparison with typical ESA spectra of tetra–oxo molecular complexes in crystals [2,3].

The next interesting fact is that σ_{ESA} for zirconate glasses depends on ZrO_2 concentration, which is depicted in Fig. 3. This may be evidence that one cannot treat isolated complexes as a source of optical properties of this glasses, and instead a certain level of delocalization should be considered. It seems that with rising concentration of the complexes, transitions between lower and higher excited state become faster. Indeed, the "spontaneous" lifetimes of the higher excited state derived from the familiar formula [9],

$$\tau_{ESA} = \frac{g_{ESA}(\nu)}{8\pi\sigma_{ESA}(max)} \left[\frac{c}{\nu}\right]^2 \qquad (2)$$

where $g_{ESA}(\nu) \sim 1/\Delta\nu$ is a lineshape of ESA spectrum, are:
$\tau_{ESA}(4\%) = 86$ ns, $\tau_{ESA}(6\%) = 68$ ns, and $\tau_{ESA}(8\%) = 54$ ns. These times are almost as short as for typical allowed transitions ($\sim 10^{-9}$s). Their decrease with concentration, an effect often observed for lower states, may be indicative of some energy transfer processes in the higher states.

The ESA/luminescence decays and σ_{ESA} and σ_{ST} spectra for tungstate and niobate glasses are presented in Figs. 4 and 5. Figure 4 shows the comparison of ESA decays to those of the luminescence. Inserts illustrates the same decays but on a logarithmic scale. For these glasses the decays are not quite single–exponential (which is particularly distinct

for the tungstate glass), but the identity of ESA and luminescence decays proves that, like before, both occur from the same state.

In Fig. 5 we illustrate the ESA crossection spectra compared to stimulated emission spectra for the tungstate and niobate glasses. In general, the level of σ_{ESA} is here similar to that of zirconate glasses and severely dominates σ_{ST}. For the tungstate glass the shape and position of maximum σ_{ESA} is very similar to that of zirconate glasses. As mentioned in I, there are indications that the W–O complex in tungstate glass is of tetrahedral coordination. Then, as long as we deal with d^0 configuration, the ESA occurs between the states 2e and $4t_2$ separated by 10Dq energy. The ESA spectrum of this glass, peaking around 24000 cm^{-1}, is especially interesting in comparison with tungstate crystals ($CaWO_4$ and $ZnWO_4$ [3,4]) where σ_{ESA} spectra peaked around 22000 cm^{-1}. This ~ 2000 cm^{-1} difference can be possibly caused by a tendency towards larger electron–lattice coupling in glasses [10]. The resulting larger shift of the first excited state parabola to higher configuration coordinate value, increasing the Stokes shifts, can also decrease the thermal activation barrier ΔE. This last hypothesis finds a reasonable confirmation in the experiment (see [3,4] and I, Table III), where ΔE–s for glasses are considerably smaller that those of crystals. More precisely, considering ESA, there is a sort of balance (competition) between the tendency towards smaller crystal fields in glasses [11] and the tendency towards larger electron–lattice coupling. In our case, the ~ 2000 cm^{-1} shift of ESA to shorter wavelengths, as compared to crystalline tungstates, indicates that increased electron–lattice coupling seems to overcome the lowering of crystal field and consecutive decrease of 10Dq [12]. Because of great similarity of the ESA spectra of zirconate glasses to that of tungstate glass, it is likely that they belong to the same, tetrahedrally coordinated category. The only glass, which has a distinctly different ESA spectrum, is

niobate glass. It displays an extreme case of UV shift, which itself coul be beneficial from laser point of view. σ_{ESA} has a maximum in the UV region (far off the figure) and goes down in the σ_{ST} region. It seems to be close to zero in green–red range, but one needs to remember that it still occurs on a 10^{-18} cm^2 scale, and hence still overcomes σ_{ST}. Because ESA transitions occur between states separated by 10Dq energy, increasing 10Dq will shift the ESA spectrum towards shorter wavelengths. The ESA spectrum of niobate glass suggests then octahedral (or distorted octahedral) coordination, in view of the basic rule: $10Dq(oct.) = \frac{9}{4} 10Dq(tet.)$. This is, of course, a crude simplification, without taking into account the electron–lattice coupling and other possible effects.

5. Conclusions

The measured ESA spectra in the glasses containing metal–oxygen d^0 complexes, compared to the stimulated emission spectra, show that it is impossible to obtain laser action in these materials. However, they also indicate a proper direction of the search for laser action in d^0–type glasses. Owing to the fact that niobate glass shows the largest shift of ESA towards the UV, and that there is an indication of octahedral coordination of the N–O complex, it seems that one should search among the ions forming octahedral coordination. This may also be relevant to the closed–shell molecular complexes in crystals. However, one still has to contend with the vastly different magnitudes of σ_{ESA} and σ_{ST}. There are some other factors causing the high strength and spectral width of ESA transitions, which conspire against lowering σ_{ESA}. One of them is spin–orbit coupling, especially distinct for tungstate complexes {Z(W) = 74} [3,4]. Another is the static Jahn–Teller effect already found in the first excited state of $CaMoO_4$, YVO_4, and $YP_{0.96}V_{0.04}O_4$ by Barendswaard, van der Waals and Weber [13,14]. From the point of

view of spin–orbit coupling it would be interesting to search among complexes with a lighter central atom e.g. Ti, V, Cr or Mn. On the other hand one should realize that small spin–orbit coupling, while possibly decreasing ESA strength can also decrease the oscillator strength of luminescence which in these materials is usually spin–forbidden.

Acknowledgment

This work was partially supported by the U.S. Army Research Office under Grant No. DAAL03–88–0103.

References

[1] Cz. Koepke, A. Lempicki, and G.H. Beall, "Glasses Containing Closed–Shell Molecular Complexes, I: Luminescence", this issue.

[2] Cz. Koepke and A. Lempicki, J. Luminescence 47, (1991) 189

[3] Cz. Koepke, A.J. Wojtowicz, and A. Lempicki, "Excited–State Absorption in Excimer–Pumped $CaWO_4$ Crystal", to be published

[4] Cz. Koepke and A. Lempicki, "Excited–State Absorption in $ZnWO_4$ Crystal" to be published.

[5] Cz. Koepke and A. Lempicki, "Excited State Absorption in Solid State Molecular Complexes", in *OSA Annual Meeting Technical Digest 1990,* Vol.15 of the OSA Technical Digest Series (Optical Society of America, Washington, D.C., 1990) p. 192

[6] D.E. McCumber, Phys. Rev. 134, (1964) A299

[7] A.J. Wojtowicz, W. Meng, A. Lempicki, G.H. Beall, D.W. Hall, and T.C. Chin, IEEE J. Quantum. Electron. QE–24, (1988) 1109

[8] W.M. Fairbank, Jr., G.K. Klauminzer, and A.L. Schawlow, Phys. Rev. B 11, (1975) 60

[9] A. Yariv, *Quantum Electronics*, Second Edition (John Wiley & Sons, New York, London, Sydney, Toronto, 1975)

[10] G.F. Imbusch, T.J. Glynn, and G.P. Morgan, J. Luminescence, 45, (1990) 63

[11] T. Bates, in *Modern Aspects of the Vitrous State*, (ed. J.D. Mackenzie, Butterworths, London 1962)

[12] L.E. Orgel, *An Introduction to Transition Metal Chemistry*, (Methuen & Co., Ltd. London, 1960)

[13] W. Barendswaard and J.H. van der Waals, Molec. Phys. 59, (1986) 337

[14] W. Barendswaard, R.T. Weber, and J.H. van der Waals, J. Chem. Phys. 87, (1987) 3731

Figure captions

Fig. 1 The comparison of ESA and luminescence decays for zirconate glasses of three different concentrations: 4, 6, and 8 %. Insets show the decays on logarithmic scale.

Fig. 2 ESA and stimulated emission crossections for three zirconate glasses. For derivation of σ_{ESA} from the measured EST, the following excited state populations were used: $n^*(4\%) = 4.4\times10^{16}$ cm^{-3}, $n^*(6\%) = 3.5\times10^{16}$ cm^{-3}, and $n^*(8\%) = 3.2\times10^{16}$ cm^{-3}. They correspond to the following excitation strengths: $p = n^*/n_o = 9.2\times10^{-5}$, 4.7×10^{-5}, and 3.2×10^{-5} respectively (n_o is the ground state population). The σ_{ST} spectra were calculated with the following radiative lifetimes (taken from separate experiments [1]): $\tau_r(4\%) = 201.4$ μs, $\tau_r(6\%) = 166.7$ μs, and $\tau_r(8\%) = 165.5$ μs.

Fig. 3 Comparison of ESA crossections for three different concentrations of zirconate glasses.

Fig. 4 The comparison of ESA and luminescence decays for tungstate and niobate glasses. Insets show the decays on logarithmic scale.

Fig. 5 ESA and stimulated emission crossections for tungstate and niobate glasses. For derivation of σ_{ESA} from the measured EST, the following excited state populations were used: $n^*(\text{tungstate}) = 3.6\times10^{17}$ cm^{-3} and $n^*(\text{niobate}) = 3.9\times10^{16}$ cm^{-3}, which corresponds to excitation parameters: $p = 2.5\times10^{-4}$ and 2.4×10^{-4} respectively. The σ_{ST} spectra were calculated with the following radiative lifetimes (taken from separate experiments [11]): $\tau_r(\text{tungstate}) = 86.6$ μs and $\tau_r(\text{niobate}) = 35.7$ μs.

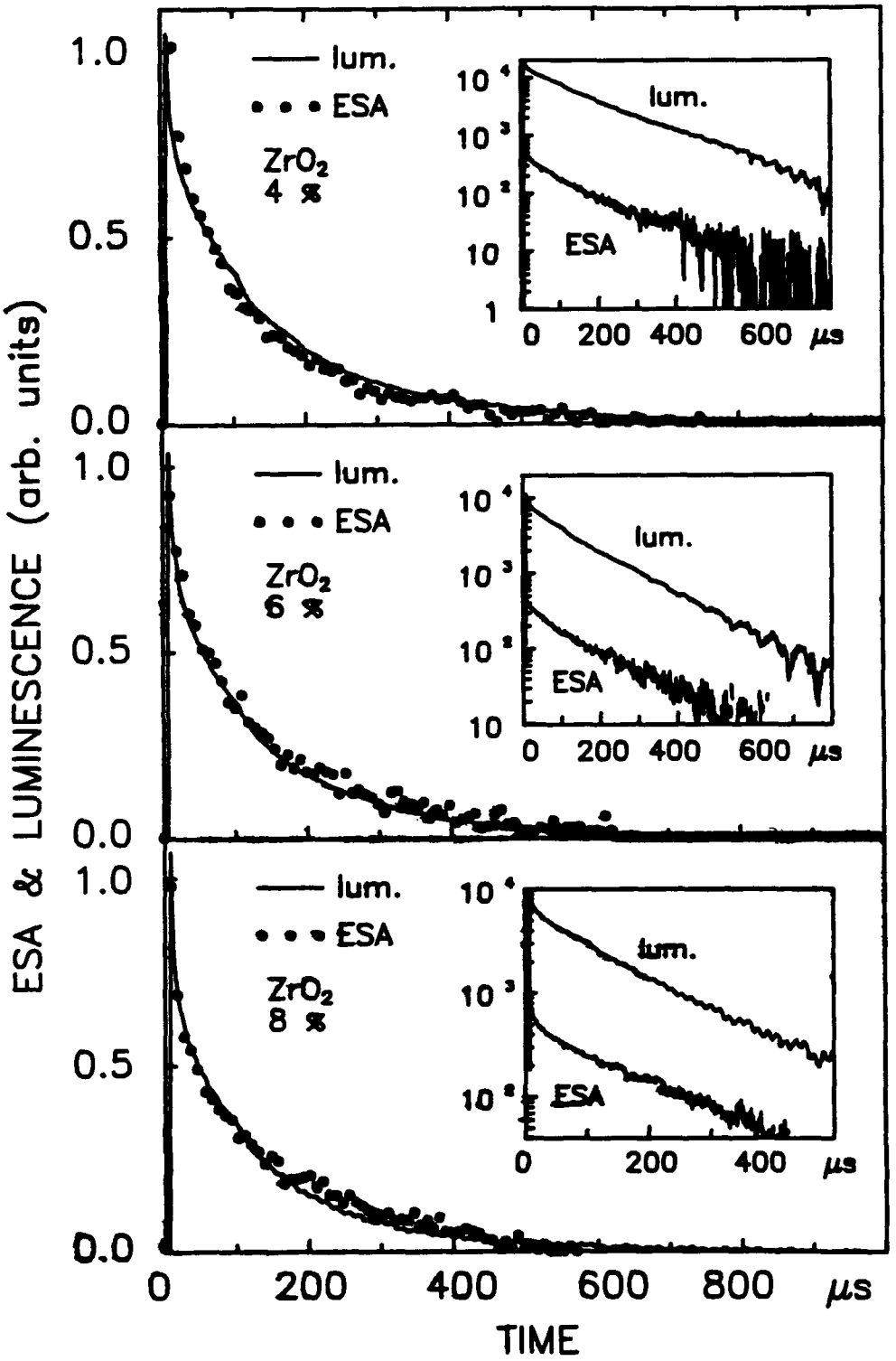

Fig. 1

Cz. Koepke et al. „Glasses Containing ... II. Excited State Absorption"

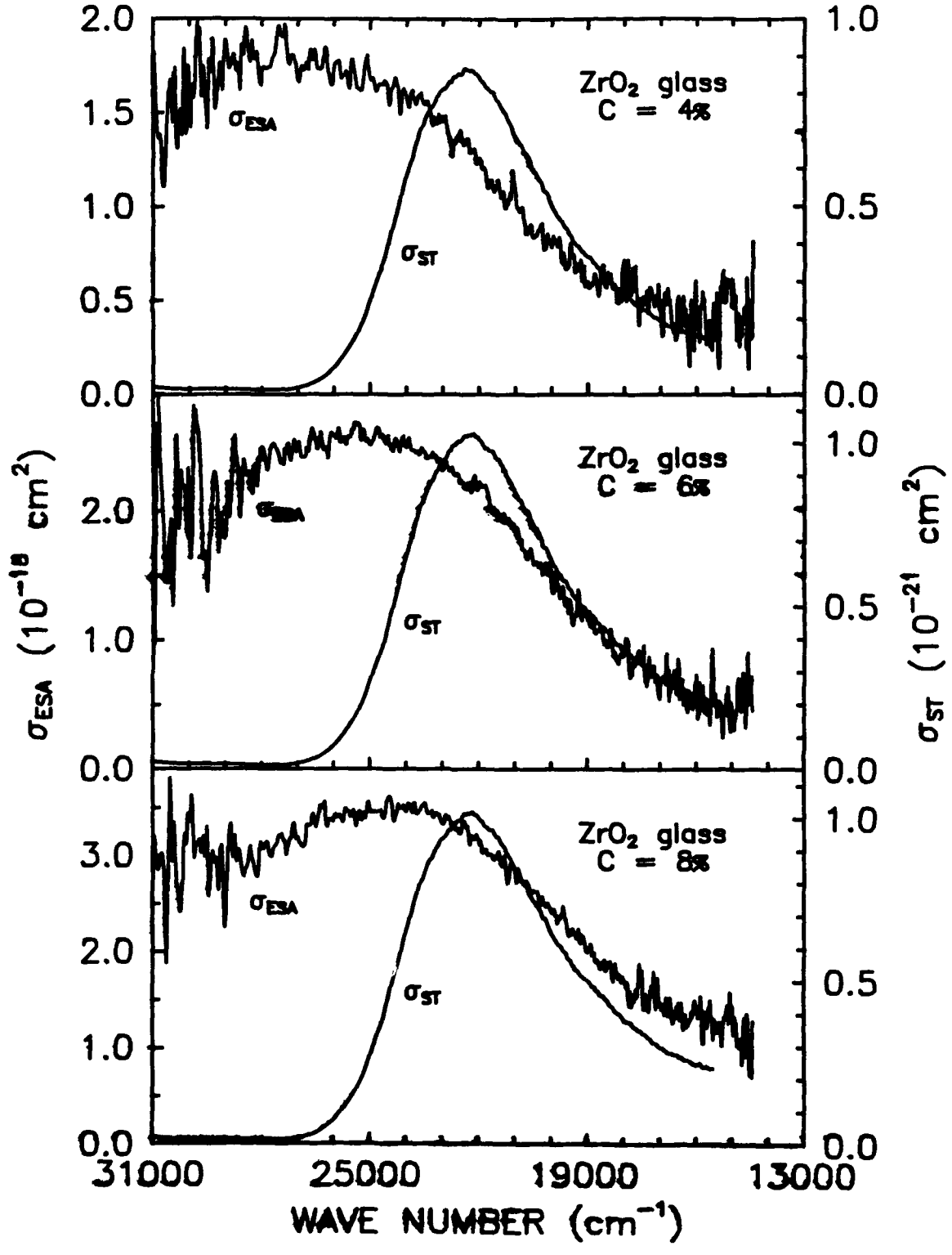

Fig. 2

Ch. Koepke et al., „Glasses Containing ... II: Excited State Absorption"

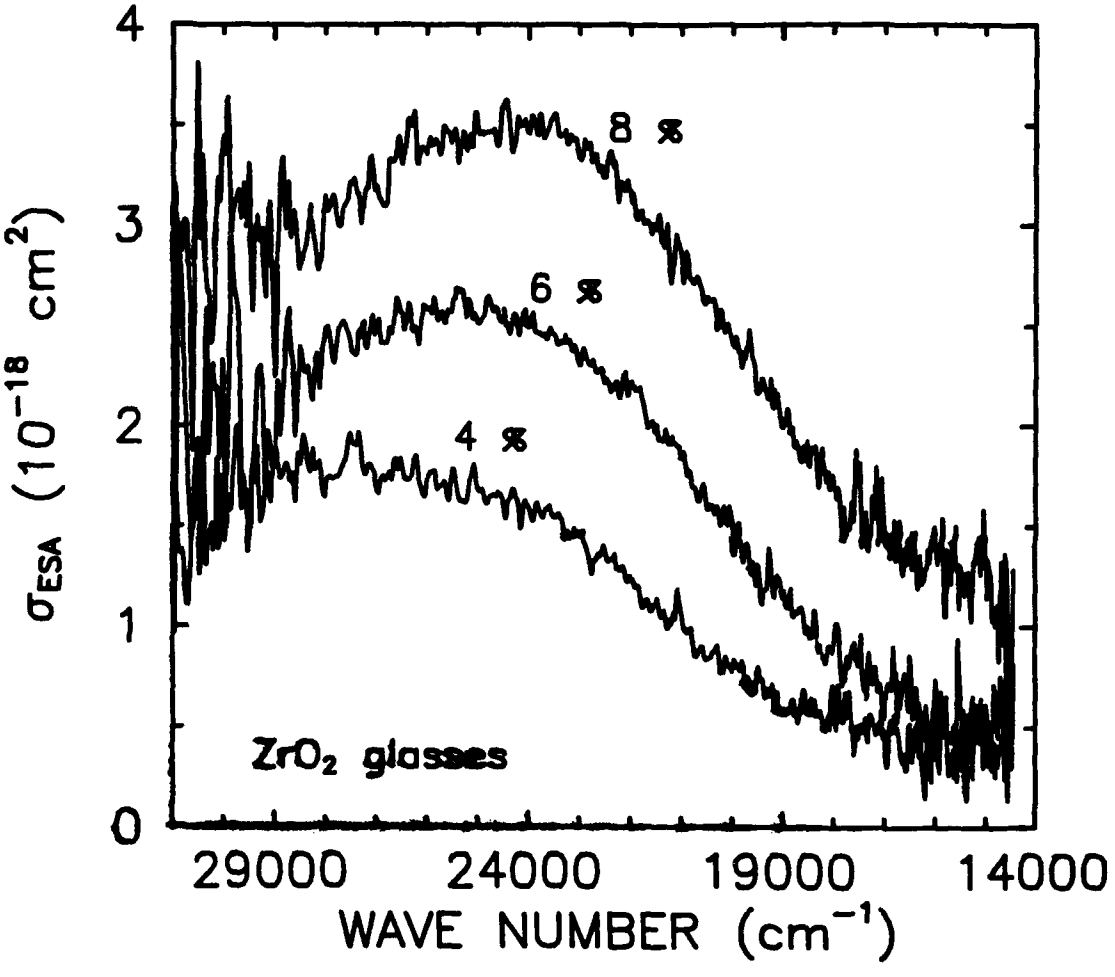

Fig. 3

Cz. Koepke et al., "Glasses Containing ... II: Excited State Absorption"

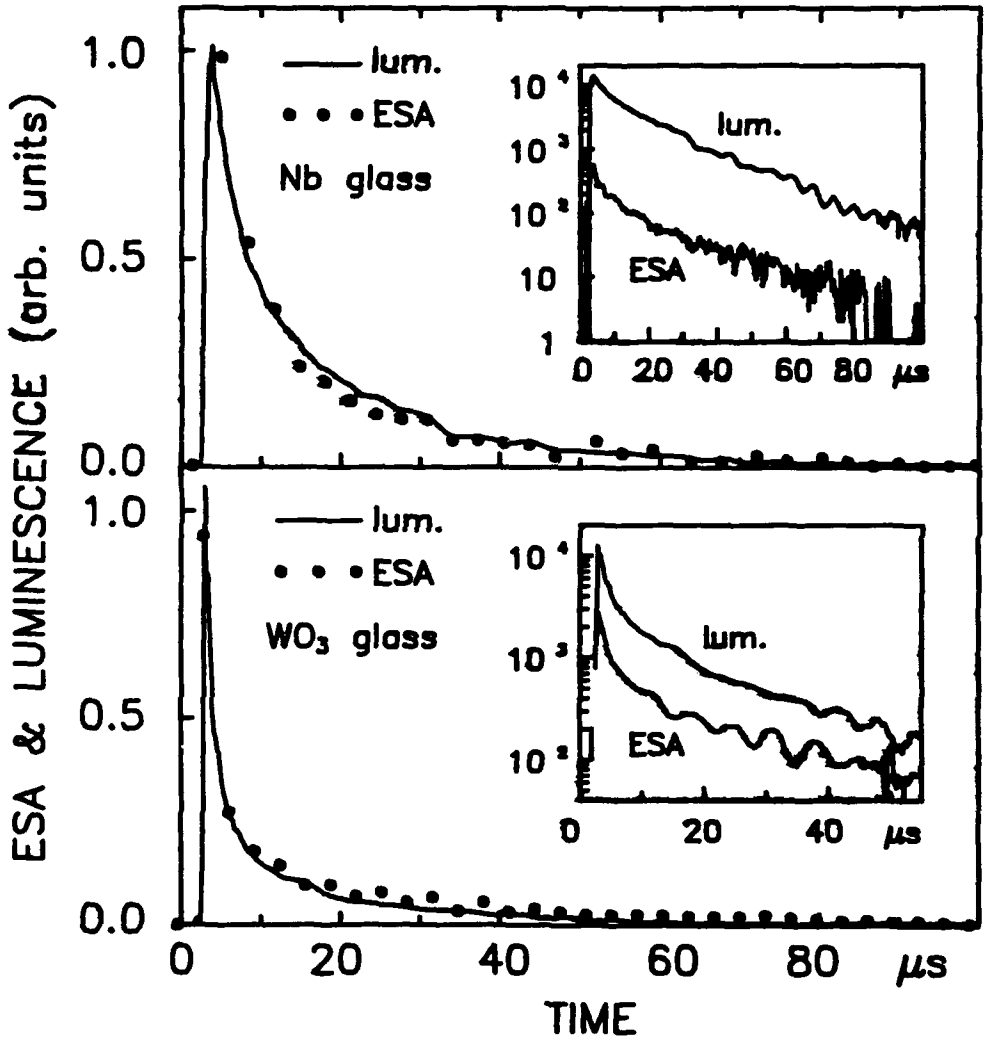

Fig. 4

Cz. Koepke et al. „Glasses Containing ... II: Excited State Absorption"

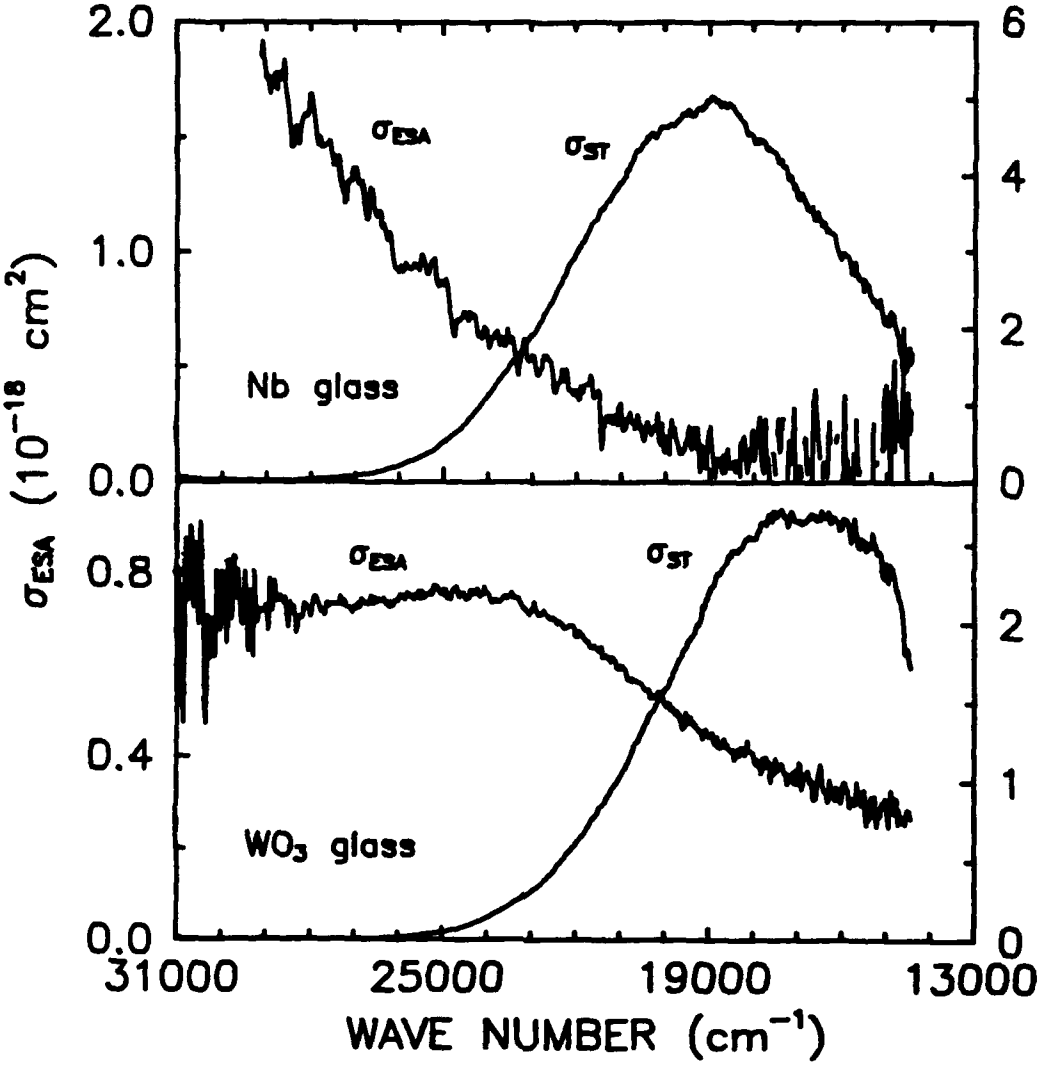

Fig. 5

Cz. Kocplue et al. "Glasses Containing ... II: Excited State Absorption"

Appendix 11

STUDY OF MOLECULAR TETROXO COMPLEXES AS POSSIBLE LASER MEDIA

Cz. Koepke*, A.J. Wojtowicz*, and A. Lempicki

Boston University, Chemistry Department, 590 Commonwealth Ave., Boston, MA 02215

Abstract

We have evaluated a series of tetra–oxo–molecular–complex materials (of d^0 electronic configuration) from the point of view of their suitability as possible tunable laser materials, emitting in the blue–green. All of them reveal a very strong, broadband excited–state absorption (ESA), occurring between $(t_1^5,2e)$ and $(t_1^5,4t_2)$ configurations separated by the energy of 10Dq. The relatively high probability of ESA transitions suggests an efficient breaking of Laporte selection rule, due to the considerable mixing of d and p–orbitals of the central ion as well as the existence of triplet terms in the terminal configuration. We compare the crossections of ESA and stimulated emission and tentatively interpret the results by means of a configuration–coordinate model. Some possible avenues of future work are indicated.

---

*On leave from Institute of Physics, N. Copernicus University, Toruń, Poland

I. Introduction

Molecular complexes in crystals hve never been systematically treated as possible tunable laser media, although some suggestions of their use were made, [1]. They are primerly known as phosphors, widely used for fluorescent lamps [2], X–ray detectors [3] and scintillators [4,5]. Relatively large quantum efficiencies, [6,7], very broad emission spectra, and negligible absorption in the visible, could make them attractive for possible laser applications. Prompted by this we have evaluated their laser–related characteristics [8–12]. For the present survey we have chosen solid–state complexes of transition metals in d^o electronic configuration.

A list of ions and their valence states giving rise to d^o configuration, is given in Table I. Table II lists the known oxy–complexes of the ions, their coordination and reported observation of luminescence. The table is based on a review article by Blasse [13]. Aside from efficiency and broad–band emission of these materials there are the following reasons why they may be considered as potential laser materials:

(a) The absorption (pump) bands are invariably situated in the near UV. They are quite intense being of "charge transfer" character [13,14]. Excimer lasers are therefore excellent pumping sources.

(b) The decay times of this class of materials are of the order of 10^{-6} sec, hence typically 10^3 times longer than for dyes. Lasers based on these materials would then have considerably higher energy storage, although naturally lower gain.

(c) Simple considerations suggest that Excited State Absorption (ESA) should not represent much of a problem.

The one–electron, molecular orbital energy diagrams of tetroxo complexes are well known [15,16,30] and an example is shown in Fig. 1 for MnO_4^- complex. It is believed that these materials luminesce from a lowest triplet term of $(t_1^5,2e)$ configuration [17,18] and hence, their luminescence is spin–forbidden but parity–allowed. On the other hand, the

a significantly higher excited state originates from the $(t_1^5,4t_2)$ configuration. A possible excited–state absorption (ESA) would then occur between the d states split off by crystal field. As a pure d–d transition ESA should then be parity forbidden (Laporte selection rule). Moreover, the $(t_1^5,2e)$ and $(t_1^5,4t_2)$ configurations are separated by an energy 10Dq, which for tetrahedral coordination falls into the infrared. Hence, one may expect that ESA should not spectrally coincide with luminescence (and gain). When interactions are taken into account the term multiplicities will obviously affect the ESA/gain competition. As will be shown, the problem of ESA in molecular complexes is not that simple and several other aspects must be taken into account.

In all cases we found a distinct "net" ESA. The present survey summarizes these results. So far we investigated $CaWO_4$, $ZnWO_4$ and $CaMoO_4$ crystals. The data obtained from the first two are supported by results obtained on a glass containing WO_4^{2-} complexes [11,19].

II. Experimental

The experimental arrangement used in our measurements has been described previously [9]. To obtain the ESA and/or gain spectra, we used a EG&G–PAR optical multichannel analyzer (OMA–III) system and a Xe flash lamp providing a polychromatic probe beam. ESA has also been measured with a krypton or argon ion laser light as the probe beam and with a fast photodiode coupled to a boxcar averager or fast transient recorder. In such a configuration we could get temporal ESA characteristics or "point–by–point" ESA spectra [8]. In all cases the samples were pumped in a transverse geometry by an excimer (308 nm) or nitrogen (337.1 nm) laser beam depending on the absorption edge of the material. In the case of $CaWO_4$ we heated the sample to thermally shift the absorption edge to such an extent, that only WO_4^{2-} complex was excited [9]. The

same setups, excluding the probe beam sources, were used for the measurement of the spectral and temporal luminescence characteristics.

The decays of the ESA and luminescence, were presented in refs. [8–11]. Usually they decay in the same manner, which proves that both originate from the same state. The only exception was $CaWO_4$ where a very long ESA component, caused by phosphorescent traps, was observed; nevertheless even in this case, after subtracting this long term, the resulting ESA decayed just like the luminescence [9].

III. Results

To determine if the laser action is possible or not, we should compare the ESA crossection σ_{ESA} to the stimulated emission crossection σ_{ST}. σ_{ESA} can be easily calculated from the directly measured excited–state transmission: $EST = I_p/I_u$ (I_p – probe beam intensity after passing through the pumped medium, I_u – probe beam intensity after passing through unpumped medium), via the following relation [20]:

$$\sigma_{ESA}(\nu) = -\frac{\ln\ EST(\nu)}{N^{\star}L} + \sigma_{GSA}(\nu) \qquad (1)$$

where $N^{\star}$ is the number of excited complexes per cm^3, calculated from the exciting beam fluence and UV absorption characteristics of a given sample, L is the length of the medium, and σ_{GSA} is the ground–state absorption crossection, orders of magnitude smaller than σ_{ESA} and σ_{ST} in their spectral region.

Having the luminescence spectra and knowing the quantum efficiencies (or radiative lifetimes), one can derive the stimulated emission crossection spectra $\sigma_{ST}(\nu)$ using the

following formula taken from a generalized McCumber theory of phonon–terminated lasers [21,22]:

$$\sigma_{ST}(\nu) = \frac{\mathscr{L}(\nu)}{8\pi\tau \int_0^\infty \mathscr{L}(\nu)d\nu} \left[\frac{c}{n\ \nu}\right]^2 \qquad (2)$$

where $\mathscr{L}(\nu)$ is the measured luminescence spectrum, τ is the radiative lifetime, and n is the refractive index.

The results are compiled in Fig. 2. The parameters used in (1) and (2) are listed in the caption. In all the cases the σ_{ESA} is from one to two orders of magnitude greater than σ_{ST} and overlaps the luminescence, which of course precludes any laser action in these materials.

The data of $CaWO_4$ (Fig. 2b) were taken at 497 K; the sample was heated to shift the absorption edge and thus, obtain a "pure" excitation of WO_4^{2-} complexes (at RT the contribution of WO_3–Schottky defects was quite substantial [9]). Also, $CaWO_4$ data were taken with a gated OMA detector, to get rid of the long ESA component, which alters the ESA spectrum. Figure 2b shows additionally the σ_{ESA} and σ_{ST} of WO_4^{2-} complex in a glass, which typically have larger Stokes shift due to increased electron–lattice coupling [23]. Hence, for the WO_4^{2-} complex in glass, the maximum of ESA crossection is shifted towards the UV, unlike that of WO_4^{2-} in $CaWO_4$ or $ZnWO_4$. The maximum of σ_{ST} is shifted towards longer wavelengths in comparison with that of tungstate crystals. However, the level of $\sigma_{ESA}(WO_4^{2-}$ in glass) is considerably greater than $\sigma_{ESA}(WO_4^{2-}$ in crystals).

The Table III specifies the crossection values taken from the spectra.

IV. Configuration coordinate model

The existence of strong, broadband ESA, overlapping the luminescence, raises a number of questions. First of all, we know that there is a very strong electron–phonon coupling, which influences the luminescence band shape and would affect ESA as well. Next, ESA, just like ground state absorption, favors these transitions which are most probable. Consequently ESA, starting from the lowest triplet of the $(t_1^5,2e)$ configuration will occur to the triplet terms of the $(t_1^5,4t_2)$ configuration. This is one of the causes of the high ESA strength. Still another effect which can affect the ESA spectrum is a static Jahn–Teller (J–T) effect, found by Barendswaard at al.,[24,25], in YVO_4, $CaMoO_4$, and probably occurring in other tetroxo–ion crystals such as $CaWO_4$ (there are some related data in ref. [26]) and possibly in $ZnWO_4$. The J–T effect, shifting of the equilibrium point of the first excited state can severely influence the ESA/gain spectral overlap. Further, spin–orbit coupling surely occurs in these materials (this is why they luminesce in the first place). It may be relatively small, obscured by J–T effect, in $CaMoO_4$ [27,28], but distinctly larger in $CaWO_4$ and $ZnWO_4$ because of the heavy central atom. Spin–orbit coupling will mix multiplicities, modify the triplet–singlet term ordering of the $(t_1^5,2e)$ and $(t_1^5,4t_2)$ configurations, and influence the ESA/gain oscillator strengths and spectral widths.

A qualitative way to deal with this complexity of spectroscopic data is the creation of a single configuration coordinate (SCC) model, assuming linear coupling to a full symmetry mode. Such a model is obviously oversimplified but it is reasonable to see how far it can lead and where it fails.

For the construction of SCC diagrams we need the maxima of the emission lineshapes obtained from experiment, and the Stokes shift. In order to determine the Stokes shift one has to know the position of the absorption lineshape maximum. Since absorption spectrum is dominated by strong, parity and spin allowed singlet–singlet

transitions, it is difficult to experimentally determine the full absorption band. To circumvent this we assume equal contributions to the Stokes shift from emission and absorption. This is a consequence of linear coupling to one mode. As an example of the procedure we take $CaWO_4$ where emission lineshape peaks at 19470 cm^{-1}. An analysis of the known emission lineshapes enable us to determine the position of zero–phonon line (ZPL) which is about 28000 cm^{-1}. The maximum of absorption lineshape would then be 36530 cm^{-1}. Butler, on the basis of semiempirical molecular orbital calculations, gives about 37000 cm^{-1} for the lowest energy, spin forbidden transition $(t_1^6)\ ^1A_1 \longrightarrow (t_1^5,2e)\ ^3T_1$, [1, p. 296]. The agreement is thus reasonable, proving the consistency of our approach. With these values we can now construct the adiabatic potential curves.

The total energy (electronic and vibrational) in harmonic approximation for the ground state, $(t_1^6)\ ^1A_1$, will be:

$$E_1(Q) = A \cdot Q^2 \qquad (3)$$

and for the first excited state, $(t_1^5,2e)\ ^3T_1$:

$$E_2(Q) = A \cdot (Q - Q_o)^2 + B\ , \qquad (4)$$

where B is equal to the ZPL energy for the $(t_1^6)\ ^1A_1 \longrightarrow (t_1^5,2e)\ ^3T_1$ transition, Q_o is the equilibrium position of the (first) excited state and $2 \cdot A \cdot Q_o^2$ is equal to the Stokes shift. If we choose the units so that $Q_o = 1.0$ then the Stokes shift for this particular center alone will determine the shape of all the parabolas.

To include ESA into our model we have to determine the final state for the ESA transition. The initial state is the same as for the luminescence transition, $(t_1^5,2e)\ ^3T_1$. The other states of the $(t_1^5,2e)$ configuration are too close, (3000 to 6000 cm^{-1} for unrelaxed, (Q = 0), WO_4^{2-} complex, [1, p. 296]), to give a spectrum in the visible even when a large lattice relaxation is included. The most likely candidate is therefore one of the states due to the $(t_1^5,4t_2)$ configuration. Assuming that ^3T is the lowest energy state and that term

splittings are about the same for both configurations, the electronic energy difference between the first and the second excited states (the system being in the equilibrium position for the ground state, Q = 0) is equal to 10Dq(0), which is about 9120 cm^{-1}, [29,30]. Then:

$$E_3(Q) = A \cdot (Q - Q_o)^2 + B + 10Dq(Q) \qquad (5)$$

where 10Dq(Q) is the difference in energy between $(t_1^5, 2e)$ and $(t_1^5, 4t_2)$ configurations. In a linear coupling model

$$10Dq(Q) = 10Dq(0) + C \cdot Q \qquad (6)$$

where 10Dq(0) is an electronic contribution to the total energy and the parameter $C = 2AQ_oQ_1$ describes the change in the equilibrium position of the second excited state in comparison to the first excited state. This procedure leads to diagrams of Fig. 3, associated with particular materials.

In addition we attempt to determine the theoretical limits of the SCC model by considering two extreme cases, shown on top of Fig. 3. In the first idealized case we assume that the $4t_2$ one–electron state is characterized by a strongly diffused wave function, characteristic of an efficient tungsten–tungsten energy transfer and high electron mobility. This approach certainly lacks any direct experimental support based e.g. on photoconductivity, [30]. It has, however, some credibility since d states of t_2 symmetry do mix with p states of the metal ion (see e.g. [16]) which may have the tendency of forming a conduction band. This mixing would strongly influence the ESA oscillator strength. In this extreme case the effective wave function would be so strongly delocalized that charge distribution in the second excited state corresponds to the same equilibrium point as that for ground state. In the second limiting approach we assume that the $4t_2$ one–electron function is made exclusively of d type one–electron orbitals and is, therefore, strongly localized on the tungsten ion. The ESA band in this model would be very narrow

with an energy around 9120 cm^{-1}. In view of the same equilibrium position for both excited state parabolas, there would be no mixing between p and d orbitals of the central ion and the ESA transition would have a rather weak oscillator strength. We illustrate the whole set of SCC diagrams in Fig. 3. The parameters are specified in Table IV, all, except 10Dq–s [29], are taken from experimental data.

DISCUSSION

As it is seen from Fig. 3, all the SCC diagrams fit into the range of the described theoretical framework. The tungstates fit very well, being close to "delocalized" case and thus producing broad ESA band. Interestingly, the SCC diagram of the tungstate glass whose structure is not well known, and whose coordination is thought to be fourfold ($\sim T_d$ symmetry) [19], explains the large ESA bandwidth only with T_d symmetry (10Dq = 9120 cm^{-1}). Assuming six fold coordination (O_h), and 10Dq = (9/4)×9120 cm^{-1}, we would obtain lower and higher excited–state parabolas having nearly the same equilibrium coordinate, i.e. yielding a narrow ESA line which is contrary to observation. Thus, the observed width and position of the ESA band tends to confirm the presumed coordination.

The only material which does not fit into our SCC model, is the $CaMoO_4$ crystal, whose SCC diagram, being rather close to "localized" case, cannot explain the large ESA bandwidth. For this case the simple model apparently fails. However, Van der Waals and collaborators [25,31], found a strong, static Jahn–Teller effect in the first excited state of $CaMoO_4$. It is very likely that the J–T distortion in this state and consequent displacement of the first excited state parabola, is responsible for the large ESA bandwidth in $CaMoO_4$.

Spin–orbit coupling plays a rather minor role in this material [27]. In absence of spin–orbit mixing ESA becomes a strictly triplet–triplet transition of considerable strength. In tungstate materials ESA is also strong but results from an opposite balance of

effects. There is an efficient breaking of Laporte selection rule due to considerable admixture of p–orbitals in the second excited state. The increase of ESA due to this selection rule breakdown is mitigated by the large heavy atom effect (Z = 74) which causes singlets and triplets to acquire less well defined multiplicities.

CONCLUSIONS

The fact, that two d stater separated by 10Dq of approximately 9120 cm^{-1} provide a broad ESA band in the visible, overlapping the emission, can than be qualitatively understood as a result of large electron–lattice coupling in the first excited state and a relative displacement between the two excited–state parabolas. In the case of $CaMoO_4$ the large ESA linewidth is connected with displacement of the lower excited state parabola due to a Jahn–Teller effect. For tungstates, the shift of the higher excited state equilibrium is connected with the admixture of p–orbitals of the central ion and $2p_\sigma$–orbitals of the ligands into the terminal ESA state. Another aspect of the ESA is its very high crossection. This derives from two sources: by breaking of the Laporte selection (LS) rule, like in tungstates, where transitions are no longer between pure d–d states, or by rather pure triplet–triplet (T–T) transitions, like in calcium molybdate.

Another effect contributing to the ESA strength and, perhaps, affecting its shape is spin–orbit coupling (SOC). Spin–orbit coupling in these materials evidently exists, relaxing the spin–selection rule and causing luminescence. It is strong in tungstate materials, and much weaker in $CaMoO_4$.

Summarizing, the ESA transitions in tetroxo complexes, occurring between the states of $(t_1^5,2e)$ and $(t_1^5,4t_2)$ configurations always have a high oscillator strength and broad spectrum, both precluding laser action. The resulting ESA strength and linewidth, including the J–T broadening, may be formally expressed as

$$\sigma_{ESA}(\tilde{\nu}) = \sigma_{ESA,T-T}(\tilde{\nu}) + \sigma_{ESA,LS}(\tilde{\nu}) \pm \sigma_{ESA,SOC}(\tilde{\nu}) + \sigma_{ESA,J-T}(\tilde{\nu}) \,. \quad (7)$$

The first term is present in all our cases, the second and third, have an essential influence in tungstates, the last one, influences the ESA in $CaMoO_4$.

We conclude that in systems with large electron–lattice coupling the estimation of the spectral position of ESA should necessarily take into account various aspects of this interaction.

Any further search for laser materials among molecular ions should then be guided by the following strategies:

1. *Spectral separation.*

Since 10Dq for tetrahedral complexes is already the lowest possible, there is no way to move it to the red. Octahedral complexes have 10Dq about twice as large. This may cause a significant shift of the ESA band to the blue or even UV. As shown in the case of WO_4^{2-} in glass, amorphous materials may be even more promising because of their naturally larger Stokes shift [23].

2. *Decrease the ESA cross section.*

As has been shown, ESA in tetroxo complexes is mostly induced by the allowedness of the $2e \longrightarrow 4t_2$ transitions, due to p–orbitals of the central ion mixed with its d–orbitals, or, by triplet terms in the $(t_1^5,4t_2)$ configuration in which case we deal with T–T transitions. Since there are always triplet terms in the $(t_1^5,4t_2)$ configuration, this is a fundamental problem making spectral separation the main hope.

3. *Increase the stimulated emission cross section.*

One should try to increase the stimulated emission crossection. However, the transition from the lowest excited state to the ground state happens to be spin and symmetry forbidden. In order to increase the oscillator strength of luminescence, we have just one degree of freedom: increase spin–orbit coupling by the use of heavy ions. However,

SOC may also alter ESA crossections. Thus, once again spectral separation becomes the dominant alternative.

Acknowledgment

We greatly appreciate the support of U.S. Army Research Office under the Grant DAAL03–88–0103.

References

[1] W. Krupke and M.J. Weber, *Prospects for New Dielectric Solid State Lasers*, at Topical Meeting on Tunable Solid State Lasers, October 26 – 28, 1987, Williamsburg, Virginia, Technical Digest, vol. 20, p. 2, MA1–1.

[2] K.H. Butler, *Fluorescent Lamp Phosphors, Technology and Theory*, (The Pensylvania University Press, University Park and London, 1980)

[3] F.A. Kröger, *Some Aspects of the Luminescence of Solids*, (Elsevier Publ. Co., Amsterdam 1948)

[4] R.H. Gillette, "Calcium and Cadmium Tungstate as scintillation counter crystals for gamma–ray detection", Rev. Sci. Inst. vol. 21, pp. 294–301, 1950.

[5] T. Oi, K. Takagi, and T. Fukazawa, "Scintillation study of $ZnWO_4$ single crystals", Appl. Phys. Lett. vol. 36, pp. 278–279, 1980.

[6] P. Pringsheim, *Fluorescence and Phosphorescence,* (Interscience Publishers, Inc., New York, London, 1949)

[7] H.V. Leverenz, *An Introduction to Luminescence of Solids,* (Dover Publications, New York, 1968)

[8] Cz. Koepke and A. Lempicki, "Excited state absorption in $Bi_4Ge_3O_{12}$", Chem. Phys. Lett. vol. 172, pp. 227–230, 1990.

[9] Cz. Koepke and A. Lempicki, "Excited state absorption in $CaMoO_4$", J. Luminescence, vol. 47, pp. 189–191, 1991.

[10] Cz. Koepke, A.J. Wojtowicz, and A. Lempicki, "Excited–State Absorption in Excimer–Pumped $CaWO_4$", to be published

[11] Cz. Koepke and A. Lempicki, "Excited–State Absorption in $ZnWO_4$ Crystal", to be published

[12] Cz. Koepke, A. Lempicki, and G.H. Beall, "Glasses Containing Closed–Shell Molecular Complexes, II: Excited State Absorption", to be published

[13] G. Blasse, "The luminescence of closed–shell transition–metal complexes. New developments", Structure and Bonding, vol. 42, pp. 1–41, 1980.

[14] T. Ziegler, A. Rauk, and E.J. Baerends, "The electronic structures of tetrahedral oxo–complexes. The nature of the "charge transfer" transitions", Chem. Phys. vol. 16, pp. 209–217, 1976.

[15] C.J. Ballhausen and H.B. Gray, *Molecular Orbital Theory,* (W.A. Benjamin, Inc., New York, Amsterdam, 1964)

[16] M. Karplus and R.N. Porter, *Atoms and Molecules; an introduction for students of physical chemistry,* (W.A. Benjamin, New York, 1970)

[17] W.A.J.A. van der Poel, M. Noort, J. Herbich, C.J.M. Coremans, and J.H. van der Waals, "The lowest triplet state of $K_2Cr_2O_7$. Optical spectra and optically detected electron spin resonance at 1.2 K", Chem. Phys. Lett. vol. 103, pp. 245–252, 1984.

[18] W. Barendswaard, R.T. Weber, and J.H. van der Waals, "An EPR study of the luminescent triplet state of VO_4^{3-} in YVO_4 and $YP_{0.96}V_{0.04}O_4$ single crystals at 1.2 K", J. Chem. Phys. vol. 87, pp. 3731–3738, 1987.

[19] Cz. Koepke, A. Lempicki, and G.H. Beall, "Glasses Containing Closed–Shell Molecular Complexes, I: Luminescence", to be published

[20] W.M. Fairbank, Jr., G.K. Klauminzer, and A.L. Schawlow, "Excited–state absorption in ruby, emerald, and MgO:Cr^{3+}", Phys. Rev. vol. B 11, pp. 60–76, 1975.

[21] D.E. McCumber, "Theory of phonon–terminated optical masers", Phys. Rev. vol. 134, pp. A299–A306, 1964.

[22] A.J. Wojtowicz, W. Meng, A. Lempicki, G.H. Beall, D.W. Hall, and T.C. Chin, "Spectroscopic Characteristics of Chromium Doped Mullite Glass–Ceramics", IEEE J. Quantum Electron., vol. QE–24, pp. 1109–1113, 1988.

G.F. Imbusch, T.J. Glynn, and G.P. Morgan, "On the quantum efficiency of chromium–doped glasses", J. Luminescence, vol. 45, pp. 63–65, 1990.

[24] W. Barendswaard, J. van Tol, and J.H. van der Waals, "The metastable triplet states of $K_2Cr_2O_7$ and YVO_4 at 1.2 K: zero–field splitting and lifetimes of the spin components", Chem. Phys. Lett. vol. 121, pp. 361–366, 1985.

[25] W. Barendswaard and J.H. van der Waals, "The photo–excited triplet state of $CaMoO_4$. A 60–80 GHz E.P.R. study at 1.2 K", Molec. Phys. vol. 59, pp. 337–353, 1986.

[26] R. Biederbick, G. Born, A. Hofstaetter, and A. Scharmann, "EPR investigations on the hole centres in $CaWO_4$ at T=4.2 K", Phys. Stat. Sol. vol. B 69, pp. 55–62, 1975.

[27] J.H. van der Waals, "Spin–orbit coupling in the tetroxo anions of the d^0 transition metals and the identification of their lower triplet states", Int. Rev. Phys. Chem. vol. 5, pp. 219–228, 1986.

[28] F.S. Ham, "Jahn–Teller Effects in Electron Paramagnetic Resonance Spectra", in *Electron Paramagnetic Resonance*, ed. by S. Geschwind (Plenum Press, New York–London, 1972) pp. 1–119.

[29] R. Kebabcioglu and A. Müller, "SCCC MO calculations on the ions WX_4^{2-}, MoX_4^{2-} and VX_4^{3-} (X = O, S, Se)", Chem. Phys. Lett. vol. 8, pp. 59–62, 1971.

[30] R. Grasser, E. Pitt, A. Scharmann, and G. Zimmerer, "Optical properties of $CaWO_4$ and $CaMoO_4$ crystals in the 4 to 25 eV region", Phys. Stat. Sol. vol. B 69,pp. 359–368, 1975.

[31] J.H. van der Waals, "Jabłoński's ideas applied to inorganic chemistry: a search for metastable triplet states of the d^0 transition metal tetroxo anions", Acta Phys. Polon. vol. A 71, pp. 809–821, 1987.

Table I *Closed Shell Transition Metal Ions*

Valence	+4	+5	+6	+7
3d	Ti	V	Cr	Mn
4d	Zr	Nb	Mo	–
5d	Hf	Ta	W	–

Table II *Complexes of Transition Metal Ions*

Ion valence	Complex	Structure	Luminescence	Example
+4	TiO_4^{4-} Titanate	Tetr.	yes	
	TiO_6^{8-} Titanate	Oct.	yes	$BaTi(PO_4)_2$
	TiO_5^{6-} Titanate	Square pyram.	?	
	ZrO_6^{8-} Zirconate		?	
	HfO_6^{8-} Hafneate		?	
+5	VO_4^{3-} Vanadate	Tetr.	yes	
	NbO_4^{3-} Niobate	Tetr.	yes	
	NbO_6^{3-} Niobate	Oct.	yes	$LiNbO_3$
	NbO_6^{7-} Niobate	Oct.	yes	Li_3NbO_4
	TaO_4^{3-} Tantalate	Tetr.	yes	
	TaO_6^{7-} Tantalate	Oct.	yes	$Mg_4Ta_2O_9$ $MgTa_2O_6$
	TaO_8^{11-} Tantalate	Zircon	yes	
+6	CrO_4^{2-} Chromate	Tetr.	no	
	MoO_4^{2-} Molybdate	Tetr.	yes	$CaMoO_4$
	MoO_6^{6-} Molybdate	Oct.	no	
	WO_4^{2-} Tungstate	Tetr.	yes	$CaWO_4$ $ZnWO_4$ etc.
	WO_6^{6-} Tungstate	Oct.	yes	A_2BWO_6
+7	MnO_4^- Manganate	Tetr.	no	

Table III. *Maximal values of cross–sections for ESA and stimulated emission transitions.*

Material	σ_{ESA} (cm^2)	σ_{ST} (cm^2)	$\sigma_{ESA}/\sigma_{ST}\big\|_{max\ ST}$
$CaWO_4$	2.6×10^{-19}	7.5×10^{-21}	30.7
$ZnWO_4$	6.3×10^{-19}	3.2×10^{-21}	171.8
WO_4^{2-} glass	7.5×10^{-19}	2.7×10^{-21}	129.6
$CaMoO_4$	10.0×10^{-19}	3.8×10^{-21}	157.8

Table IV. *Parameters used to calculate SCC diagrams presented in Fig. 3.*

All parameters are expressed in cm^{-1}.

Material	Z–P line	Emiss. line.max.	ESA line.max.	10Dq
$CaWO_4$	28000	19470	20500	9120
$ZnWO_4$	26200	18980	20870	9120
WO_4^{2-} glass	24500	15900	23350	9120
$CaMoO_4$	24000	15700	19650	13620

Captions to figures

Fig, 1 Molecular orbital diagram for tetrahedral MX_4 complex showing correlation with metal and ligand orbitals. We indicate the transitions for ground state – and excited state absorptions. The sequence of molecular orbitals corresponds to the example of MnO_4^- complex.

Fig. 2 Excited–State Absorption and Stimulated Emission cross–sections for $CaMoO_4$ crystal (a), $CaWO_4$ crystal and tungstate glass (b), and $ZnWO_4$ crystal (c). To determine σ_{ESA} and σ_{ST} we used the following parameters: $CaMoO_4$: $N^* = 3.9 \times 10^{17}$ cm^{-3}, $\tau = \tau(RT)/\phi(RT) = 40.0$ μs; $CaWO_4$: $N^* = 1.5 \times 10^{18}$ cm^{-3}, $\tau = \tau(RT)/\phi(RT) = 15.3$ μs; Tungstate glass: $N^* = 3.6 \times 10^{17}$ cm^{-3}, $\tau = \tau(RT)/\phi(RT) = 86.6$ μs; and $ZnWO_4$: $N^* = 4.5 \times 10^{16}$ cm^{-3}, $\tau = \tau(RT)/\phi(RT) = 36.0$ μs.

Fig. 3 Single configuration coordinate diagrams of tetroxo complexes in crystals and glass. Two top diagrams illustrate theoretical limits: extreme cases of fully delocalized and fully localized terminal ESA state, calculated for exemplary parameters of $CaWO_4$ crystal. Q_1–s denote the equilibrium positions of the higher excited state parabolas, with an assumption that the first excited states equilibrium positions: $Q_o = 1$.

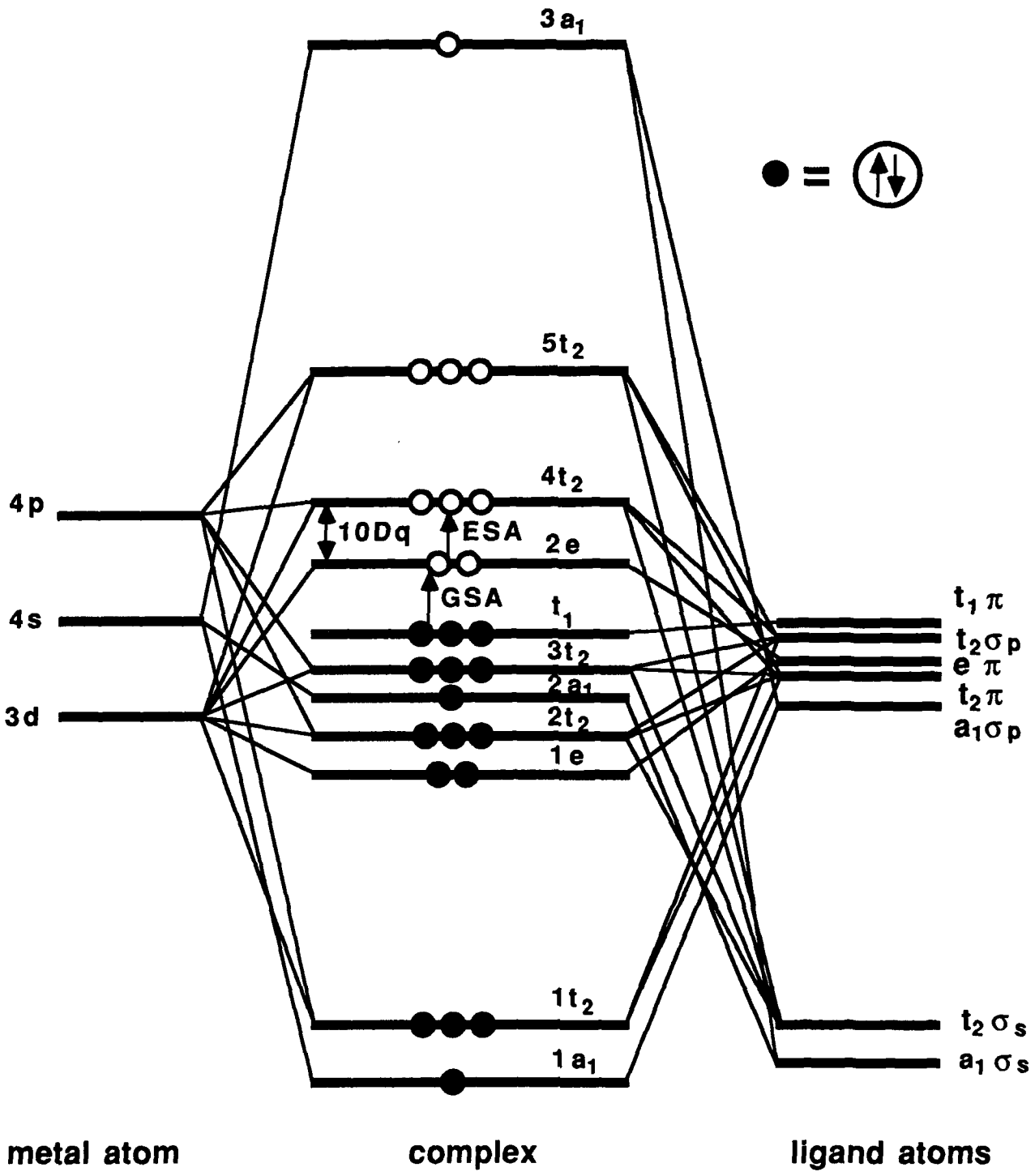
3a1
● = ⇅
5t2
4t2
4p
10Dq
ESA
2e
GSA
4s
t1
t1 π
t2σp
3t2
e π
2a1
t2 π
3d
2t2
a1σp
1e
1t2
t2 σs
1a1
a1 σs
metal atom
complex
ligand atoms

Fig. 1

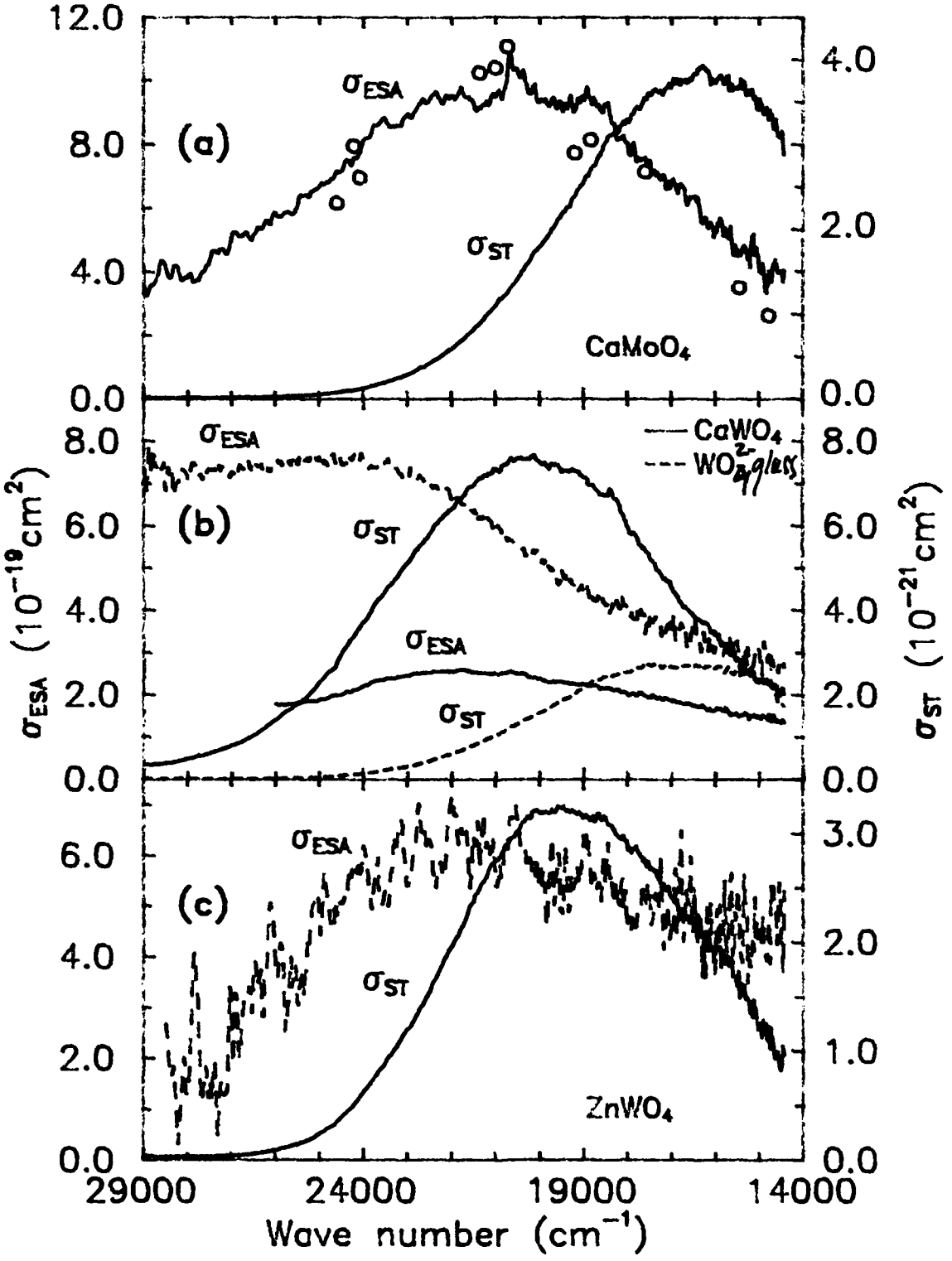

molecul1.ptt

Fig. 2

1
1.5
0.6
0.6

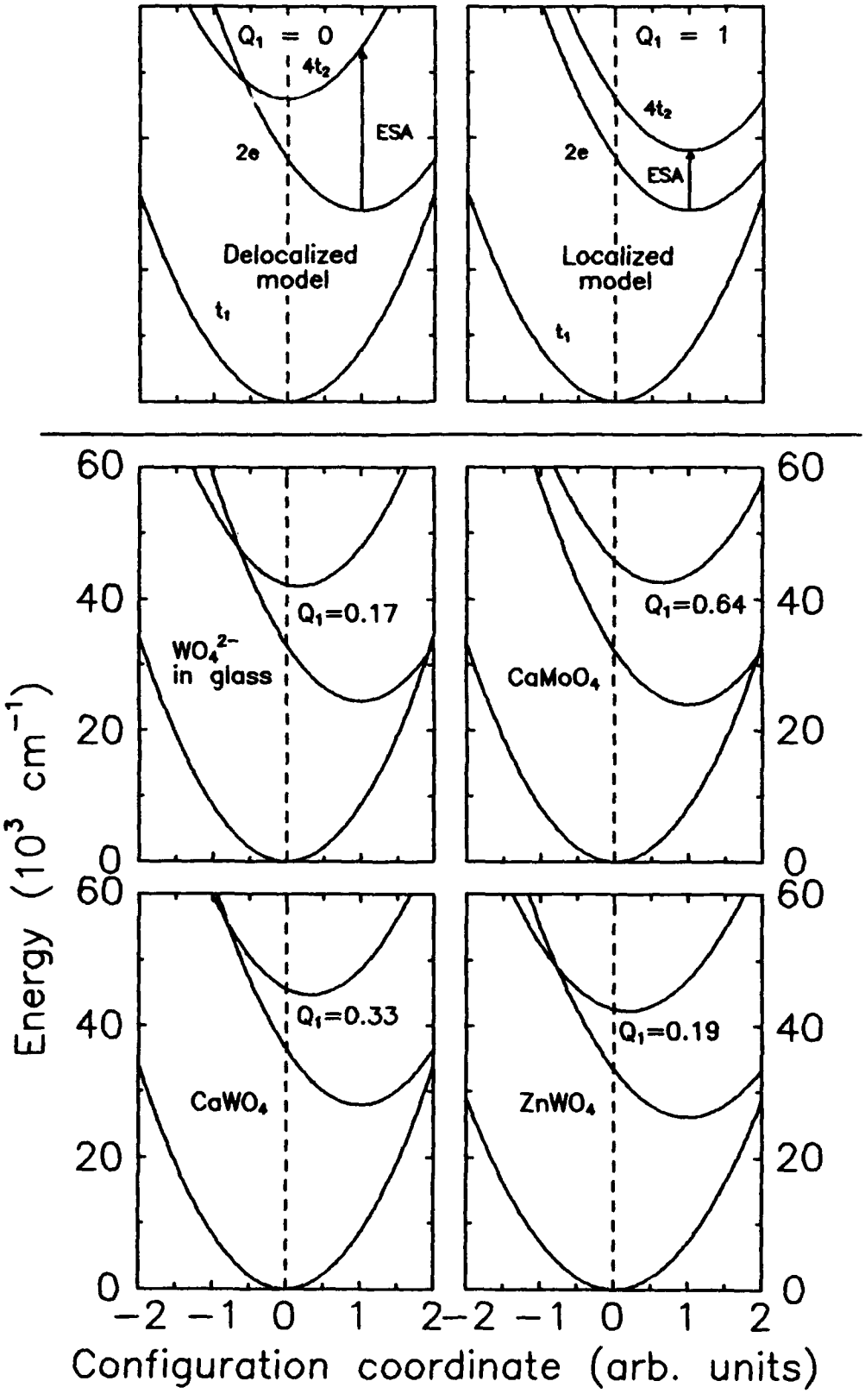

Fig. 3

Allparab.plt

1.5
1.5
0.4
0.4

LUMINESCENCE QUENCHING OF STRONGLY COUPLED SYSTEMS

Cz. Koepke*, A. Lempicki, and A.J. Wojtowicz*

Boston University, Chemistry Department, 590 Commonwealth Ave. Boston, MA 02215

Abstract

We examine the case of temperature quenching of luminescence of broad–band emitters. On the basis of published and newly acquired data, we conclude that the theory of nonradiative transitions based on coupling to a single vibrational mode, whether calculated in the Mott–Seitz terms or improved by the procedures developed by Struck and Fonger, is totally incapable of accounting for observed radiationless rates. There is no evidence for the operation of selection rules for nonradiative transitions.

---

*On leave from Institute of Physics, N. Copernicus University, 87–100 Toruń, Poland.

Introduction.

This paper deals with the problem of temperature quenching of luminescence of strongly coupled or broad band systems. We will present some new experimental results and review others, reported in the literature. Attempts to interpret these results in terms of conventional theory of nonradiative transitions, generally end up in failure.

Volumes have been written on the subject of nonradiative transitions in solids, [1–5], and it is not our intention to review the subject in any detail. Reduced to the bare bones, the nonradiative rate is invariably given by a product of two terms:

$$W_{nr} = C\, L(\omega \rightarrow 0) \qquad (1)$$

where C is a constant proportional to an electronic matrix element between initial and final electronic states and the operator is the non–adiabatic operator for a particular promoting mode, [6]. If there is coupling to more than one mode, C would involve summation over these modes. The quantity L is a normalized lineshape function, whose argument is the emission frequency taken in the vanishing limit. The physical origin of this is the fact that in nonradiative transitions there is no photon to carry the excess energy of the excited system, hence to satisfy energy conservation the frequency has to approach zero. This fact has been recognized before, [7] and leads to the bothersome conclusion that relevant values of the lineshape are totally outside experimental reach. All that experiment can provide is the product of eq. (1) or the total nonradiative rate W_{nr}.

All the theoretical effort has been directed at the calculation of the lineshape function, without much regard for the possibility of an experimental test. In all cases, except one, [7], the constant C has been treated either as an adjustable parameter or assigned a value in the neighborhood of 10^{13} sec^{-1}, taken from an early argument given by Mott and Seitz, [8,9]. One should mention that only in the case of week coupling is the

calculation of L fairly straightforward, and leads to the well known "gap law". In all other cases it leads to serious mathematical and conceptual difficulties.

Faced with this rather poor guidance from theory, what does the experimenter do? Invariably he fits the data to an Arrhenius equation, first suggested by Mott and Seitz,

$$W_{nr} = s \exp(-\delta E/kT) \qquad (2)$$

where s is usually referred to as a "frequency factor" of the order of a vibrational frequency and δE is an thermal activation energy. Although eq.(2) has a clear physical meaning, its justification has often been called into question, notably by Struck and Fonger, who argued that the assumption of a single barrier and the neglect of tunneling is not realistic, [10].

The values of the two constants, s and δE, as obtained from experimental fits, are often impossible to interpret on the basis of simple theory. The barrier δE is invariably much smaller than the barrier obtained from single configuration coordinate diagram, [7,11,14]. The frequency factor s can vary over some 13 orders of magnitude, as will be seen from our collection of data. It is therefore obvious that s in eq. (2) cannot be regarded as an universal constant represented by a vibrational frequency, as was the original intention of Mott. Values of s smaller than 10^{13} have sometimes been used as possible evidence for the existence of selection rules for nonradiative processes, [12–15]. This would be superficially plausible if one could identify s with the electronic matrix element C of eq. (1). However, there are strong arguments that such selection rules cannot exist because it is difficult to conceive of solids in which mixing promoting modes are absent. In one case of Cr^{3+} in elpasolites, [7] the matrix element has been calculated from first principles and found to lead to a frequency factor close to its canonical value of 10^{13} s^{-1}.

Experimental Results

We recently measured the temperature quenching of luminescence of a number of broad band emitters, [16]. The measured, wavelength integrated intensity was fitted to an expression, which combines eq.(1) with the definition of quantum efficiency η,

$$\eta = \tau/\tau_r \tag{3}$$

and

$$1/\tau = 1/\tau_r + W_{nr} \tag{4}$$

where τ is the observed decay time and τ_r is the radiative lifetime. Eqs. (1) through (4), yield

$$\eta = 1/[1 + s\,\tau_r \exp(-\delta E/kT)]\,. \tag{5}$$

If we assume that $\tau = \tau_r$ at low temperature, the quantum efficiency η is simply the integrated intensity, normalized to unity at low temperature.

One should emphasize that although a fit to eq.(5) requires two adjustable parameters, s and δE, the choice is quite unique and extremely sensitive to any variation. Examples of the fits can be found in refs. [11,14,16,27,28]. It is remarkable how well this simple equation fits the experimental data and it is therefore compelling to regard it as expressing some degree of truth.

Using a fit to eq. (5), our recently obtained data [16], plus those of other authors, are compiled on the left hand side of the Table I. Additionally we list the observed Stokes shift, Sts_{exp}. One can immediately see the extraordinary large range of s values and an overall tendency of s increasing with δE, illustrated in Fig. 1.

Discussion

The question which we pose is whether the Mott–Seitz equation, so successful in reproducing experimental data, can be retained, while reinterpreting the meaning of s and δE. There are two immediate arguments which would indicate that this is not possible. First, the existence of one barrier is unphysical in view of the Boltzmann occupancy of vibrational levels, each of which has a different barrier to contend with. Still δE may be some kind of effective barrier. The second argument is more powerful. The form and spirit of the Mott–Seitz equation indicates that the quantities s and δE should be independent, s being a more or less universal, temperature independent constant, related to a vibrational frequency, while δE is involved in the temperature dependence. However, the range of s values and the relation indicated by Fig. 1 seem to contradict the Mott–Seitz equation. Nevertheless, we shall still attempt to justify this formula by generalizing the quantities s and δE.

Limiting ourselves to a harmonic approximation and coupling to a single mode, we adopt the Struck and Fonger notation and express the nonradiative rate as

$$W_{nr} = N_{uv}\, U_{pu} \tag{6}$$

where N_{uv} is a constant of the order of 10^{13}, essentially replacing the Mott frequency factor s and U_{pu} is the lineshape as calculated by Fonger and Struck. The lineshape in the linear coupling case is given by:

$$U_{pu} = \sum_{m=0}^{\infty} (1-r_v)\, r_v^m \langle u_{p_u+m} | v_m \rangle^2 \tag{7}$$

where $r_v = \exp(-\hbar\omega/kT)$ is the Boltzmann factor between vibrational states, $\langle u_{p_u+m} | v_m \rangle$

are Franck–Condon overlap integrals between lower $|u_n\rangle$ and higher $|v_m\rangle$ vibrational state (n indexes the vibrational levels of electronic ground state, m refers to those of the excited state), and p_u is the ratio of zero–phonon line energy to the phonon energy: $p_u = h\nu_o/\hbar\omega$. For the nonlinear coupling case the formula (7) becomes somewhat more complicated [10] but the overall sense is the same. We rewrite eq.(1) in the form

$$W_{nr} = N_{uv}\, s' \exp(-\delta E/kT), \qquad (8)$$

$s = N_{uv}s'$, where $N_{uv}s'$ can now be regarded as a new "effective frequency factor" in which $N_{uv} = 10^{13}$ and s' is given by

$$s' = U_{pu} \,/\, \exp(-\delta E/kT). \qquad (9)$$

The calculation of U_{pu} proceeds according to the prescription of Fonger and Struck by using the Manneback recursion formulas for the overlap integrals [10,17]. The quantity s' can be viewed as a correction factor, designed to account for the departure of the observed (or rather fitted) frequency factor from the expected value of 10^{13} s^{-1}. A similar approach was demonstrated by Struck and Fonger [10]. Eq. (8) represents a departure from the Mott–Seitz picture because it introduces a temperature dependence in the pre–exponential factor. This is an unavoidable consequence of trying to reconcile eq. (2) with Struck and Fonger eq. (6). All that we can expect is that the temperature dependence of the effective frequency factor $N_{uv}s'$ will be weak and that the Mott–Seitz equation will still retain its basic applicability.

We have performed these calculations for several cases, all listed on the right hand side of Table I, labled QMSCC, a name used by S–F for quantum mechanical single coordinate calculations. In the first instance we restricted the calculations to a linear coupling model, or in the language of Struck and Fonger, to a Manneback angle θ of 45°.

Linear coupling case

The objective is to calculate $s = N_{uv}s'$ with s' derived from eq. (9). The parameters needed for this calculation are the photon frequency and the dimensionless measure of the Franck–Condon offset a_{uv} defined by

$$a_{uv}^2 = 4\,S \tag{10}$$

where S is a Huang–Rhys parameter. We take the phonon frequency from experiment, whenever it is available, otherwise we fix it at 400 cm^{-1}, which is a reasonable figure for the investigated cases. Having the phonon frequency, a_{uv} is uniquely defined by the Stokes shift Sts:

$$a_{uv}^2 = 2\,Sts/\hbar\omega \tag{11}$$

which is more directly observable in experiment. We therefore list the experimental value of the Stokes shift Sts_{exp} in Table I, together with a value Sts_{need}, needed to achieve the reproduction of the value of s. Since in turn, the Stokes shift determines the value of a classical barrier height ΔE, determined by the intersection of two parabolas, we also include its values in Table I.

On the basis of the values listed in Table I, we observe that the inclusion of Struck and Fonger technique for recognizing multiple barriers and tunneling, while enabling us to account for the observed "effective frequency factor" s, requires Stokes shift and barriers totally at variance with experiment. Also, for two cases where values of the phonon energy are known, we observe that using actual Sts_{exp} one can fit the value of s but only by applying artificially high phonon energies; $\hbar\omega$ = 950 cm^{-1} for $CdWO_4$ (instead of 250 cm^{-1}), or 605 cm^{-1} for Sillimanite: Cr^{3+} (instead of 363 cm^{-1}). Fonger and Struck [18]

encountered a similar problem: in order to fit radiationless transition rates they had to use a phonon energy substantially larger than that needed to fit optical line shapes. Hence, we must conclude that there in no way a single coordinate, linear coupling model can be made compatible with eq. (1) in which δE and s are obtained from a fit. We therefore explore next the case of nonlinear coupling.

Nonlinear coupling case

We shall consider now the nonlinear coupling by introducing the Manneback angle $\theta = \arctan\sqrt{\omega_v/\omega_u} \neq 45^o$, where ω_v and ω_u are respectively the phonon frequencies of the excited and ground states. In calculating the correction factor s', we shall now treat the angle θ as the independent variable, while the Stokes shift will be kept at its experimental value. The results are given in Table I under the heading "Nonlinear coupling". There are two things which require comment. First the required angle θ is unusually small, (except perhaps for the K_2NaGaF_6:Cr^{3+} and Tungstate glass), making the ratio of phonon frequencies unphysical. The introduced nonlinearity can also alter severely the fits to the temperature dependencies, as can be seen in ref. [19] where even a relatively small change of the Manneback angle ($45^o \longrightarrow 44^o$) was capable to shift the entire $\eta(T)$ curve to unrealistically lower temperatures. One can decrease the required nonlinearity, still fitting the experimental s values, but like in the linear coupling case, only by using higher values of $\hbar\omega_u$. In the aforementioned cases of $CdWO_4$ and Cr^{3+} in Sillimanite, using a realistic $\theta = 44^o$, one can fit s with: $\hbar\omega_u = 795\ cm^{-1}$ and $\hbar\omega_u = 465\ cm^{-1}$ respectively; both values far from experimental ones. Secondly we notice that the barrier height ΔE, although smaller than in the case of linear coupling, is still considerably larger (except Cs_2NaYCl_6 case) than the Mott barrier δE. Hence introduction of arbitrary nonlinear coupling is still incapable of bringing an agreement with the Mott–Seitz equation.

We should note here that by forcing an equality between W_{nr} as given by eqs. (2)

and (6), we have made sure that at room temperature the nonradiative rates as determined experimentally and by the linear or nonlinear model are all equal. This of course does not have to hold at other temperatures. To illustrate this point we plot in Fig. 2 the radiationless transition time as a function of temperature, for the case of zirconate glass (6%). The experimental points (circles) derived from the fit to Mott formula, are compared to $\tau_{nr}(T)$ dependencies calculated with linear and nonlinear coupling model. Theoretical curves were calculated taking care of the s value to be the same as in experiment, i.e. using fitting parameters from right–hand side of Table I. The curve yielded by the linear case (long dashes) seems to be closer to the experimental points, one should remember however, that the curve was calculated with a Stokes shift (different from experimental one) that fits the experimental value of s. Despite of this, the dynamic range of calculated τ_{nr} is here still too large in comparison with experiment. The nonlinear case data have even wider dynamic range and deviate from experiment even more than the linear case data. This is surprising, especially in comparison with the Table I, where the nonlinear model yielded values of ΔE closer to experiment than the linear one. One needs to keep in mind, however, that the Manneback angles θ used to fit the calculated s to the experimental one are rather small, giving unphysically small ratio of the higher to lower phonon. Finally, we note that all the $\tau_{nr}(T)$ curves cross at T = 300 K, which is caused by the fact that s' of eg.(9) was calculated at room temperature. This is of course the basic inconsistency between our (or S–F) approach, and the Mott formula which regards s as temperature independent.

Conclusions

The conclusion so far is that linear or nonlinear coupling to a single mode cannot reproduce the experimentally observed nonradiative rates. The next degree of complexity

one can add to this problem is the introduction of linear coupling to a a distribution of many vibrational modes [20]. This complication departs from the limited goal set at the begining. Moreover as shown in Ref.[7], it does not seem to improve the situation. As it can be concluded from the set of results illustrated in Fig. 1, the Mott–Seitz equation in its traditional form mixes s and δE parameters, thus producing an artificial proportionality between δE and s. Should there still be any suspicion that there exists selection rules governing nonradiative rates, we have divided the materials listed in Table I into three classes, which should differ in the form of the promoting mode matrix element C of eq. (1). Thus, in Fig. 1 we use asterisks for Ce doped crystals and glass (allowed optical transitions); dots for chromium doped crystals (transitions allowed through the doublet–quartet interaction), and circles for molecular complexes (forbidden triplet–singlet transitions). If selection rules were operative one would expect that these three classes would fall in different curves. Yet there is no such tendency and we must conclude that *selection rules do not operate.*

The final conclusion must be that in many, and we suspect most cases of broad band emitters, or equivalently strong electron–lattice coupling, the elementary theory of nonradiative rates, simply does not work. One is therefore left with a case by case consideration of a proper remedy. In the case of Cr^{3+} in elpassolites [7] the remedy turned out to be the inclusion of quadratic coupling to a non totally symmetric mode. In other cases anharmonicity may be the answer [21]. This is a very frustrating state of the theory because it does not, at this time, provide any predictive ability, like the one offered by the gap law of weakly coupled systems. The Mott–Seitz theory fails entirely as long as s is defined as a fixed "frequency factor". The ability of the Mott–Seitz formula to fit experimental data must therefore be regarded as totally fortuitous.

Acknowledgment

We wish to thank Prof. R. Bartram for very useful suggestions. We gratefully acknowledge the support of the U.S. Army Research Office under Grant No. DAAL03–88–0103.

References

[1] F.A. Krõger, *Some Aspects of the Luminescence of Solids*, (Elsevier Publ. Co., Amsterdam 1948)

[2] R. Englman, *Non–Radiative Decay of Ions and Molecules in Solids*, (North Holland, Amsterdam 1979)

[3] F. Auzel, in *Radiationless Processes*, ed. B. Di Bartolo and V. Goldberg (Plenum Press, New York 1980)

[4] K. Huang, Chin. Phys. 1, (1981) 717

[5] R. H. Bartram, J. Phys. Chem. Solids 51, (1990) 641

[6] S.H. Lin, J. Chem. Phys. 44, (1966) 3759

[7] R.H. Bartram, J.C. Charpie, L.J. Andrews, and A. Lempicki, Phys. Rev. B 34, (1986) 2741

[8] N.F. Mott, Proc. Roy. Soc.(London), A 167, (1938) 384

[9] F. Seitz, J. Chem. Phys. 6, (1938) 150

[10] C.W. Struck and W.H. Fonger, J. Luminescence, 10, (1975) 1

[11] L.J. Andrews, A. Lempicki, B.C. McCollum, C.J. Giunta, R.H. Bartram, and J.F. Dolan, Phys. Rev. B 34, (1986) 2735

[12] P.J. Gardner and M. Kasha, J. Chem. Phys. 50, (1969) 1543

[13] L.J. Andrews, A. Lempicki, and B.C. McCollum, Chem. Phys. Lett. 74, (1980) 404

[14] A.J. Wojtowicz and A. Lempicki, Phys. Rev. B 39, (1989) 8695

[15] R. Knochenmuss, Ch. Reber, M.V. Rajesekharan, and H.U. Gudel, J. Chem. Phys. 85, (1986) 4290

[16] Cz. Koepke, A. Lempicki, and G.H. Beall, "Glasses Containing Closed–Shell Molecular Complexes, I: Luminescence", to be published

[17] C. Manneback, Physica XVII, (1951) 1001

[18] W.H. Fonger and C.W. Struck, Phys. Rev. B 11, (1975) 3251

[19] K.C. Bleijenberg and G. Blasse, J. Sol. Stat. Chem. 28, (1979) 303

[20] M.H.L. Pryce, in *Phonons*, ed. by R.W.H. Stevenson (Plenum Press, New York, 1966)

[21] M.D. Sturge, Phys. Rev. B 8, (1973) 6

[22] A.D. Bross, IEEE Trans. Nucl. Sci. 33, (1986) 144

[23] R. Ruchti, B. Baumbaugh, J. Bishop, N. Biswas, J. Busenitz, N. Cason, J. Cunningham, R. Gardner, S. Grenquist, V. Kenney, E. Mannel, R. Mountain, W. Shephard, A. Baumbaugh, K. Knickerbocker, C. Wegner, R. Yarema, A. Rogers, B. Kinchen, J. Ellis, R. Mead, and D. Swanson, IEEE Trans. Nucl. Sci. 33, (1986) 151

[24] Cz. Koepke, A.J. Wojtowicz, and A. Lempicki, "Excited–State Absorption in Excimer–Pumped $CaWO_4$ Crystal", to be published

[25] G.B. Beard, W.H. Kelly, and M.L. Mallory, J. Appl. Phys. 33, (1962) 144

[26] C.E. Tyner and H.G. Drickamer, J. Chem. Phys. 67, (1977) 4103

[27] Cz. Koepke and A. Lempicki, "Excited–State Absorption in $ZnWO_4$ Crystal", to be published

[28] H. Grassmann, H.G. Moser, and E. Lorenz, J. Lumin. 33, (1985) 109

[29] Li–Ji Lyu and D.S. Hamilton, J. Lumin. 48 & 49, (1991) 251

ble I.

ATERIAL	EXPERIMENT				Ref.	QMSCC, LINEAR COUPLING		QMSCC, NONLINEAR COUPLING		
	$a\,(s^{-1})$	$\Delta E\,(cm^{-1})$	$\hbar\omega\,(cm^{-1})$	$Sta_{exp}\,(cm^{-1})$		$Sta_{need}\,(cm^{-1})$	$\Delta E\,(cm^{-1})$	θ (deg)	$\hbar\omega_y/\hbar\omega_g$	$\Delta E\,(cm^{-1}$
Zirconate										
ns 8%	$6.7\cdot10^{4}$	887	400*	9600	[16]	20070	7170	40.45	0.727	5347
6%	$1.1\cdot10^{5}$	1008	400*	9600	[16]	20030	7201	40.47	0.728	5374
4%	$1.0\cdot10^{5}$	1048	400*	9600	[16]	19880	7320	40.54	0.732	5472
Tungstate										
-ass, 20%	$7.4\cdot10^{5}$	363	400*	17320	[16]	20093	5271	43.93	0.927	4870
obate										
glass, 1%	$1.2\cdot10^{6}$	887	400*	15400	[16]	21270	5842	42.74	0.855	5003
..limanite										
$:Cr^{3+}$	$3.6\cdot10^{6}$	1700	363	4818	[14]	7243	8033	43.10	0.876	6587
Ce : glass					[22,23]					
C–20	$2.3\cdot10^{9}$	1476	400*	10580	+ our data	28400	4121	37.50	0.590	2892
WO_4	$5.4\cdot10^{9}$	2420	400*	17060	[24]	23940	5367	42.50	0.840	4559
	$1.6\cdot10^{10}$	2742	–	–	[25]					
$CdWO_4$	$8.0\cdot10^{9}$	2500	250	11200	[25,26]	22060	4161	40.37	0.724	3494
WO_4	$7.0\cdot10^{11}$	3629	400*	14440	[27]	20853	5966	42.44	0.835	4979
	$2.5\cdot10^{12}$	4033	–	–	[28]	–	–	–	–	–
$Ce:Cs_2NaYCl_6$	$3.8\cdot10^{10}$	4250	228	3187	[11]	6805	4594	41.49	0.782	3744
$Ce:K_2NaScF_6$	$1.2\cdot10^{12}$	7270	380	3002	[11]	4550	15837	43.66	0.911	12698
$:K_2NaGaF_6$	$5.2\cdot10^{12}$	9240	378	3009	[11]	3685	22361	44.46	0.963	19857
$:LaF_3$	$1.0\cdot10^{11}$	2400	–	–	[29]	–	–	–	–	–
:YAG	$4.0\cdot10^{13}$	6500	–	–	[29]	–	–	–	–	–
$Ce:CaF_2$	$1.0\cdot10^{14}$	6700	–	–	[29]	–	–	–	–	–
$:YLiF_4$	$4.0\cdot10^{15}$	14000	–	–	[29]	–	–	–	–	–
$Ce:YAlO_3$	$1.0\cdot10^{17}$	9700	–	–	[29]	–	–	–	–	–

sumed value

Caption to Table I

Compilation of parameters characterizing nonradiative processes.
s – frequency factor obtained by use of Mott–Seitz formula, δE – energy barrier obtained by use of Mott–Seitz formula, $\hbar\omega$ – phonon energy, Sts_{exp} – experimental Stokes shift, Sts_{need} – Stokes shift needed to fit s value in QMSCC linear model, ΔE – energy barrier resulting from QMSCC linear model, θ – Manneback angle used to fit s in QMSCC nonlinear model, $\hbar\omega_y / \hbar\omega_u$ – ratio of phonon energies, ΔE – energy barrier resulting from QMSCC nonlinear model.

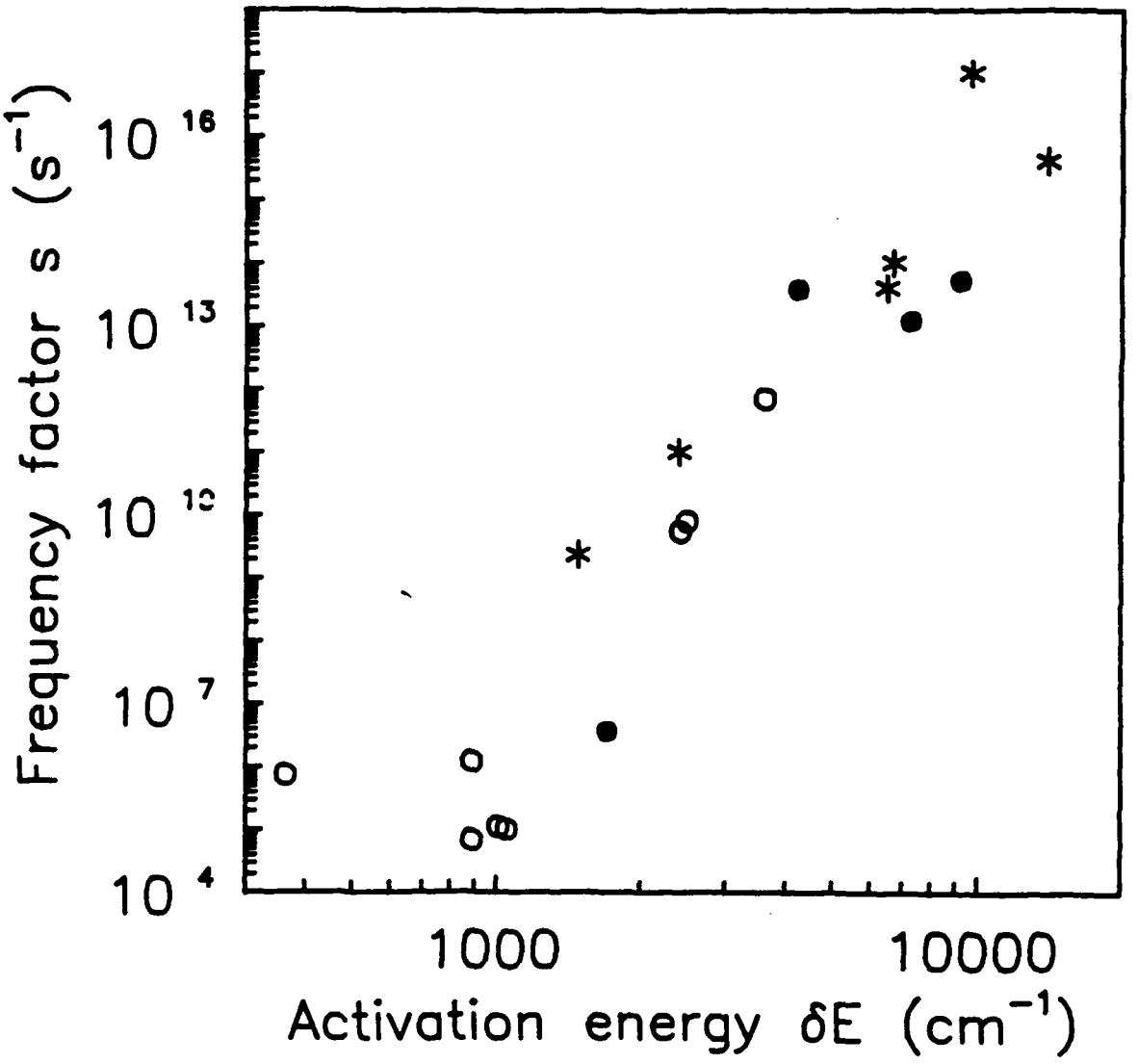

Fig. 1

Gachkine et al. „Luminescence Quenching"

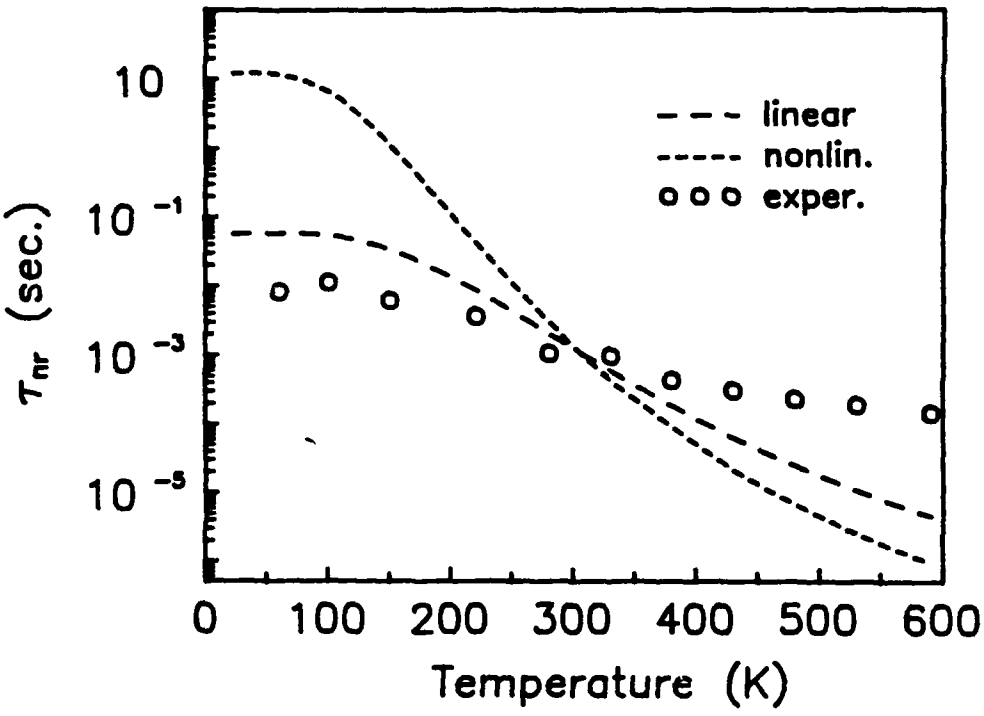

Fig. 2

G. Kaplyanskii et al. "Luminescence Quenching..."

Captions to figures

Fig. 1 Correlation between the barrier δE and "frequency factor" s, parameters taken from Table I. Different symbols were supposed to distinguish three classes of materials, by means of different "ratiationless selection rules" (see text).

Fig. 2 Comparison of the temperature dependence of nonradiative decay time τ_{nr} for three cases: experimental (derived from fit to Mott formula), QMSCC linear model, and QMSCC nonlinear model. All data correspond to the case of zirconate glass (6%).